Frugal Design and Robotic Surgery

by

Stephen Alan McKinley

A dissertation submitted in partial satisfaction of the
requirements for the degree of
Doctor of Philosophy

in

Engineering-Mechanical Engineering

in the

Graduate Division

of the

University of California, Berkeley

Committee in charge:

Professor Paul Wright, Co-chair
Professor Ken Goldberg, Co-chair
Professor Dennis K. Lieu
Professor Eric Paulos

Summer 2016

Frugal Design and Robotic Surgery

Abstract

Frugal Design and Robotic Surgery

by

Stephen Alan McKinley

Doctor of Philosophy in Engineering-Mechanical Engineering

University of California, Berkeley

Professor Paul Wright, Co-chair

Professor Ken Goldberg, Co-chair

A new era of robotic surgery is poised to begin when critical patents held by Intuitive Surgical (IS) expire in 2016. IS market dominance for decades has led to an effective monopoly that will be challenged by several commercial enterprises working on next generation general robotic surgery systems. Robotic surgery has the potential to alleviate the skill-gap between experienced and inexperienced surgeons through the automation of sub-tasks within surgical procedures.

The primary objective of this dissertation is to explore the process of design itself through the presentation of these devices. The common intention throughout the presented case studies is **Frugal Design**.

Secondarily, this dissertation explores limitations of current **surgical automation** and addresses the design considerations of hardware modifications to the daVinci Research Kit which enable automation.

Part I (Chapter 1) of this dissertation describes the considerations that make a design frugal and the methodology used by the author across three conceptual examples including:

- an inexpensive physical environment for machine learning,
- a device for cloud-enabled irrigation optimization, and
- an interchangeable tool interface for surgical robotics.

Part II of this dissertation presents frugal design case studies for system components that enable an automated silicone-phantom tumorectomy.

Chapter 2 provides an overview of existing technology and related work in the field of surgical automation.

Chapters 3, 4, 5, and 6 describe designs for devices that enable automation of the four subtasks involved in a tumorectomey: *Palpation*, *Incision*, *Debridement*, and *Closure*. Specifically, these devices include:

- an inexpensive palpation probe to locate tumors (Chapter 3),
- an interchangeable tool interface for surgical robotics (Chapter 5),
- a fluid injector for surgical robotics (Chapter 4), and
- a passive needle orientation fixture (Chapter 6).

Part III of this dissertation describes the design **theory behind** the author's work presented in Part 1 (examples) and Part 2 (case studies). In Chapter 7, a short history of design theory in the Bauhaus school of (1919-1933) is presented through examples taken from the author's work. Chapter 8 serves as a link to **future efforts** by the author by bridging the presented frugal design work into the global development effort of frugal innovation.
The design theory material in Part 3 is presented for three reasons:
First: Conceptual design depends on the practitioner's ability to abstract design criteria into diverse functional solutions. The author's practice in this area involves the artistic study of functionalist abstraction as unconstrained exploration of the design space. That practice is presented to elucidate the creative origins of the solutions presented herein, and to provoke creative problem solving in others
Second: A socially-progressive responsibility, inherent in the Bauhaus ideology, is modernized in Chapter 8 as Frugal Design, which borrows its motivation from a new trend in development for emerging markets known as Frugal Innovation.
Third: A parallel is drawn to the climate of artificially intelligent automation in present-day Bay Area research in Berkeley, Stanford, and Silicon Valley to the Bauhaus, which was founded as a reaction to increasing automation during the first machine age in Germany.

To My Brothers,
for their fearless inspiration.

To my Mother and Father,
for their limitless encouragement.

In memory of Professor David A. Dornfeld,
thank you for having believed in me.

Art is communication, design is self-evident.

All of the research presented henceforth was completed at the AUTOLAB on the University of California, Berkeley campus under the direction of Professor Ken Goldberg.
All photos, logos, and graphics in this work are original creations by the author (except otherwise noted below in this preface). Some of these have been previously published (as cited below in this preface); these previously published graphics are included so as to present this work within context of the greater research effort at the University of California, Berkeley; and in the greater scientific community.
All of the artwork (chapter headings, accents, and appendices) presented in this work are original and previously unpublished works of the author completed during the period of time during which the henceforth presented research was completed. The pieces are included in an attempt to present a more complete picture of the design process used by the author.

Chapters 1 (Introduction) and 2 (Surgical Overview) are previously unpublished works providing an introduction to Frugal Design and a related work survey of surgical practices. Figure 1.1 has been adapted from Bramstedt Surgical. Figure 1.2 (lower left) and 1.3.a were created by Intuitive Surgical. Figure 1.4 was published by Cavusoglu in [22]. Figure 1.5 was published in [164]. Figure 1.6 was published in [134]. Figure 1.7 (left) was published in [73], and Figure 1.7 (right) was published in [102].

Chapter 3 (PALP) was partially published in a conference paper:

S. McKinley, A. Garg, S. Sen, R. Kapadia, A. Murali, K. Nichols, S. Lim, S. Patil, P. Abbeel, A. M. Okamura, and K. Goldeberg, "A disposable haptic palpation probe for locating subcutaneous blood vessels in robot-assisted minimally invasive surgery," in *CASE*, 2015.

This chapter was also submitted as a provisional patent (U.S. Provisional Application No. 62/183,633). Additional work using the devices featured in this chapter was presented in a conference paper (Note: Only contributions made by the author are presented here):

A. Garg, S. Sen, R. Kapadia, Y. Jen, S. McKinley, L. Miller, and K. Goldberg, "Tumor localization using automated palpation with gaussian process adaptive sampling," *International Conference on Automation Science and Engineering (CASE)*, 2016.

Chapter 4 (FLIP) was submitted as a provisional patent (U.S. Provisional Application No. 62/183,638) and presented as a poster in:

S. McKinley, A. Garg, S. Lim, S. Patil, and K. Goldberg, "Automated delivery instrument for stem cell treatment using the da vinci robotic surgical system," `http://bit.ly/29Kzog2`, 2015, poster presented at International Society for Stem Cell Research Conference 2015, Stockholm, Sweeden.

Chapter 5 (SWAP) was partially published as:

S. McKinley, A. Garg, S. Sen, D. V. Gealy, J. P. McKinley, Y. Jen, M. Guo, D. Boyd, and K. Goldberg, "An interchangeable surgical instrument system with application to supervised automation of multilateral tumor resection," *International Conference on Automation Science and Engineering (CASE)*, 2016.

This chapter was also submitted as a provisional patent and presented in a video (which won Best Video at Hamlyn Surgical Challenge 2015) as:

S. McKinley, A. Garg, J. McKinley, Y. Jen, D. Gealy, D. J. Boyd, P. Abbeel, and K. Goldberg, "Robot-assisted surgery: Autonomous tumor localization and extraction," `http://bit.ly/29LhVXr`, 2016, best Video Winner at Hamlyn Surgical Challenge 2015.

Chapter 6 (SNAP) was partially published as a conference paper (Note: only contributions made by the author are presented here):

S. Sen, A. Garg, D. V. Gealy, S. McKinley, Y. Jen, and K. Goldberg, "Automating multiple-throw multilateral surgical suturing with a mechanical needle guide and sequential convex optimization," *IEEE International Conference on Robotics and Automation (ICRA)*, 2016.

Chapter 7 (Design) and 8 (Frugal) are original contributions by the author. Their purpose is to communicate the greater design philosophies of Frugal Design and the Bauhaus Design School with respect to human augmentation (represented here by Autonomous Surgery). In these chapters, the author describes a set of experiences through which others may learn to be better designers: socially conscious creators in the style of the Bauhaus.

All chapters featuring previously published material have been rewritten to present their contributions as a structured, coherent body within the context of the author's research. All co-authored material is used with permission.

Stephen Alan McKinley
August 2016

444 Soda Hall
University of California
Berkeley, CA 94705

Acknowledgments

Professor Goldberg; thank you for the opportunities you have presented me over the past two years. Working under your guidance in the AUTOLAB I have learned to write, research, and teach in an academic setting. It has been an honor working with you; thank you for encouraging my passion.

I would like to extend thanks to my qualification exam and dissertation committees. Professors **Hayden Taylor**, **Eric Paulos**, and **Liwei Lin**, thank you for guiding me through the qualification exam. Professor **Dennis Lieu**, thank you for co-advising me and helping me develop my research at Berkeley. Professor **Paul Wright**, thank you for encouraging me to pursue inspiration from the Bauhaus.

This dissertation represents far more than the photos and words shown below. This dissertation comes at the end of five years of graduate school starting in Berkeley, then moving to San Diego, and back to Berkeley. I have been afforded the unique opportunity to work in three different groups here at Berkeley, and have gained experience at two start-ups during this time. These pages don't show the failures, the hardships, and the dead-ends upon which I embarked, and from which I learned far more than was necessary to complete my degree.

Thankfully I was not alone for this journey. Foremost I thank my **Mother** and **Father** for their unwavering support. Thank you also for encouraging me to build and create, and for showing me that the outcome of a project is measured primarily by the experience gained in its pursuit.

I would not be here if it were not for my brothers. Michael, Jonathan: it is rare and truly special that we share such a strong and productive bond. Thank you both for being such willing participants in the adventures that have enriched my experience. **Michael**, thank you for your strength and humility; I have learned how to succeed from your example. **Jonathan**, thank you for your patience and creativity; I cannot understate your importance in building my artistic practice. Though we do not know where these experiences will lead us, I have learned how to *live* my art through your example.

Thank you **David Gealy** for your humor and energy: hard work has always been fun while working at your side. **Jeff Mahler**, **Michael Laskey**, **Zoe McCarthy**, and **Menglong Guo**; thank you for your inspiration and companionship during the past two years working together in 444 Soda. **Animesh Garg** and **Sanjay Krishnan**; thank you for your invaluable feedback and guidance throughout our time together.

Jon Anderson; thank you for teaching me how to be a manager. Thank you for allowing me to work alongside the machinists at Oakland Machine Works. That experience taught me to 'Respect the Process' above all else. I will never forget your optimism, vitality, and diplomacy.

> We have no interest in making museum pieces, we are creating experiences.
>
> *Johannes Itten*

Part 1
Introduction

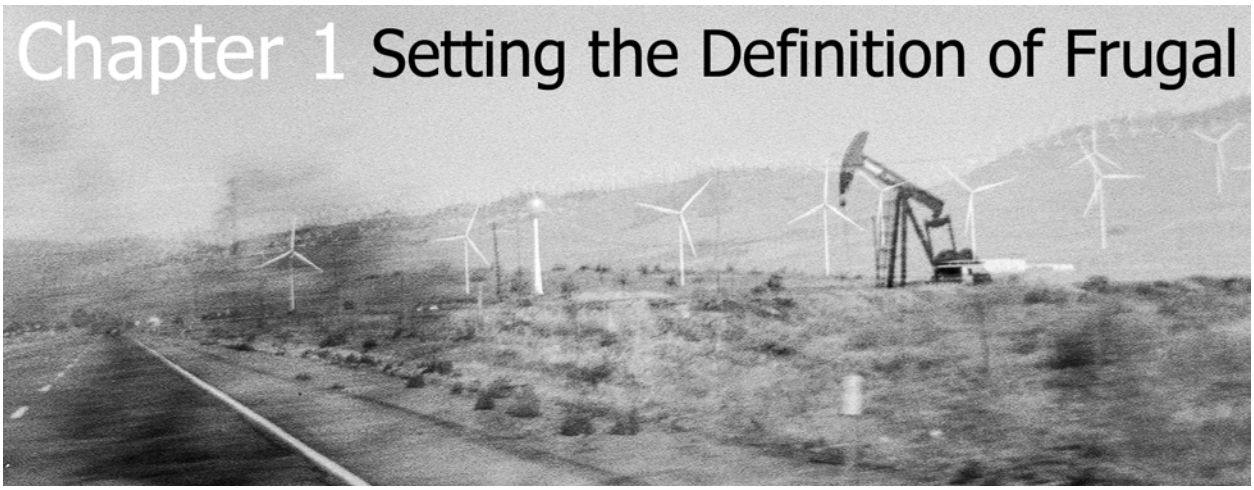

Introduction

Design is a systematic relationship between creativity and intent that repeatably creates extensions to the human experience.

For a designer, although the delineation between art and engineering is blurred, a noticeable constraint of economy is consistently prevalent in engineering. Functionalist (as in: form-follows-function) design is taken to the extreme when designing for affordability [32] and aesthetic legibility [83, p. 41]. Functionalist technological development as applied in resource-scarce environments has been termed 'Frugal Innovation' [16]. A key component of Frugal Innovation (as reviewed in Chapter 8) is the creative use of locally sourced materials and talent to solve problems that are unique to an area of need [126]. Also important for a frugal innovation is an intent for socially progressive technological advancement, especially among marginalized populations.

The first part of this dissertation (an Introduction) extends the concept of 'Frugal Innovation' beyond emerging economies to a broad variety of applications in all economies. The central principle of 'Frugal Design' is making use of available resources: modifying materials and equipment that are available rather than constructing entirely from scratch. This offers benefits in cost reduction, waste minimization, and accessibility. **Five Considerations for a Frugal Designer** are presented here (in Section 1.4 of this Chapter) as guidance for creators of all skill levels.

The second (and predominant) part of this dissertation presents four case studies in Frugal Design applied to robotic surgery. The third part of this dissertation examines the supporting design theories behind the Bauhaus, functionalism, and Frugal Innovation.

Consider the following three examples, which introduce the concept of Frugal Design. The first example is a test bed for **self-learning machine intelligence** algorithms. The second example is an **irrigation tool** in development for farmers. The final example is a system for interchangeable tools in **robot-assisted surgery**.

1.1 Example: Frugal Robotic Self-Learning Platform

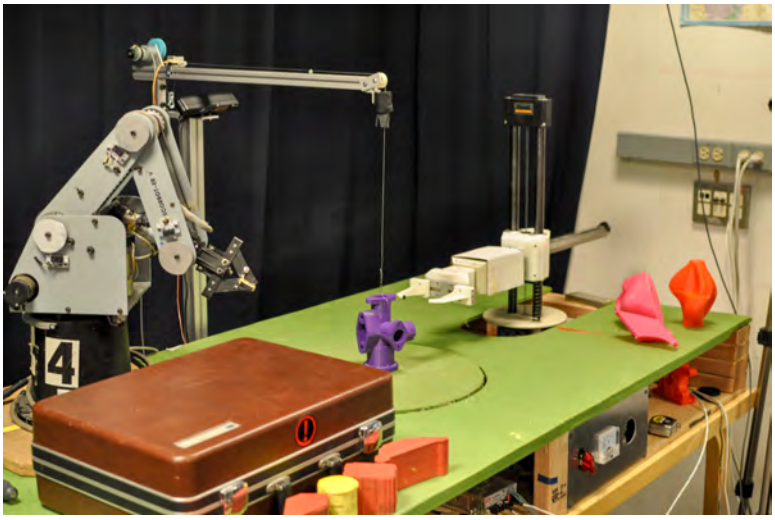

Figure 1.1: "Izzy and Zeke Table" *(S. McKinley, D. Gealy, M. Guo. 2016)* is low-cost implementation of robotic self-learning. Two robots (Izzy and Zeke) can be set up for simultaneous training and data collection experiments. A center turntable orients an object in the center of the table below a crane that lifts and resets objects once grasped. It has been used for research (M. Laskey's 2016 *Learning from Demonstrations* [79] and *Grasping in Clutter* [78]) (Mahler 2016 *Synthesis of Grasps* [89]).

Problem Statement: Enable hardware-based self-learning for robot manipulation.

Researchers in the Automation Laboratory (AUTOLAB) are working to create tools for automation in surgery, industry, and the home. However, without robots dedicated to grasping in the lab, the algorithms being developed were experimentally evaluated in simulation.

The Dexterity Network **(Dex-Net)**, developed by Jeffrey Mahler et al. pre-computes (and ranks) grasp configurations for robot-object interaction using analytic modeling [88]. **Dex-Net** requires a robot-computer interface that can repeatably evaluate grasp success on various objects and reset the physical configuration before each trial.

SHIV (short for: (Svm-based reduction in Human InterVention), developed by Michael Laskey et al. investigates the reduction in data for learning-from-demonstration [79]. **SHIV** requires that a human be able to tele-operate the robot in a two-dimensional simplified state space configuration.

A barrier to physical implementation of these algorithms is the high cost of a robotic system and physical distance from existing experimental hardware (such as robots shared by labs housed in different buildings). Geographic distance between the researchers and experimental hardware limits productivity. To surmount this limitation, the author began looking for existing resolutions to this need in the environment. Disused bio-lab robots from the 1990's were resurrected from a nearby lab by building new motor-drivers and power hardware. A table was constructed using plywood and furniture scraps from an alley near campus. Green fabric was placed on the table for visual neutrality, and a turntable was built from a third robot to allow for an additional degree of freedom that is shared by both robots.

Frugality: The experimental system (shown in Figure 1.1) is constructed from reclaimed sheets of plywood, construction materials, fabric, and legacy robots (nicknamed Izzy & Zeke) reclaimed from the refuse pile.

1.2 Example: Facilitating Frugal Irrigation

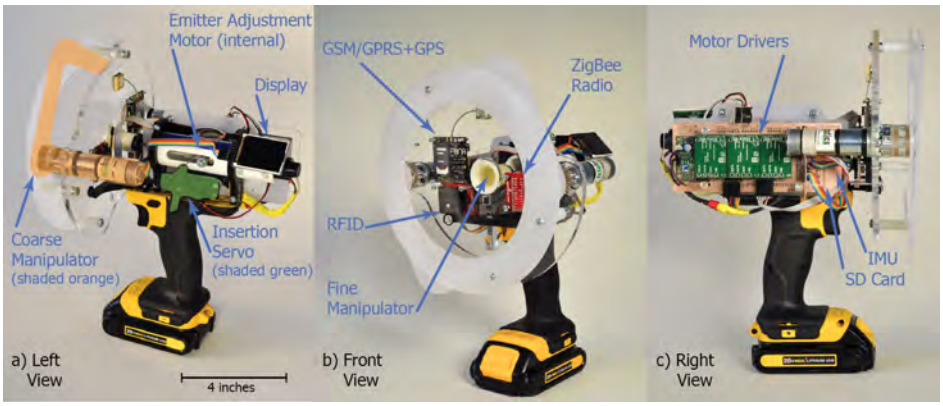

Figure 1.2: "The Device for Auto-Tuning of Emitters (DATE)" *D. Gealy, S. McKinley, M Guo. 2016* The DATE is a frugal design solution to irrigation efficiency during drought. [45]

Problem Statement: Lower the distributed cost of intelligent irrigation in vineyards.

Agricultural irrigation consumes 85% of the world's freshwater [47]. As global human populations continue to grow, increasing demand for irrigation water strains water supplies limited by drought and variability due to climate change [169]. The Device for Auto-Tuning of Emitters (DATE) was designed to interface with inexpensive and pervasive passive drip irrigation emitters (shown in Figure 1.3 inset). Passive emitters placed near plants are gripped with the coarse manipulators and adjusted by the fine manipulators as dictated by a control algorithm running in the cloud [45].

Figure 1.3: The DATE is designed to interface with inexpensive passive irrigation emitters distributed in a field to alleviate the financial burden placed on farmers in California's drought.

Frugality: Cost is kept low by placing actuation and sensing on a single device that can be moved through the agricultural field. Prototyping costs were minimized by utilizing existing components such as the body of a commercially available drill, which contained a battery, and power system.

As a result of sustained drought in California, the Central Valley agricultural region's water availability in 2015 was at 48% of average levels resulting in a total economic impact of $2.7 billion and a loss of 21,000 jobs [57]. The DATE project is one way to improve crop yield and food stability and currently has a patent pending.

1.3 Example: Frugal Design and Robotic Surgery

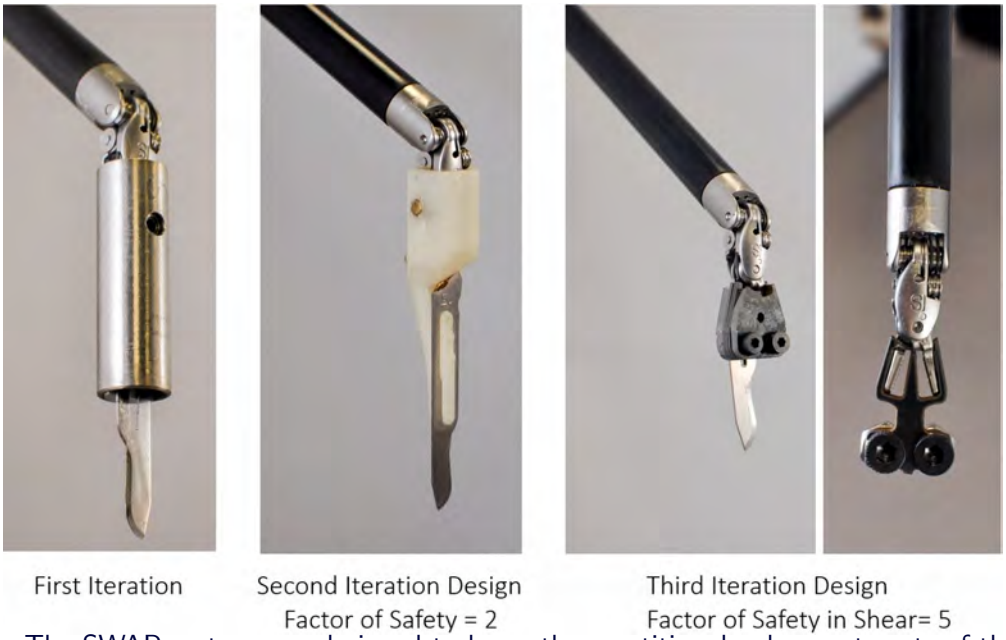

Figure 1.4: The SWAP system was designed to lower the repetitive development costs of the research equipment in AUTOLAB. **Left:** The first iteration of SWAP was bolted to the end-effector and held a stock no.15 scalpel blade. **Center:** The second iteration (as investigated in Chapter 5) was designed with a 3D printed plastic body and used brass screws to fixture the device to existing geometry. **Right:** Two views of the most recent iteration as constructed from water-jetted sheetmetal.

Problem Statement: Redesigning surgical tools for automation using existing geometric features.

Laparoscopic surgical end-effectors allow for smaller incision wounds [116] and decreased surgical time [99], but currently available modular tools do not have a wristed degree of freedom thus decreasing surgeon efficacy. Interchangeable low-cost instrument mounts (as illustrated in Figure 1.4), were developed to enable automated tumor resection.

Frugality: These interchangeable tools make use of geometric indentations at the base of each jaw (seen in Figure 1.4 at far right) to interface with existing tools. Reusing the same tool while swapping individual end-effectors lowers overall cost of equipment during surgery. These devices were initially prototyped from a section of steel tubing and standard scalpel blades. Shown in figure Figure 1.4 are the design iterations to reduce cost and increase resistance to external disturbances. See Chapter 6 for more design details of the interchangeable surgical tool system.

This invention is used as the basis for an ongoing investigation into multi-step surgical procedure automation that forms the core engineering contribution of this dissertation [96, 94, 98, 44, 136]. Part 2 of this dissertation contains studies of the robotic surgical system and three other Frugally Designed surgical automation inventions.

1.4 Five Considerations of a Frugal Designer

First Consideration: Empathize with Need

The designs presented in this dissertation are all borne from perceived needs. In literature, Ulrich presents established methods for problem identification and classification [163, p. 16]. In practice, designers find themselves solving problems characterized as needs or wants within their own lives. Many humans intuitively: we (as a species) are uniquely best at creating tools and solving problems.

Interviews, field excursions, and surveys are good ways to find problems, but rarely are we so lucky as to have others deliver challenges for us to solve. A designer must be able to dive into a problem and *live* within it to perceive a present need. A creator must be able to selectively engage the passion which drives invention.

In this way, the designer is much like an actor placing their self within a character. A competent designer can switch between several problems just as an actor can transition between characters. A designer can argue for a design passionately, yet feel confident enough to drop it and move toward group consensus when needed. An empathetic designer seeks to find, understand, and feel, the societal and emotional causes of the presented problem.

In the examples presented above, the need for the DATE irrigation project only became evident after travelling to vineyards in Lodi, California to interview growers: to see the dust on the ground, and perceive the fear in their eyes. The Izzy & Zeke table was developed only after working in close contact with the algorithmists in AUTOLAB, and feeling their passion for machine intelligence. The surgical projects were personally motivated by the memories of the author's relatives lost to cancer. **In all three of these cases, inventions were found by making the realization of the problem a personal necessity to the designer.**

Define Success on Need Fulfillment: After discovering a need, a list of criteria can be tabulated that define the success of a design. This list can include many different physical properties and constraints, the inputs to the desired system, and the desired output of the system.

Consider example 2 above (the DATE device). The initial need is to lessen the effect of the drought on farmers. From communication with the farmers, it was determined that an open problem was overwatering: water outputs for all types of drip irrigation are actuated for blocks of hundreds of emitters at once. Ideally, each plant should be individually monitored and maintained to maximize yield and quality while minimizing water consumption.

This need was narrowed to a subset of farmers on vineyards through the observation that vines are irrigated through irrigation networks laying above the surface of the soil.

The DATE device, which represents a modular subsystem within the greater problem formulation, has the following Functional Requirements:

- Hand-held (limits weight, and defines physical characteristics)
- Intuitive for farmers (defines user-interface constraints)

- Prototype Cost (less than $1000)
- Final Unit Cost (less than $300)
- Positively identify an individual plant within a field of thousands
- Receive instruction from a cloud-based control algorithm
- Adjust water output to an individual plant
- Allow for all-day use

Design is fundamentally difficult because each design requirement can be met with a large number of possibilities. This realm of possible working solutions is known as the 'design space' and grows larger as the list-of-design-requirements increases in length, which in turn, requires a greater complexity of interacting design parameters. The design space can be imagined as a non-convex high-dimensional surface with a success axis dependant upon many parametric axes. Individual conceptual designs (as informed by TRIZ or Axiomatic methods) are discontinuous from each other within this space. An example of conceptual designs to satisfy the functional requirement of robot locomotion could be treads, wheels, and legs; each of these surfaces in the design space cannot be reached from parametric optimization within the conceptual surface.

Second Consideration: Focus on What is Available

Frugal Design shrinks the design space by focusing on locally available resources. The University of California, Berkeley is a rich ecosystem of technology. Legacy equipment can often be found decomposing in alleys, old hallways, or on loading docks, provided you keep your eyes open. These forgotten projects can provide valuable insight and components for future endeavors. Every past design can be analyzed to find what made it succeed or fail, as formalized by a method such as TRIZ, who's creators note that new designs consistently recycle existing resolutions to functional requirements in novel combinations [3].

The Izzy/Zeke table (example 1 above) was conceived almost entirely from reclaimed materials and has already born the fruit of several research papers and a new hardware-based research direction for the AUTOLAB.

The research presented in this dissertation has been accomplished in the AUTOLAB, while working with some brilliant computer scientists in the world. It is important to note that in this setting software approaches are generally far less expensive than similar hardware approaches because of the rapid iteration cycle and negligible material costs for algorithms.

However, **hardware enables automation**. Most of the problems approached by the designs presented within this dissertation arise where the limits of algorithms are found. For example, the SNAP (Surgical Needle Alignment Positioner) studied in Chapter 6 was created because the existing surgical system (relying on vision processing algorithms) could

not estimate the orientation of a surgical needle with precision adequate for automated suturing.

In another example, the DATE irrigation system represents a co-development of both hardware (autonomous agents) and software (machine learning and optimization) systems. A resolution to need is found by utilizing available expertise in both hardware and software design.

Chapter 8 reviews existing literature in 'Frugal Innovation,' a practice established for the development of technologies in emerging economies. In those settings, the available resources and talent is very different from those found at UC, Berkeley. However, a **Frugal Designer** will be able to identify approaches that match the specific location and needs.

Third Consideration: Quickly Generate Conceptual Prototypes

After determining an open need, the designer must then invent an approach that fulfils the Functional Requirements of the need. The process of inventing new ideas, called *conceptualization*, has necessarily been an area of interests for artists, designers, and all other forms of creators.

Some creators find designs as impulses or inspirations that strike them in 'eureka' moments. This approach may be sufficient in design problems with fewer constraints (more artistic problems), but cannot be called optimal and is certainly neither repeatable nor transferable to other designers (due to the relationship between the designer and their source of inspiration).

A systematic method for invention can be communicated and repeated on-command by others (see [163] for another example of this process). Systematic invention exists in two steps: **abstraction** and **realization** (see [77, p. 66] for a visualization of this process).

During **abstraction**, a problem definition is decomposed into visualized possibilities as allowed by the designer's imagination. In engineering literature, there are many established practices to guide this process such as TRIZ [3], Axiomatic Design [148], and Parameter Analysis [77]. There have been some comparisons made as to their efficacy ([176]), but it is the author's belief that a conceptualization strategy's true success is dependent upon the disposition of the designer (Axiomatic design being more rigid, TRIZ being more ad-hoc). For the most part, structured design methods are ignored by designers because of the difficulty in posing a problem within a deliberate framework [163, p. 20]. All of these methods are similar in that they prompt the designer to view a design requirement from as many different possible permutations of design space as possible. These abstractions can be listed out in terms of complexity, cost, and/or feasibility to inform conceptual exploration.

Realization of these abstractions should first be accomplished with expenditure of minimal resources through sketches.

Using an iterative method, the designer attempts to search within the parametric space of a design concept to reach a pre-determined success metric. Simultaneously, designs from competing conceptual spaces must be considered. The balance between exploration of novel

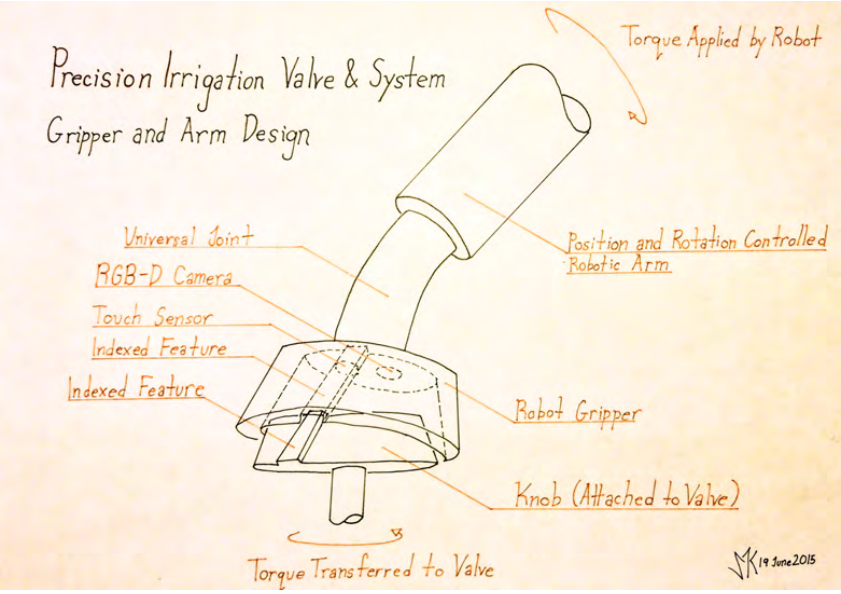

Figure 1.5: Gripper and Arm Concept: a visualization to illustrate the following functional design criteria: A flexible shaft coupling a tool to the plant-located emitter, the presence of a vision system to identify valves, the presence of a knob on the emitter, the presence of some sort of indexing feature on the knob, the transferal of torque between the tool and the emitter so as to change the output water flow delivered to the plant, and additional sensors.

conceptual designs and exploitation of known parametric design spaces defines the speed and novelty of innovation.

Examples of concept illustrations for the DATE device (example 2 above) are shown in Figure 1.5 and the Appendix (on page 91). These concept sketches were used as illustrations for patent disclosures and grant applications before physical prototype development occurred (this patent disclosure is currently being pursued in full). Artwork conceptualizations serve as examples of how abstract visualization can be used to effectively inform device design. Each functional requirement of the precision irrigation system (and two sub-systems) were imagined visually in this way before being written in patent claims or prototyped physically.

Visual exploration (sketches and renderings) of abstracted functional requirements is a frugal first step in the prototyping process of individual concepts. Exploring parameters within conceptual designs is accomplished through minimal prototypes.

Fourth Consideration: Design for Modularity

Physical realization of functional prototypes can be made frugal through the use of modularity.

Kroll notes that "as the number of functions [or design requirements] increases, both the magnitude of the required design effort and the product cost also increase" [77, p. 26]. By designing many compartmentalized modular subsystems, the overall magnitude of the initial conceptual design is capped. Additionally, experimental exploration of the design space is much easier if modular subsystems can be interchangeable. As the design moves away from a conceptual (research) stage, modular subsystems can be merged or discarded as necessary.

The DATE device (example 2 above) represents a modular sub-component of a larger sensing/actuation system that controls water usage across a farm. The DATE itself could be replaced with an entirely different concept if its success proved inadequate. Within the

design for the DATE, is another collection of sub-systems that can also be interchangeable as the (DATE) system design space is explored.

Fifth Consideration: Frugal Design Represents Accessibility

In the final two chapters of this dissertation, design is investigated from the perspective of social progressivism. The Bauhaus discussed in Chapter 7, sought to create artifacts for human use that resonated with their users through functional minimalism.

A modern approach to socially progressive technological development can be observed in the current Frugal Innovation movement discussed in Chapter 8. Inexpensive designs should not be created simply to be consumed by individuals with lower income, but are intended to help better their condition.

In an era of unprecedented materialism, designers should be motivated to create devices that solve problems within our environment and better the human condition. At the University of California, Berkeley; designers are privileged with resources and opportunities that allow for the consideration of global accessibility separate from commercial considerations present in the existing economy. Please note: the author claims this consideration in the Frugal Design process not as a mark of accomplishment, but as a motivating creed for the designer.

Increasing data availability and automation can help humans work together more effectively and efficiently. It is up to the designer to ensure that in the future of intelligence, automation will augment all humans, not just the select few that can afford it. Automating robotic surgery can commoditize the skills possessed by expert surgeons, making healthcare more accessible. Part II of this dissertation focuses on cases of Frugal Design as applied to robot assisted minimally invasive surgery.


Part 2
Case Studies
in Frugal Design

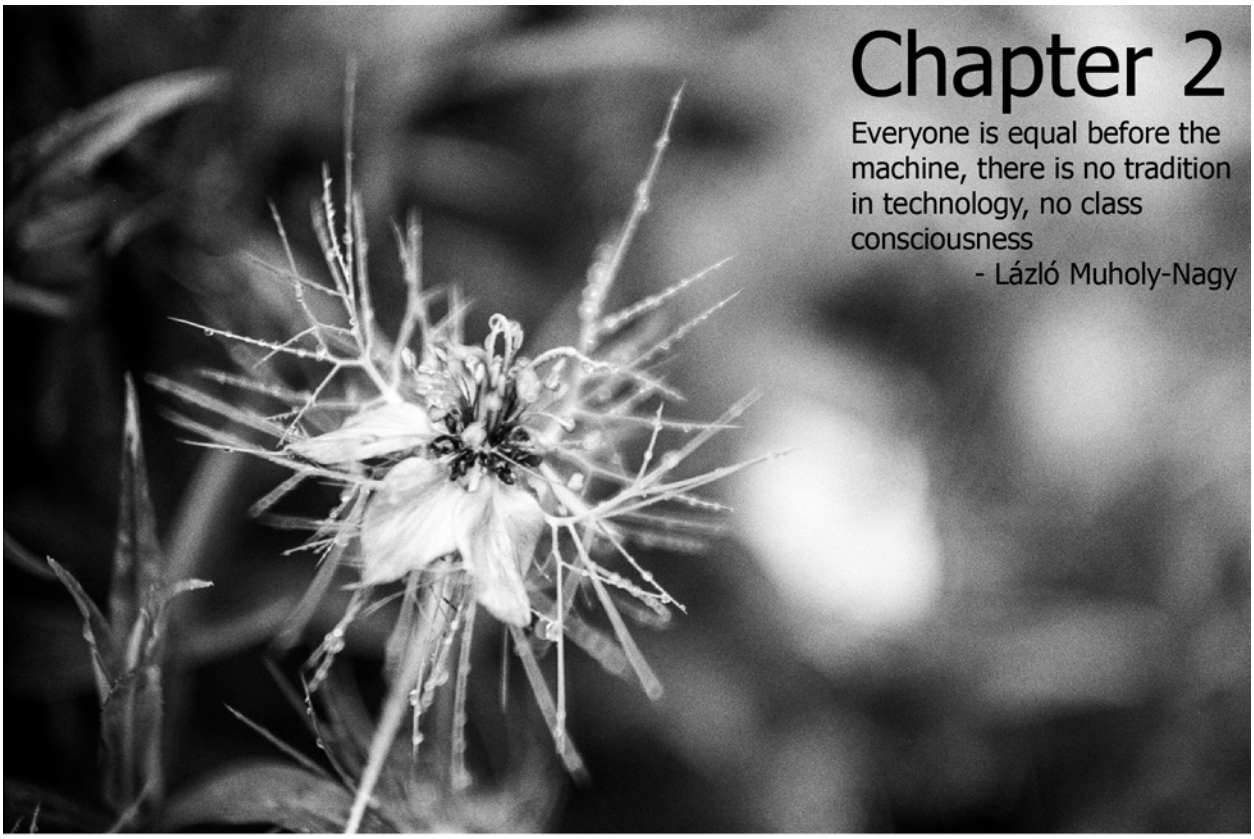

A Background in Robotic Surgery

2.1 Definitions and Related Work

The goal of a surgical procedure is to treat a disorder of the human body through physical manipulation such as cutting, sewing, implantation, or removal of tissue and foreign bodies. A successful surgery minimizes any collateral tissue trauma while accessing the location of the disorder. Historically, surgery has been a manual exercise which requires an open pathway for the surgeon's hands and view. Minimally Invasive Surgery (MIS) seeks to lessen the collateral impact of surgical trauma by utilizing smaller instruments and remote viewing devices. Minimally invasive operations are classified by the cavity within which the operation takes place; these include laparoscopy (within the abdominal cavity), thoracoscopy (chest cavity), arthroscopy (joints), pelviscopy (pelvis), and angioscopy (blood vessels). A device designed to view the interior of the body is generally known as an **endoscope**; a device designed specifically for viewing the abdominal cavity is known as a **laparoscope**, whereas a device designed to view the inside of a joint would be known as a arthroscope. In practice, many of these tools can be used for surgeries in multiple body cavities (cross-over between laparoscopic and pelviscopic tools are common).

Figure 2.1: **Left:** A traditional laparoscopic tool consists of a stiff shaft (1) connected to a gripper (2) that pivots around a hinge (3); this closing motion is translated to an end-effector (4) that can be scissors, grippers, retractors, etc. **Right:** Laparoscopic tools inserted through cannulae in the abdomen.

Laparoscopy specifically describes a class of surgical procedures that use fiber-optic instruments or miniaturized cameras (known as laparoscopes) to facilitate a surgeon's view through the abdominal wall without the need for large incisions. A laparoscope was first used for patient diagnosis in 1910, but would remain unpopular until 1966, when a device was invented for automatic inflation of the abdominal cavity to create a workspace within the body [8].

The first manual corrective laparoscopic surgery was performed in 1987 using miniaturized instruments inserted along with a laparoscope [64]. This initial surgery, a cholecystectomy (removal of the gall bladder), represented a disruptive shift in the history of surgery. by 1993, 67% of cholecystectomies were performed laparoscopically [50]. To fix internal injuries, it was no longer necessary to make an incision large enough for a surgeon's hands to fit within the body of the patient.

The manual laparoscopic process involves making small incisions (0.5-2cm) through the abdominal wall. A device called the trocar is then inserted into each incision. The trocar consists of a metal tube (called the cannula) attached to a seal so that the abdomen can be positively pressurized with carbon dioxide gas (as illustrated in 2.2). The abdomen is inflated to create a working space within the body and laparoscopic tools (shown in 2.1), consisting of end-effectors connected to shafts, are inserted through the cannula. Because the shaft pivots around the trocar port, manual control of the tools is difficult and uncomfortable leading to back and neck pain among 12% of laparoscopic surgeons [14]. Laparoscopic tools lack articulation at the wrist and are prohibitively difficult for novice surgeons to master [64].

Roboticists current with surgical research quickly noted the potential for improvement, noting that "in many ways endoscopic surgery is similar to teleoperation of a remote manipulator" [159]. These researchers were imagining that the linkage between surgeon and patient could be replaced with a robotic device that would allow for more precise control and lower the barrier to entry for novice laparoscopic surgeons.

Robotic Minimally Invasive Surgery (RMIS) uses mechatronic devices to augment human surgical performance during laparoscopy. Early RMIS prototypes were developed in 1995 by Johns Hopkins university and International Business Machines (IBM) [156]. By the year 2000, Intuitive Surgical Systems had been granted FDA clearance for a master/slave

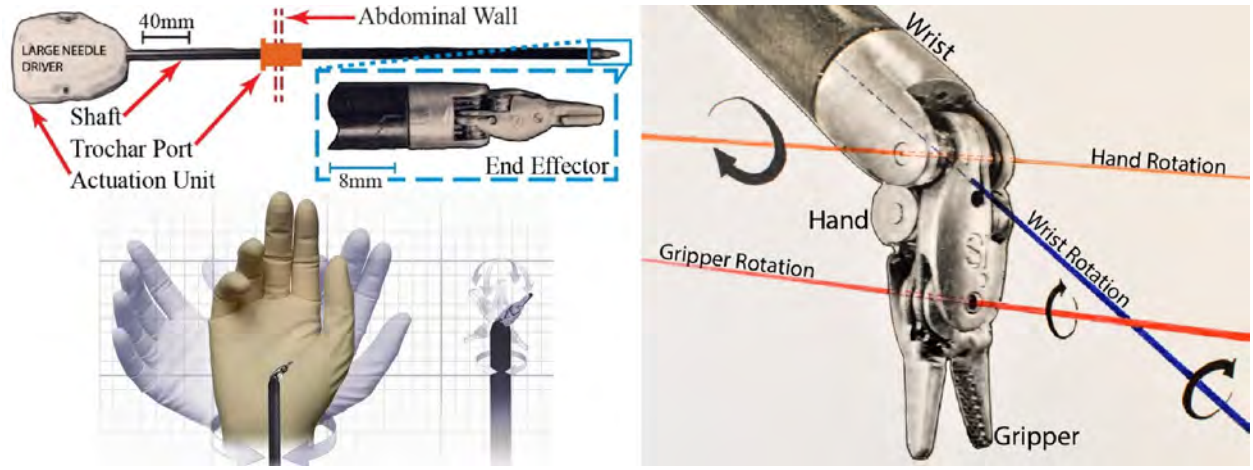

Figure 2.2: **Top Left:** A schematic view of a da Vinci Classic instrument inserted through a trocar port into the abdominal cavity. **Lower Left**: The endoscopic surgical retractors of the daVinci Robotic Surgical Assistant can fit in locations unaccessible to surgeons. **Right:** The wristed surgical retractor has three degrees of freedom mimicing the human hand.

Robotic Surgical Assistant (RSA) which translated a surgeon's movements through an exoskeletal master to a robotic slave system that mimics the motion of the master within the patient's body. Hardware for this device was based on research by IBM and Stanford Research Institute (SRI International) in the 1990's [154, 52].

The master exoskeleton for the daVinci system (shown in 2.3a) consists of two arms and a stereoscopic headset. Each arm follows 6 Degrees of Freedom (DOF) position/rotation (x, y, z, yaw, pitch, roll) as well as an additional gripping DOF represented by forefinger-thumb pinching. The slave arms (also shown in 2.3b) translate the motion of the surgeon-controlled exoskeleton to a scaled movement within the body cavity of the patient. RSA's allow several advantages over traditional laparoscopy, including continuous motion scaling, stereoscopic 3D visualization, and surgeon hand tremor filtration [115].

Critical patents [84, 86, 85, 24] filed in 1996-1998, have allowed Intuitive Surgical to monopolize the field of RMIS for the past two decades. Intuitive Surgical reported that by 2014 there were 500,000 surgeries per year using 3000 daVinci RSAs working in the United States. For comparison, there are an estimated 400,000 operating rooms in the world [40]. Each daVinci system currently costs approximately USD 2 Million; as Intuitive Surgical's patents protecting RMIS expire, a new era of democratized RMIS approaches.

(a) Master exoskeleton with two 7 DOF manipulators.

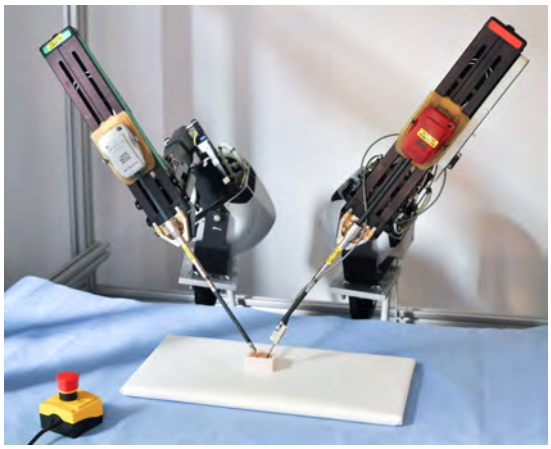

(b) Surgical arms controlled by telepresence.

Figure 2.3: The da Vinci Robotic Surgical Assistant (RSA) consists of a master exoskeleton and two slave arms. The daVinci Robotic Surgical Assistant is controlled by a surgeon's hand movements.

2.2 Prior Work on RMIS at UC Berkeley

A Hardware Approach: Fearing, Sastry, and Cavusoglu (1985-2001)

Starting in 1985, Berkeley faculty members Ron Fearing, Shankar Sastry, and Murat Cenk Cavusoglu worked in parallel with SRI and IBM to develop hardware systems for RMIS with tactile feedback to the surgeon. Research by Fearing et al classified basic solid mechanics for compliant robot grasping with fingers [36]. This research led to the development of individual tactile fingertips [35] and micro-machined tactile arrays [51] which were used in a surgical context to search for inclusions of varying stiffness within a flesh phantom made from silicone and latex by placing a tactile sensor on a participant's fingertip [175]. This group went on to develop several micro-sensor arrays for tactile sensing with the interest of communicating tactile feedback to a surgeon. Also at Berkeley, Brouwer et al conducted experiments with porcine tissue and instrumented laparoscopic instruments to benchmark stiffness and force characteristics in real flesh with the intent to create better training environments for surgeons [18].

Sastry et al published on the basic challenges of telesurgery in 1996 [133] and considered game theory based hybrid control of surgical retractors [23] while Tendrick and Cavusoglu also worked on developing prototype end-effectors and master manipulators in 1997 [158] [21]. Cavusoglu et al working with Sastry developed a prototype 6-DOF laparoscopic workstation in 1998 known as the 'Berkeley Surgical Robots' (see Figure 2.5) [22].

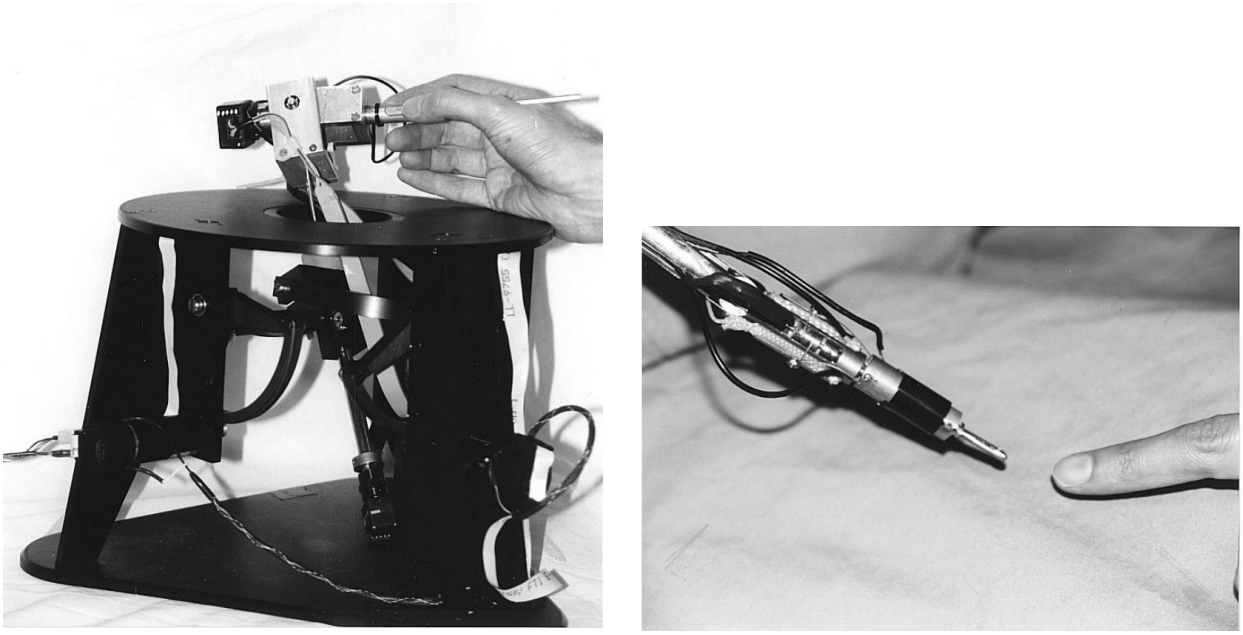

(a) An initial prototype of the Berkeley Surgical Robot surgeon manipulator shows part of a large hardware effort by Sastry et al to create a RMIS system [22].

(b) The Berkeley Surgical Robot patient-side manipulator shown with a human finger for scale [22].

Figure 2.4: The Berkeley Surgical Robot Prototypes (1999)

An Algorithmic Approach: Goldberg and Abbeel (2009-2015)

A decade after these hardware developments, research groups led by Ken Goldberg and Pieter Abbeel started developing machine learning algorithms to control surgical robots. In 2009, Jur van den Berg et al revitalized the Berkeley Surgical Robots [22] to perform knot tying based on demonstrations observed from expert surgeons (see Figure 2.5) [164]. Jansen et al explored simulated tissue retraction in 2009 with the Goldberg group in a simulated environment inspired by the daVinci RSA made by Intuitive Surgical Systems [66]. Berensen et al explored learning from experience with application in needle hand over during a simulated suturing environment inspired by the daVinci RSA [13].

The Abbeel group explored the limits of learning in a surgical setting with a 2013 case study in simplified suturing by Schulman et al [135]. In this study, a PR2 by Willow Garage was used with large (10cm) knitting needles to suggest that learning and accomplishing suturing is possible if the perception problems posed by surgical environments were solved (see Figure 2.6)

Following success with automating the Berkeley Surgical Robot, the Raven II surgical research platform was acquired. Autonomous multilateral debridement with the Raven (see Figure 2.7a) was accomplished by Kehoe et al (with Goldberg and Abbeel)[73]. Success with

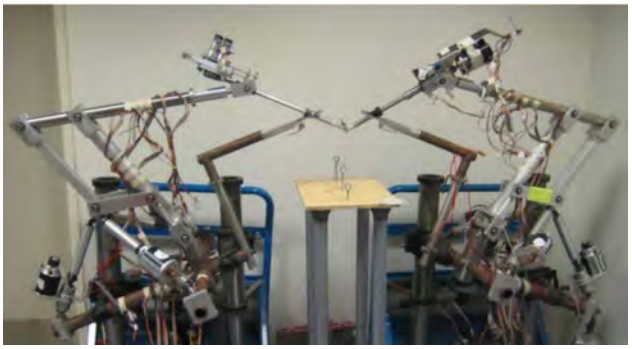

Figure 2.5: The Berkeley Surgical Robot performing knot tying [164]. Note the phantom used to practice suturing constructed from wood and steel eyebolts.

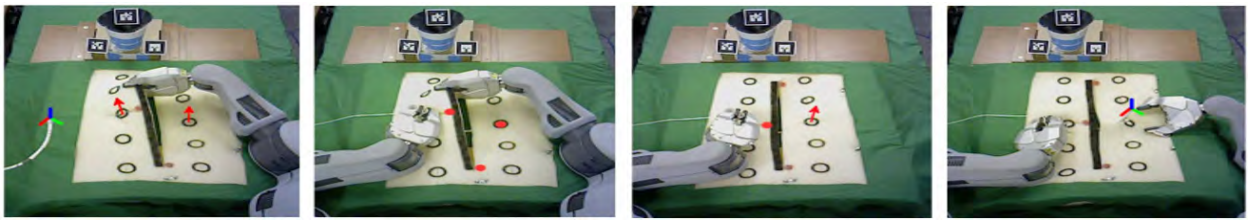

Figure 2.6: A humanoid PR2 robot performing over-sized suturing with knitting needles [135]. If perception of small needles in a surgical environment can be solved, a policy for suturing can be learned by a surgical robot.

the Raven was limited by inaccurate position control through planetary gearboxes and loose cable drives. Attempts were made by Mahler et al to learn control of the cable driven robots using machine learning techniques [87].

In 2014, researchers at Intuitive Surgical Systems released 26 first generation daVinci RSA systems for academic research as the daVinci Research Kit (dVRK). These systems contained only the hardware developed by Intuitive Surgical. Researchers at Johns Hopkins University led by Peter Kazanzides developed firmware and software to be distributed to the research teams with dVRK hardware [72]. At Berkeley, Murali et al was successful in automating multilateral tasks such as gauze cutting and simple debridement using Learning by Observation (a machine learning technique) [102].

Traditional laparoscopic surgery using hand-held tools can be uncomfortable and even dangerous for a surgeon. Robotic minimally invasive surgical systems reduce the ergonomic and training difficulties for surgeons, but there is still a high cognitive load for surgeons during lengthy surgeries. Supervised automation of selected subtasks in Robot Assisted Minimally Invasive Surgery (RMIS) has potential to reduce surgeon fatigue, operating time, and facilitate remote tele-surgery.

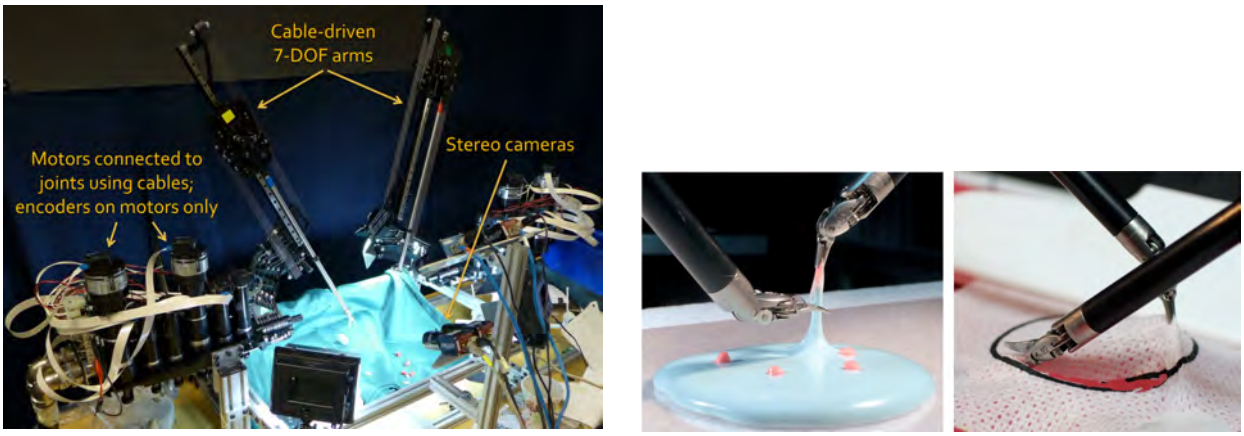

(a) The Raven II surgical robot performing multilateral (two handed) debridement [73]. Note that the surgical phantoms in this setting are 1cm cubes of foam.

(b) The daVinci RSA performing autonomous debridement and circle cutting [102].

Figure 2.7: Surgical Automation Research Platforms (2014)

2.3 Introduction to Case Studies in Robotic Surgery

This work presents hardware solutions to algorithmic limitations in automating surgical procedures with the daVinci Research Kit (dVRK).

A complete surgery can be thought of as a compilation of many individual tasks and subtasks. For example, an inguinal hernia repair can be considered to have nine separate **tasks**: 1) Incision of inguinal (groin) area, 2) Identify external oblique aponeurosis (a type of tendon) and external ring, 3) Open up inguinal canal, 4) Identify spermatic cord, 5) Identify indirect or direct sac of inguinal hernia, 6) Removal of indirect inguinal hernia sac, 7) Placement of mesh, 8) Closure of external oblique aponeurosis, and 9) Closure of wound [67].

Each of these tasks can be further decomposed into **subtasks**; for instance task 5 can be decomposed into: 5.1) transverse incision of aponeurosis, 5.2) lateral and medial incision of aponeurosis, 5.3) retraction of flaps to form a pocket, and 5.4) insertion of tools into pocket [67]. Further decomposition results in generalized primitives called **surgemes** such as 'orientation', 'insertion', and 'grasping' [129]. Comparing surgery to writing, the basic set of surgical motions can be thought of as the "Language of Surgery" with surgemes acting as words within a sentence.

Although there is a large variance in surgical subtasks between operations [146], a set of skills required for competency in most RMIS settings [131, 33] has been described as the Fundamental Skills of Robotic Surgery (FSRS) [139]. The FSRS skills can be classified in four groups: (a) basic console operation, (b) psychomotor skills, (c) basic surgery skills and (d) intermediate surgery skills [146].

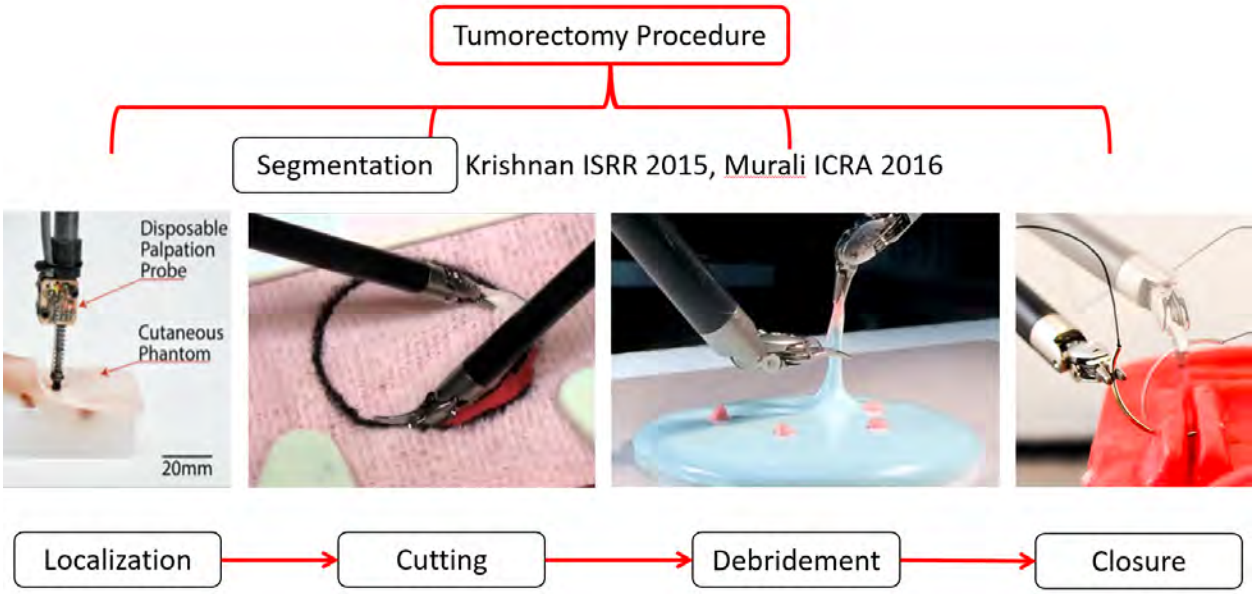

Figure 2.8: Tumorectomy (surgical removal of a tumor) can be decomposed into four subtasks: Palpation, Incision, Debridement, and Closure.

Basic console operation includes instrument, and camera control; psychomotor training includes peg placement and spatial end-effector control using the master-slave system. Other examples of basic surgical skills are needle handling and tissue cutting; intermediate surgical skills are comprised of sub-tasks such as vessel dissection and tissue retraction.

Each surgical subtask (such as cutting, grasping, debridement, and cauterizing) requires a different set of skills and specialized instruments [1]. Many of the instruments designed with tele-operation as their primary use-case make automation challenging. For example, making incisions with a scissors instrument is difficult for an automated system as compared to a scalpel because of the necessity to make an initial notch and maintain correct pose while cutting [102]. Therefore, in conjunction with the algorithmic advances, the design of a complementary set of surgical instruments to facilitate automation would be beneficial.

Automated surgery could encompass a vast quantity of procedures; we chose to define a simulated tumor resection surgery as our test medium, as it comprises several clearly delineated sub-tasks which require several different instruments.

Chapter 3: Texture/Contrast

A Frugal Palpation Tool for RMIS

3.1 Overview

Robotic surgical assistants (RSAs) such as the Intuitive Surgical's da Vinci system (described in chapter 2) have been shown to be effective in facilitating precise minimally invasive surgery [27, 165], by providing increased dexterity and control for the surgeon. **However, these devices lack a sense of touch.** Tactile and force sensors have potential to provide haptic feedback enabling the surgeon to perform an array of survey operations such as in-situ diagnosis and localization.

3.2 Introduction

During open surgery, a surgeon can directly palpate tissue allowing localization of a number of subcutaneous (residing below external organ membranes) or subserous (residing below internal organ membranes) inclusions based on changes in tissue reaction force relative to surrounding substrate (parenchyma) [167]. Even though robot-assisted minimally invasive surgery (RMIS) is frequently used in cancer surgeries [110], the lack of force perception in RMIS has been shown to increase tissue trauma and accidental tissue damage [28]. Williams

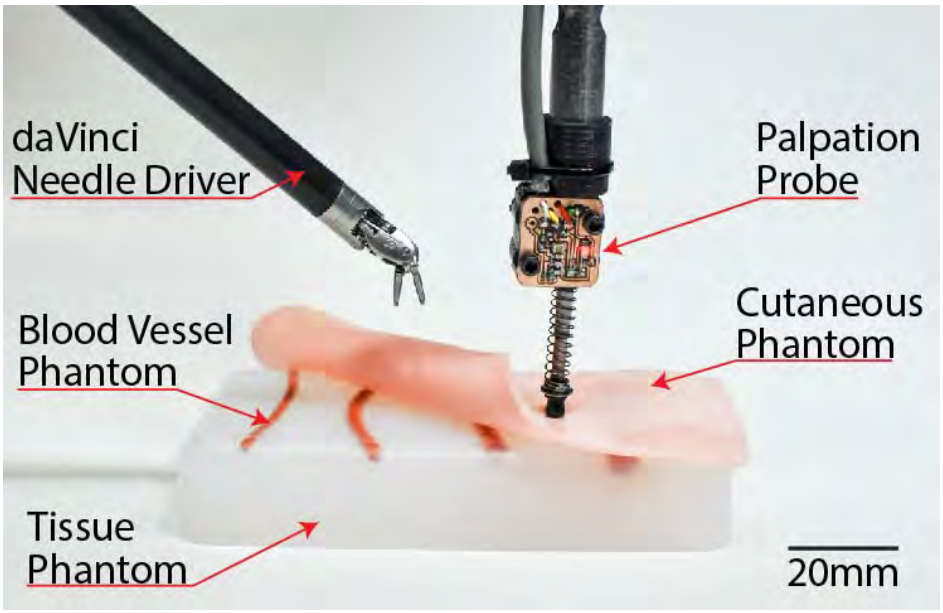

Figure 3.1: A disposable palpation probe (PALP) mounted on the tip of an 8 mm diameter dVRK needle driver tool is shown alongside a regular 8 mm diameter da Vinci tool and with a tissue phantom with subcutaneous vessels. This device is a low-cost extension to an existing da Vinci tool for acquiring tactile information from surface probing in robot-assisted minimally invasive surgery.

et al. [172] show that the lack of tactile or force feedback in RMIS, as compared to open surgery, can lead to increased likelihood of leaving behind target cells during debridement in a diseased region.

A recent survey of medical tactile force sensors by Konstantinova et al. [75] reports that numerous devices exist to estimate tactile information during static (point based) measurements. However, a gap exists in scanning soft tissue surfaces in a dynamic (continuous) manner. Another major limitation in clinical use of tactile force sensing in RMIS is the need for sterilization of tools [6]. After every use, end-effectors are cleaned in an autoclave using high-pressure, high-temperature steam. Most haptic sensors have delicate components, such as resistive strain gauges or electromagnets, which cannot withstand such a harsh sterilization process. Hence, there is a need to develop low-cost single-use tactile or force sensing devices for RMIS which operates in real-time, to provide reproducible and repeatable measurements.

Contributions: A novel low-cost, disposable, haptic palpation probe (called PALP) to be used with the da Vinci RSA tools is shown in Figure 3.1. The probe is designed to sense relative deflection differences for localization of subcutaneous or subserous inclusions such as blood vessels or tumors. It is an indentation based device using a displacement-based contact sensing mechanism. A spherical indenter of 4.5 mm diameter allows quasi-static sliding palpation for continuous measurements analogous to human fingertip sensation.

The design details of PALP are discussed along with sliding indentation experiments on silicone-based tissue phantoms. Silicone inclusions of varying diameters

($\{1.58, 2.38, 3.175, 4.75\}$ mm) placed at varying depths ($\{1, 2, 3, 5\}$ mm) were used to evaluate probe sensitivity. For characterization of robustness to sliding surface speed, the probe is mounted on a CNC milling machine (as shown in Figure 3.5) and is palpated across the tissue phantom at varying indentation depths ($\{1, 3, 8\}$ mm) and sliding speeds (0.5-21 mm/s). PALP is also demonstrated as a tool mounted on the dVRK to perform automated sliding palpation in the silicone-based tissue phantoms. Initial results suggest a potential for the clinical utility of automated sliding palpation in both supervised and semi-supervised telesurgery.

3.3 Background and Related Work

Tactile force sensing is used by humans to explore, manipulate, or respond to their environment [25]. Robotic tactile sensing is applied in diverse fields including surgical devices, industrial equipment, and manipulation on micro scales [17]. Palpation sensors are a subclass of tactile and force sensors that mimic the biological sense of cutaneous touch. In RMIS, palpation sensors can estimate relative tissue stiffness and allow the surgeon to adjust force control input for safer tissue manipulation. It has been demonstrated that a RMIS tool equipped with tactile sensing under autonomous control reduces the maximum applied force to the tissue by more than 35% compared to manual palpation with the same instrument [162]. Other studies have compared human sensing with probing sensors for tumor localization and have found probing sensor arrays to be more effective in requiring lesser forces for inclusion identification [53, 132].

Methods of tactile force sensing: Tactile feedback can be obtained by using a number of transduction principles [75, 122] Refer to Girão et al. [46] and Tiwana et al. [161] for a detailed survey of existing tactile and force feedback devices in the context of robotic and biomedical applications respectively. Tactile sensing can be classified based on its underlying transduction principles: mechanical [41], piezoresistive [149], capacitive [138], piezoelectric [123], strain gauge [59], optical [109], and magnetic [150]. Attempts have also been made to estimate robotic-surgical end-effector forces by relating motor torques and displacements of instruments to mathematical models representing the stiffness of both the environment and instrument [5].

Existing tactile force sensors for RMIS: Konstantinova et al. [75] provide a survey of a number of RMIS tactile feedback devices and compare them based on desired features for tactile probes in RMIS such as: (a) repeatability, (b) reliability, (c) speed of sensing, (d) static versus dynamic response, (d) miniaturized form and (e) cost. Also, RMIS tools are between 5 mm to 12 mm in diameter [93], hence the sensor needs to be small enough to pass though the trocar port and be placed proximal to the tool-tip. Further, strict certification requirements for medical devices warrant that these probes have high accuracy and stable response.

Murayama et al. [103] devised a sensor array for lump detection in breast cancer aimed at identifying large (> 10 mm) inclusions close to the surface (< 20 mm) but it faces limited

adoption in laparoscopic procedures given its large size (45 mm in cross-section). Beccani et al. [11] developed a wireless sensor based on external static magnetic fields within a small workspace. Developments in MicroElectroMechanical System (MEMS) devices have allowed a multitude of sensors to be miniaturized inexpensively; Peng et al. [118] proposed a MEMS tactile sensor which can provide fast relative elasticity measurement. Gafford et al. [42] proposed a monolithic approach to build a tri-axis force sensor for medical applications. However, none of these methods provide continuous tangential sliding surface measurements.

Liu et al. [81] used a force sensitive wheeled probe to gather a rolling mechanical image to observe that a continuous measurement approach is more sensitive to differences in force profiles caused by simulated tumors than single-site data acquisition. However, rolling teeth cause periodic perturbations impairing the continuous measurement. An improved design by Liu et al. [80] with a greater complexity is able to identify spherical inclusions larger than 3 mm in diameter at a depth of less than 2 mm.

Escoto et al. [34] employed sliding detection by sweeping an array of capacitive touch sensors and ultrasound sensors across tissue. This work is designed to palpate tissue readily accessible from both sides, such as portions of the lung and liver and the sensing elements were both relatively large, at 90mm in length.

Non-contact sensing methods such as intraoperative MIS ultrasound probes [92] and optical coherence tomography (OCT) devices [180] have also been explored. These methods provide lower resolution compared to contact probes [75] and are limited to sensing within a comparatively low subcutaneous depth (0-2 mm).

Requirements for sterilization of devices are also considerations for the design of surgical tools [6]; heat, pressure, and humidity during treatment for tool reprocessing can destroy sensors. In the case of single-use devices a design for manufacturability in a sterile environment is required but considerations for reprocessing are circumvented. The simplicity of the design presented in this work allows for a low-cost single-use disposable.

While many of the tactile and force sensors described by Konstantinova et al. [75] have a subset of desired characteristics, limitations such as repeatability, ease of manufacturing, and cost, have slowed wide-spread adoption in clinical settings. Many of these sensors are often operable only in a discrete mode for orthogonal point measurements and cannot survive sterilization. As concluded by [75], "A number of devices have been developed to provide accurate tactile information during static measurements from one point. However, to detect information about mechanical properties of an organ, it is required to perform dynamic tissue scans." There is a need for RMIS compatible sensors with rapid response time for stable measurements in sliding or rolling modes.

This chapter presents a novel low-cost, single-use RMIS tool-tip deflection measurement device for localization of subcutaneous blood vessels. The design of PALP achieves high speed sliding palpation (tested up to 21 mm/s) while maintaining high sensitivity in deflection (50μm) and force (4mN least count). The PALP measures displacement-based force properties of tissue using a commercially available MEMS-based Hall Effect encoder as its core sensor. Hall Effect sensors measure minute changes in electric potential produced by magnetic flux passing through a conductor; a single sensor design favorably reduces fabri-

Property	Value
Size	Diameter < 15 mm
Sensitivity	Discern 5 mm, 5 mm deep
Input	8mm Needle Driver
Output	Subsurface relative stiffness map
Cost	< 10 \$
Material	ABS Plastic, Stainless Steel, Brass

Table 3.1: Palpation Probe Design Constraints

Property	Value
Probe-Tip Radius	2.25 mm
Force Resolution	4 mN
Maximum Linear Displacement	12 mm
Spring Rate	0.08 N/mm
Total Linear Offset of Device (from dVRK gripper)	75 mm
Magnetic Encoder	NSE5310
Pole Pair Length	2 mm
Number of Pole Pairs	6

Table 3.2: PALP Specifications

cation complexity [75]. A 4.5 mm diameter spherical probe tip at as the end-effector for tangential sliding point-contact interaction analogous to human fingertip palpation. Other physical characteristics can be found in Table 3.2. The device is tested on a flesh analogue described in Section 3.6.

3.4 PALP Design

Design Requirements

In addition to considerations for achieving high sensitivity at low-cost, the following issues were addressed:

Compact Size and Low Cost

The probe must match size constraints imposed by minimally invasive tools (diameter 5 mm to 12 mm) [93] used in laparoscopic procedures. PALP is designed to mount onto the 8 mm diameter tool-tip of the da Vinci Research Kit (dVRK) Patient Side Manipulator (PSM). The current prototype adds a total length offset of 75 mm to the needle driver tool as shown in Figure 3.3a. To limit costs, the probe sensing element is designed as a single-use add-on to an existing gripping tool. The gripper and data collection board may be reused.

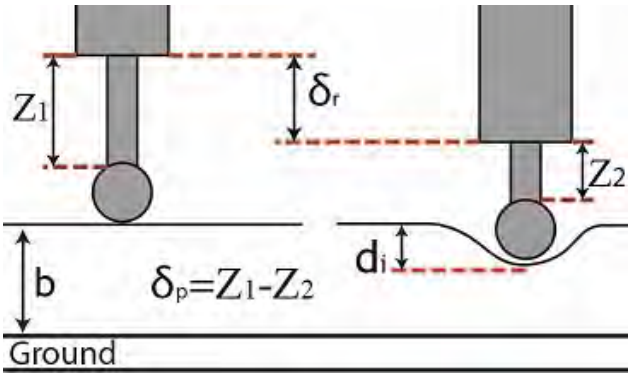

Figure 3.2: A schematic illustrating the indentation process as well as the parameters which define the relationship between indentation depth and probe-tip deflection as described in Section 3.4.

Resolution in Deflection

Palpation measurements are improved by matching the impedance of test probe to sampled tissue in that the stiffness of the spring is chosen to be proportional to the stiffness of the sample. While searching for subcutaneous inclusions, it is essential to indent appreciably within tissue to observe a deflection in the probe, as demonstrated later in the experiments (see Figure 3.7(c)). The total displacement of the device is designed to be 10 mm with replaceable springs to allow for operation over tissues of different stiffness values.

Principle of Operation

The probe uses an end-effector with a known spring constant ($k = 0.08\,\mathrm{N/mm}$) and Hall Effect sensing to compare displacement from PALP to a known deflection value taken from a relative sample. The probe-tip displacement (δ_p) relative to the body of the device is measured with an incremental magnetic encoder and can be linearly related to a tissue reaction force (F) using Hooke's Law ($F = k\delta_p$).

For this device the indentation depth d_i can be calculated from the relative positions of the device (position of the robot arm), end effector (displacement of probe tip), and the baseline height (b) as (see Figure 3.2):

$$\begin{aligned} \delta_p &= Z_1 - Z_2 \\ d_i &= \delta_r - (\delta_p - b), \end{aligned} \tag{3.1}$$

where d_i is the depth of indentation, δ_p is the probe-tip displacement, δ_r is the displacement of PALP body along the contact normal with respect to datum, and b is the baseline height of the sample. This approach assumes that the probe is approximately perpendicular to the tissue to be sensed. The presented probe cannot articulate about the wrist joint, the search area is restricted to limit the angle from vertical to be no more than 10 degrees.

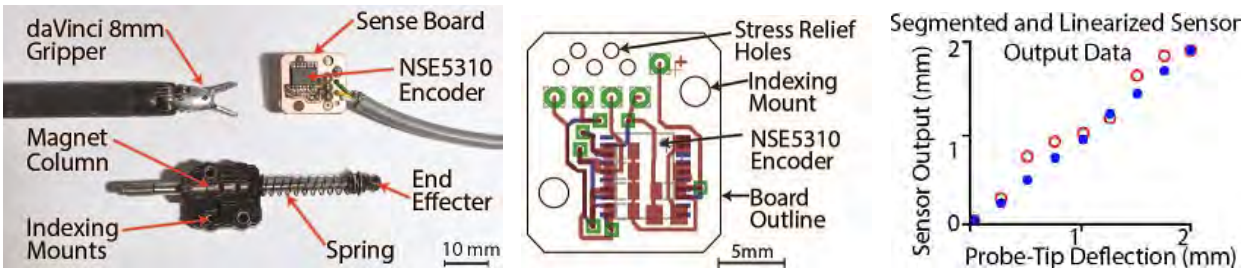

(a) Probe internal components. (b) Probe electronics. (c) Probe linearized data

Figure 3.3: An exploded view of PALP components. (a) Internal components of the probe with 8 mm da Vinci needle driver for comparison. The mounting bracket for the sensor is not shown. (b)Two layer printed circuit board design of the Sense Board showing surface mount components on top layer in red and bottom layer in blue. Connectors have been omitted from the design in the interest of minimizing size. (c) Linearization of output: Raw output of the sensor with respect to actual probe-tip position shown as red circles, cleaned data with non-linearities removed in real time signal processing as described in Section 3.5 are shown in solid blue.

3.5 System Design

Deflection of the probe tip is measured with an NSE5310 Austria Microsystems incremental magnetic Hall Effect position sensor. The power supply for the NSE5310 encoder is buffered and isolated using low-pass capacitors. The total footprint of the electronics board is less than 15 mm per edge as illustrated in Figure 3.3b. The probe tip and axisymmetric magnet column were free to rotate with respect to the shaft of the da Vinci robot allowing PALP to slide and rotate while in contact with surfaces. The NSE5310 magnetic encoder is mounted on the reverse of the electronics board located 0.125 mm from a central column of magnets which followed the movement of a 2.25 mm radius spherical indenter. Neodymium disc magnets (of 2 mm diameter and 2 mm pole pair length) were installed within the sense column with an inter-magnet air-gap of 2 mm. There were 4 magnets within the central column yielding a theoretical total displacement of 16 mm. Hard-stops were placed on the device to limit total displacement to 12 mm. The central column is made from magnetically permeable 316 Stainless Steel with a wall thickness of 0.23 mm which slid co-axially within 316 Stainless Steel bushings. Magnetic permeability is critical for allowing lines of flux to pass through the magnetic column to the NSE5310 Hall Effect sensors. An internal view of the mechanical components can be seen in Figure 3.3a.

Signal Processing and Data Linearization

An Arduino Mega microprocessor is used for signal processing, data transmission, and interfacing with the dVRK. The NSE5310 encoder transmits 14-bit position measurements to the Arduino via I2C at a rate of 300Hz. A 50 sample sliding average low-pass filter is used to condition the raw encoder measurements.

Absolute position between magnet pole-pairs is calculated as a 14-bit integer in software by comparing any two consecutive readings and shifting the most significant bit up or down by one if the differences between consecutive readings is greater or less than a shifting threshold of 4000 or -4000 respectively. The shifting threshold is chosen to be greater than 6 standard deviations of noise away from the maximum sensor value of 4096 (sensor noise is addressed below).

Sensor output is recorded at known probe-tip indentation depths by mounting the sensor in a computer numerical controlled (CNC) Bridgeport vertical milling machine, as shown in Figure 3.5, equipped with a digital readout accurate to 0.01 mm. For every probe-tip position, $10,000$ samples were collected and averaged. These data points revealed a non-linearity between probe output and CNC measured compression as illustrated in Figure 3.3c. Transitional air gaps between magnetic pole-pairs, spaced alternately every 2 mm as seen in the *Magnet Column* in Figure 3.3a, create non-linearities in magnetic flux along the axis of travel. A six degree polynomial is fit to the 4 mm repeating segment of data used by the microprocessor to scale probe-tip indentation depth to a linear output as shown in Figure 3.3c.

3.6 Experiments and dVRK Integration

Tissue Phantom with Linear Vessels

A tissue phantom comprising a cutaneous layer with subcutaneous inclusions is created for testing and characterization of the stiffness probe, as shown in Figure 3.4. Silicone Rubber *Ecoflex 00-30* (*Smooth-On*) is cast in a 1A:1B ratio into a 100 mm long, 50 mm wide, 20 mm thick mold CNC machined from a block of *Delrin* to create a subcutaneous tissue matrix; material properties can be found in the EcoFlex datasheet [142]. Linear cylindrical inclusions of Silicone Rubber (thickness $\{1.58, 2.38, 3.175, 4.75\}$ mm; Shore hardness of 70A) were arranged in the bottom of the mold prior to casting to serve as subcutaneous blood vessel phantoms. After setting, the subcutaneous phantom is unmolded and inverted. A cutaneous phantom is created using a slightly stiffer (shore harness 2A) *DragonSkin 10 Medium* Silicone Rubber (*Smooth-On*) in a 1A:1B ratio; material properties can be found in the DragonSkin datasheet [141]. Opaque pigmentation is achieved using a 0.5% by volume addition of Oil Pigment (Winton Oil Colour, Flesh Tint). The pigmented dermal layer is cast at various thicknesses ($\{1, 2, 3, 5\}$ mm) in molds milled from *Delrin* (with width of 60 mm and length of 100 mm). Upon solidification, the dermal phantom is overlaid on the subcutaneous phantom (as shown in Figures 3.1) to create the tissue phantom setup.

Calibration using CNC Tool

The probe is affixed to a *Bridgeport* CNC vertical mill (with digital encoders accurate to 0.01 mm) for sensor calibration similar to the linearization procedure in Section 3.5. The

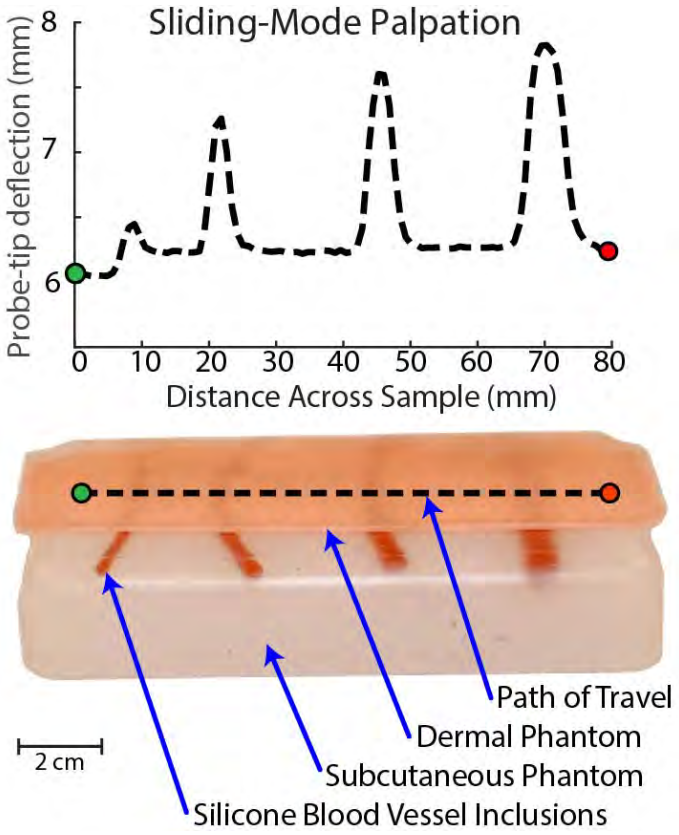

Figure 3.4: A silicone tissue phantom is shown with blood vessel inclusions and overlaid dermal phantom. Sliding palpation from starting point (green circle) to end point (red circle) over 80 mm of travel reveals the presence of subcutaneous blood-vessel inclusions as observed from the probe-tip deflection in the graph above. Depth of indentation is held constant at 8 mm, sliding speed is 1 mm/s, and skin thickness is 1 mm.

tissue phantom is mounted securely to an acrylic plate affixed in a vise. The vertical position of the sensor is held constant at an initial probe deflection of 2 mm while the tissue phantom along with a cutaneous layer (lubricated by petroleum jelly) is moved beneath the sensor at a feed rate of 1 mm/s. Each trial is conducted across the same line running transverse to the veins embedded in the tissue phantom as shown in Figure 3.4. The standard error across 10 trials, quantified by normalized root mean square difference, is found to be $0.931\,\mu m$.

Baseline sensor noise data ($> 10,000$ samples) were collected with no signal processing; the standard deviation of the noise is found to be $12.9\,\mu$m. A measured value $52\,\mu$m (4σ) above baseline can be considered statistically dissimilar from noise; and using $F = k\delta_p$, can yield a minimum palpation probe sensitivity of 4 mN.

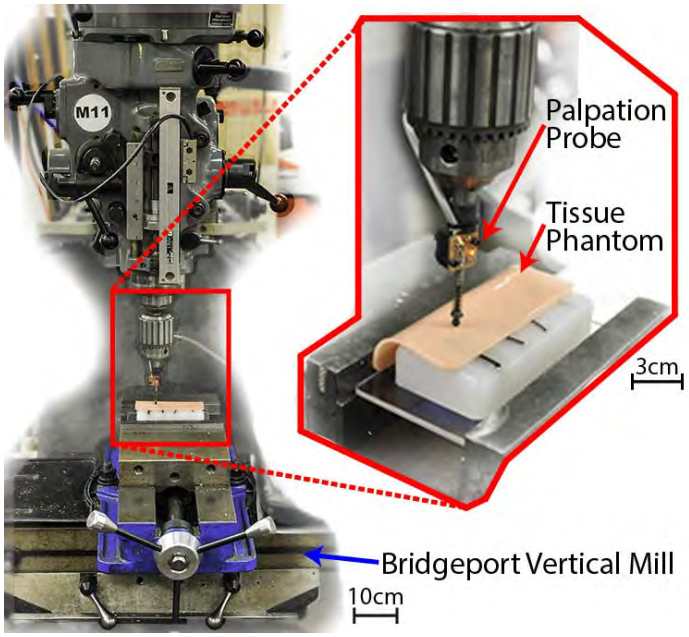

Figure 3.5: Probe characterization on a Bridgeport CNC (XY-Axis) Vertical Mill. The vertical axis movement (δ_r in Equation 3.1) is measured by a digital encoder (accurate to 0.01 mm). For every setting of indentation depth, the vertical position is held constant as the tissue phantom is moved along a linear path across the subcutaneous vessels.

Probe Characterization using CNC Tool

A surface profile is constructed by interpolating the δ_r position of probed surface contact points spaced at 10 mm intervals along areas of interest. A surface contact point is described as the first time the probe registers a non-trivial measurement upon touching the surface; quantitatively defined as the δ_r position of the sensor after statistically significant deflection ($4\sigma \approx 52$ μm) is observed at the probe-tip (δ_b). This profile accounts for physical irregularities in the sample surface shape and is used to account for surface offset represented by b in Equation 3.1.

Figure 3.4 shows the probe-tip deflection (δ_p) using a sliding measurement across the silicone tissue phantom with blood vessel phantoms and overlaid dermal phantom. The probe is slid across the surface from the starting point (green circle) to end point (red circle) over 80 mm of displacement. Parameters used in this trial were: indentation depth (δ_r) of 8 mm, sliding speed of 1 mm/s, and a skin thickness of 1 mm.

Deflection Response Characterization: Localization of a subcutaneous blood vessel (or tumor) depends on several parameters such as the *indentation depth*, *depth of the vessel* below the surface, and *speed of probe sliding*. Characterization of the probe behavior is essential to analyze the deflection response for different parameter settings.

Probe response is tested by varying each of these parameters for a fixed value of the other two as shown in the series of graphs in Figure 3.6. Each graph in the figure shows

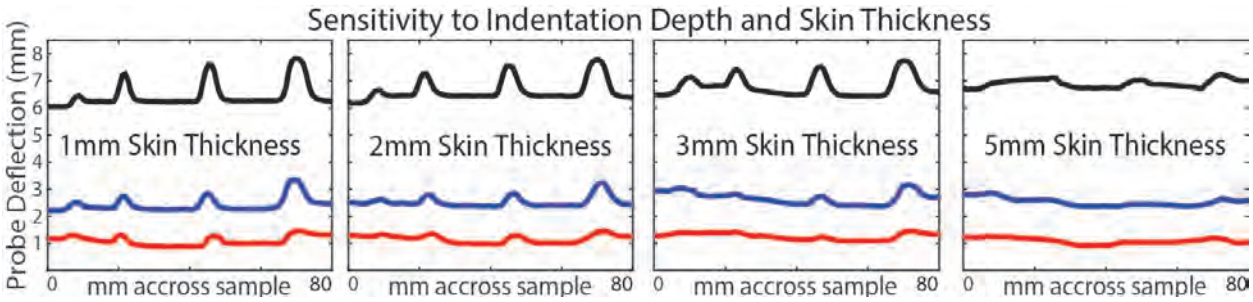

Figure 3.6: Increasing skin thickness decreases palpation probe sensitivity, while increasing penetration depth increases probe sensitivity to buried blood-vessel phantoms. Displacement of the probe-tip during sliding palpation plotted at $1\,\text{mm/s}$ surface speed; indentation depth (δ_r) of $1\,\text{mm}$ shown in red, $3\,\text{mm}$ shown in blue, and $8\,\text{mm}$ shown in black.

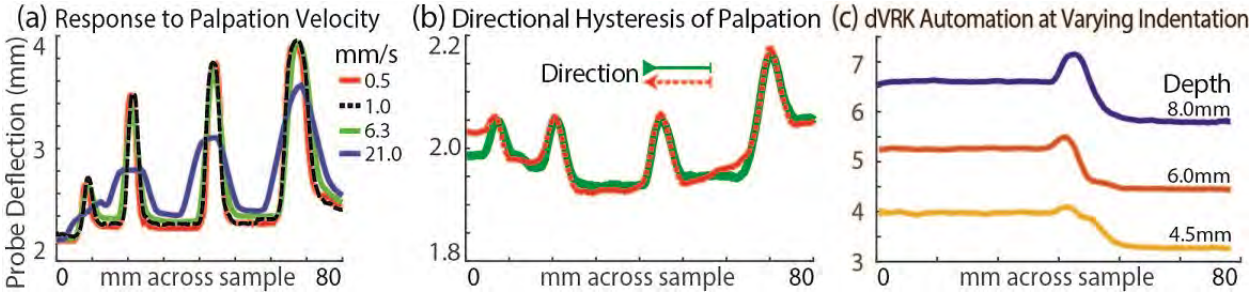

Figure 3.7: Sensor response is tested with respect to varying speed, direction, and automation by the dVRK. (a) robustness to sliding speed is tested at four surface feed-rates; $0.5\,\text{mm/s}$ is shown in red, $1\,\text{mm/s}$ is shown in black, $6.3\,\text{mm/s}$ is shown in green, and $21\,\text{mm/s}$ is shown in blue. Probe indentation depth is held constant at $8\,\text{mm}$; skin thickness is $1\,\text{mm}$. (b) Hysteresis of sliding palpation collected continuously in opposite directions without lifting the probe. The maximum maximum difference between data observed are within 4σ of noise levels, indicating very low hysteresis. Motion in the positive x-direction is shown in red; negative x-direction palpation is shown in green. This data is collected using a $1\,\text{mm}$ skin thickness and $2\,\text{mm}$ indentation at $1\,\text{mm/s}$ sliding speed. (c) Deflection of PALP at three different indentation depths with an automated routine on the dVRK.

the variation in probe-tip deflection for different indentation depths ($1\,\text{mm}$, $3\,\text{mm}$, $8\,\text{mm}$) at a fixed skin thickness and a constant sliding speed of $1\,\text{mm/s}$. The different graphs show the variation for different skin thicknesses ($1\,\text{mm}$, $2\,\text{mm}$, $3\,\text{mm}$, $5\,\text{mm}$). Similarly, fixing the indentation depth at $8\,\text{mm}$ and skin thickness at $1\,\text{mm}$, sliding speed is varied to four different settings, ($\{0.5,\ 1,\ 6.3,\ 21\}\,\text{mm/s}$) and observed the probing response as shown in Figure 3.7(a).

The probe is used to acquire deflection measurements along the same raster line in a forward and a backward pass. The results from this hysteresis analysis are shown in Figure 3.7(b); the maximum difference between the directional data is not statistically significant ($\geq 10\times$ larger than 4σ of Gaussian noise).

dVRK Integration and Vein Localization

PALP is mounted on the end of an 8 mm da Vinci Needle Driver as shown in Figures 3.1 and 3.10, extending the tool tip by 75 mm. Figure 3.7(c) shows the deflection response obtained for three indentation depths ({4, 6, and 8} mm) at 2 mm/s in single-sweep automated sliding palpation.

An autonomous palpation routine is created for the dVRK accounting for the linear offset along the insertion direction as shown in Figure 3.8: a plane representing the surface of the tissue phantom is created by recording the pose of the dVRK at the four corner points defined by point-contact of PALP ($\geq 50\,\mu$m indentation). This plane (45 mm $\times$ 25 mm) is segmented into 10 linear palpation sub-routines transversely crossing two subcutaneous blood vessel phantoms. The dVRK returned the palpation probe-tip to a home position 2cm above the area of interest between each linear segment. Continuous tangential palpation at 2 mm/s with an indentation depth of 8 mm is used to search within the area of interest on the tissue phantom. The blood vessel silicone phantoms used for these trials were 2.5 mm and 3.5 mm in diameter embedded subcutaneously beneath a layer of 1 mm thick dermal phantom. An estimate of the location of subcutaneous vessels generated by Delaunay interpolation of a raster scanning pattern is illustrated in Fig. 3.8. Start and end points of the raster path are shown overlaid above a tissue phantom as green and red circles respectively.

3.7 Discussion and Future Work

Discussion of Results

Preliminary characterization results from PALP demonstrate the ability to identify and localize a subcutaneous blood vessel phantom. As observed in Figure 3.4, as the size of underlying vessel increases the sensor deflection also increases. However, in all cases the deflection obtained is significantly above noise ($\geq 10\times$ larger than 4σ of Gaussian noise). Increasing depth of the inclusion decreases the signal-to-noise ratio from 40:1 at 1 mm skin thickness to 4:1 at 5 mm skin thickness for a vessel of diameter 4.75 mm. Signal-to-noise ratio amplifies approximately linearly with increase in indentation depth as observed in Figure 3.6. A discernible peak is obtained even in the raw data without signal conditioning for a subcutaneous vessel of 2.25 mm diameter under a 5 mm skin with an 8 mm indentation depth. As sliding speed of the probe on the phantom surface is increased, a small decrease in signal-to-noise ratio is observed as shown in Figure 3.7(a). However, even at the speed of 21 mm/s, which is comparatively high in the context of RMIS, statistically significant deflections for all 4 subcutaneous vessels are observed. Repeatability in measurements is supported by measurements obtained from forward and backward runs of the probe along the same raster line within noise levels of $50\,\mu$m($\approx 4\sigma$) as shown in Figure 3.7(b).

Experiments with autonomous palpation routines on dVRK corroborate the findings from probe characterization on CNC machine tool. Figure 3.7(c) shows a high gain in signal with increase in indentation depth with constant skin thickness and sliding speed. Further, the

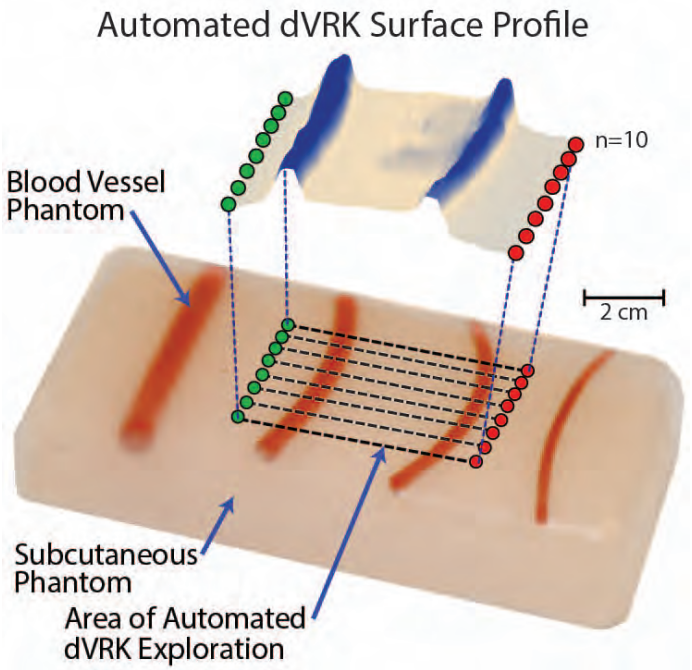

Figure 3.8: An estimate of subcutaneous blood vessels generated by a raster scan on the region of interest. Delaunay surface interpolation is used to create a continuous estimate from raster samples. Start and end points for each linear segment are shown overlaid above a tissue phantom as green and red circles respectively with indicative raster scan paths (shown as black dashed lines).

raster scan results from Figure 3.8 demonstrate that this method can be used to search and localize a subcutaneous inclusion in a large surface area and can be automated for use by RMIS devices.

Future Work

The described sensor is primarily aimed to differentiate areas of interest based on relative deflection changes. However, the tool could provide estimated stiffness values using inverse calculations as in work by Yu et al. [177] and Hayes et al [55].

This work is focused on developing a sensor for autonomous or semi-autonomous surgical procedures; however, it could also be used to provide tactile information which can be fed back to a user as Talasaz et al. [151] demonstrate. Autonomous palpation and localization can be improved with the use of active sensing algorithms. As an example, Nichols et al. [107] presented a probabilistic sensing algorithm which can be leveraged to enable autonomous searching within a target area. They used a 45 mm indentation ball limited to sensing large inclusions; the probe would extend their work to a fine grained localization of smaller inclusions. Nichols et al. relied on point measurements; the probe uses a sliding continuous measurement. Information-gathering algorithms for autonomous localization of inclusions, such as the ones compared by Goldman et al. [48], may be considered for this continuous

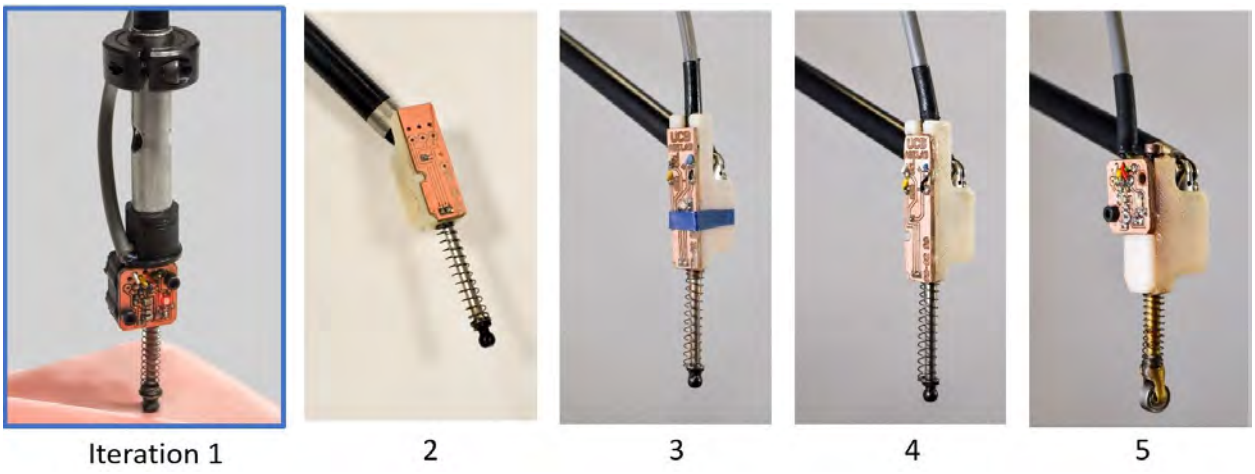

Figure 3.9: Successive iterations of the PALP. The probe was redesigned to allow for greater movement of the wrist axes (see Chapter 5) as well as to minimize overall size of the instrument.

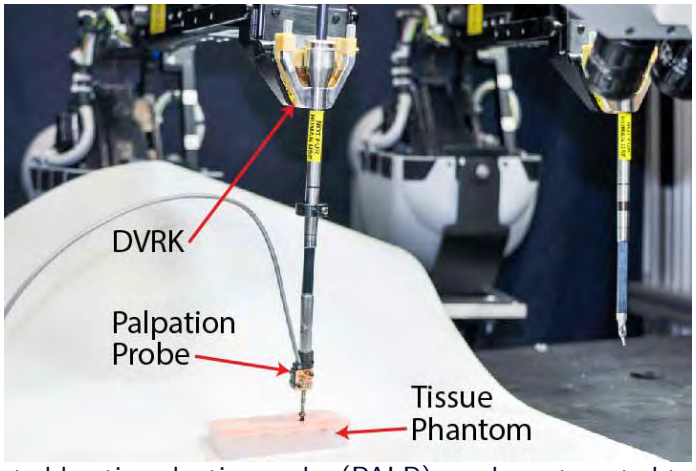

Figure 3.10: The presented haptic palpation probe (PALP) can be automated to search for blood vessel phantoms with the da Vinci Research Kit Patient Side Manipulator.

(sliding) probe.

Possessing prior knowledge of the surface profile, the insertion axis of the dVRK could be used to maintain consistent probe-tip indentation depth (linearly related to force) across non-planar surface paths while searching tissue for inclusions to allow for greater accuracy of localization as accomplished by Ibrayev et al. [60]. This chapter investigated the success of the PALP while searching for a tumor withing planar samples. To accomplish more complex searching on realistic surfaces (as seen in [60]), the probe was redesigned as shown in Figure 3.9 (see Chapter 5 for more details).

3.8 Conclusions

A low-cost, single-use palpation probe (PALP) for usage with RMIS for localizing subcutaneous blood vessels and tumors is presented in this work. The probe senses relative differences in probe tip reaction force by measuring tip deflection with respect to a known spring constant using a Hall Effect sensor. PALP fits on the end of a 8 mm diameter needle driver and extends it by 75 mm. It is an indentation based probe which can be used for quasi-static sliding palpation as well as for discrete point palpation. Discrete measurements are used for generating a surface profile of unknown silicone tissue phantoms; while quasi-static sliding is used for identifying subcutaneous blood vessel phantoms. The issue of sterilization is circumvented by use of disposable sensors.

The sensor probe is characterized for deflection response on a CNC machine tool with respect to various parameter settings such as multiple diameters of subcutaneous silicone cylinders (1.58-4.75 mm) at varying subcutaneous depths (1-5 mm) with a range of indentation depths (0-8 mm) and sliding speeds (0.5-21 mm/s). Experiments with the dVRK performed under autonomous execution suggest probing routines could be automated adaptively in minimally invasive surgeries. The probe can detect subcutaneous structures in phantoms of diameter 2.25 mm at a depth of up to 5 mm below the tissue surface and can operate up to speeds of 21 mm/s in sliding palpation.

PALP was recently used to automate a simulated-tumor resection surgery on the DVRK in recent work [96]. This probe was also recently used with algorithms developed by Miller et al. to optimize automated palpation in an RMIS setting [44].

A major limitation of the probe as described above, is the mounting strategy used to connect the probe to the DVRK. By mounting the device to the shaft of the arm wrist movement was prohibited, limiting the probe workspace to a spherical volume with a diameter of 5cm. This limitation is addressed in chapter 5.

Chapter 4: Void/Proximity

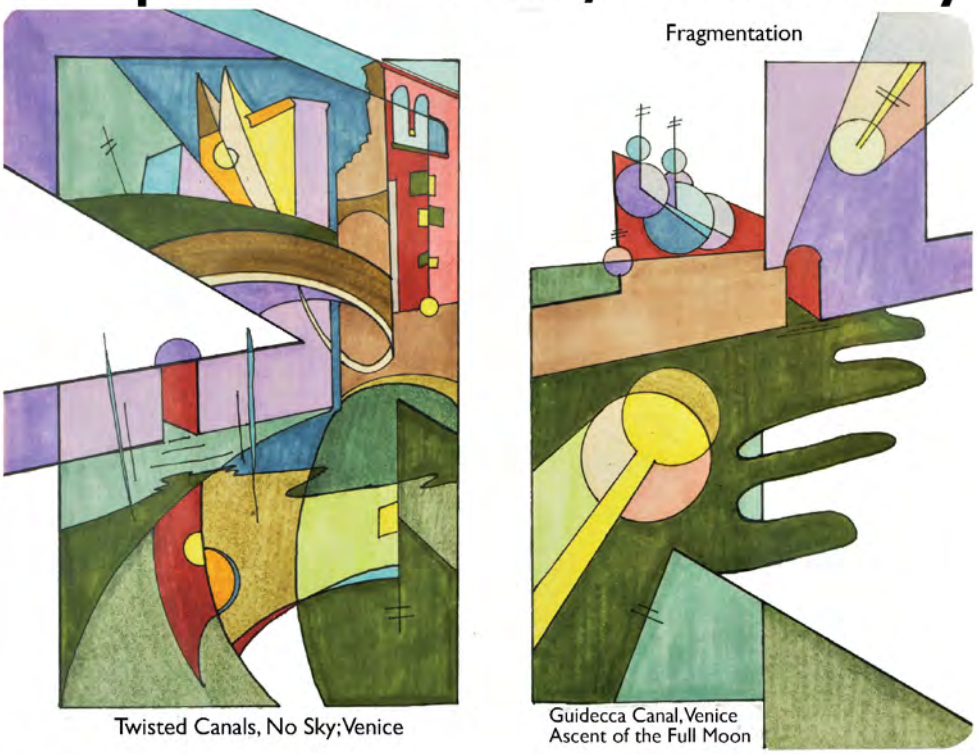

An Injection System for RMIS

4.1 Overview

Minimally-Invasive Surgical robots laparoscopically access sites within the thorax, abdomen, and pelvis; currently there are no available instruments to allow fluid delivery robotically during surgery. This chapter describes a novel stem-cell delivery instrument embodied by a remotely actuated syringe pump attached to the arm of the da Vinci system.

This work was initially motivated for use in delivering precise amounts of mesenchymal stem cells to areas with tissue trauma within the body. The device was re-purposed for use in delivering surgical glue as described in Chapter 5.

4.2 Motivation and Related Work

Recent advances in stem-cell based tissue engineering research hold promise for near-term clinical application as regenerative therapies and for the treatment of a diverse set of debilitating conditions including liver disease, connective tissue degeneration, trauma, and inflammatory diseases [170]. Mesenchymal stem cells (MSCs) are cellular progenitors found

to reside within bone marrow by Jakovlecich et al. in 1968 [38]; MSCs have shown pluripotency to replicate and differentiate into most somatic cellular types [120]. Transplants of a patient's own undifferentiated mesenchymal stem cells to areas outside of the bone marrow can prompt MSC specialization to that of their residing location providing repair or regeneration of that tissue [104].

While there is extensive research on methodologies to harness and differentiate stem cells, there is less innovation and no clear consensus on viable modes of stem cell delivery in the clinic [68]. Systemic delivery employs an intravenous injection of high volumes of cells with the expectation that some of the injected cells will migrate to the targets of interest [29]. However, systemic delivery of stem cells in very high numbers also introduces risk for pulmonary emboli or infarction, as many of the cells will become trapped in the lung [71]. Local delivery via direct injections allows a controlled and precise stem cell delivery, but delivery to organs in more inaccessible locations within the thorax, abdomen and pelvis is challenging because of the relatively high degree of invasiveness [71]. Novel procedures or delivery devices are needed to reach certain anatomic locations such as organs located within the abdominal cavity [68].

Contributions: We present an instrument mounted to a surgical robot that can deliver measured amounts of saline solution containing MSCs to desired sites within the body using Intuitive Surgical's da Vinci Robotic Surgical Assistant. We present a software interface between the existing da Vinci Research Kit (dVRK) and the proposed hardware to allow for an entire course of treatment without increasing the overall size of the dVRK end-effector in-vivo. We also demonstrate the autonomous injection process for delivery of pre-calculated amounts of the saline solution in precise locations under robotic control on tissue phantoms using a da Vinci Research Kit. The instrument is designed from commodity hardware, and the portion to be used in-vivo is a single-use disposable. This instrument facilitates the minimally invasive infusion of stem cells, where indicated, at any location already accessible by the daVinci surgical system.

Figure 4.1: This delivery instrument can provide controlled local injections of mesenchymal stem cells to hard-to-reach areas within body cavities using a single-use disposable needle tip.

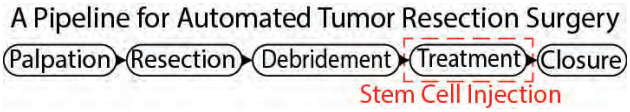

Figure 4.2: Treatment via local stem cell injection is a unique surgical sub-task within a complete autonomous tumor resection surgery.

4.3 Design of Hardware and Software Framework

This device is comprised of three components: a tool-tip mounted needle, a flexible catheter assembly, and a drive motor assembly mounted to the upper portion of the dVRK arm (behind the sterile barrier) as seen in Figure 4.3. Typical local injection volume is on the order of 10's of milliliters, with per-injection doses of 10mL to 30mL representing approximately 10 million viable MSCs [153]. This volume guided the design of the injector to include an off-board dVRK syringe pump rather than have the end-effector carry the payload. Injection force is provided by a Haydon-Kerk 21F4AC-2.5 linear actuator, powered by Allegro's A4988 microstepping bipolar stepper motor driver, and controlled by an Arduino Pro Mini 328 microcontroller. A 10mL syringe is carried by a 3D-printed enclosure along a linear stage that is mounted to the dVRK arm.

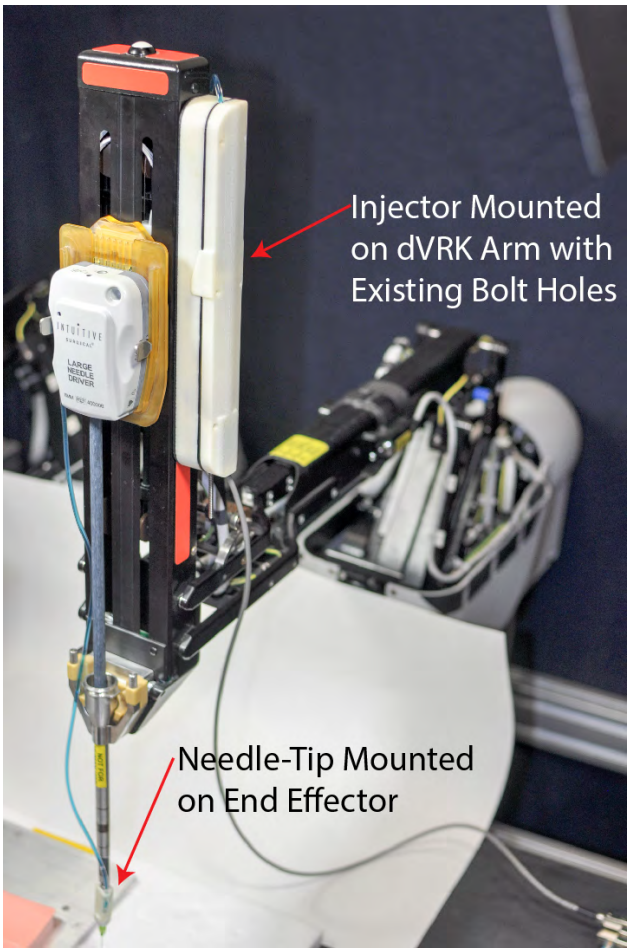

Figure 4.3: The device mounted on the dVRK surgical robot can provide controlled injection patterns around tissue of interest.

The stem cell injector was created to fit within an ecosystem of hardware designed to enable surgical automation of the dVRK Surgical Robot as described in Figure 4.4. Each device has its own address on an i2c communication bus controlled by a master point which acts as a Robot Operating System (ROS) node.

This device was designed to enable a sub-task to be performed within an end-to-end autonomous surgery as described in Figure 4.2. Figure 5.1 shows the device in use within an autonomous simulated-tumor resection surgery.

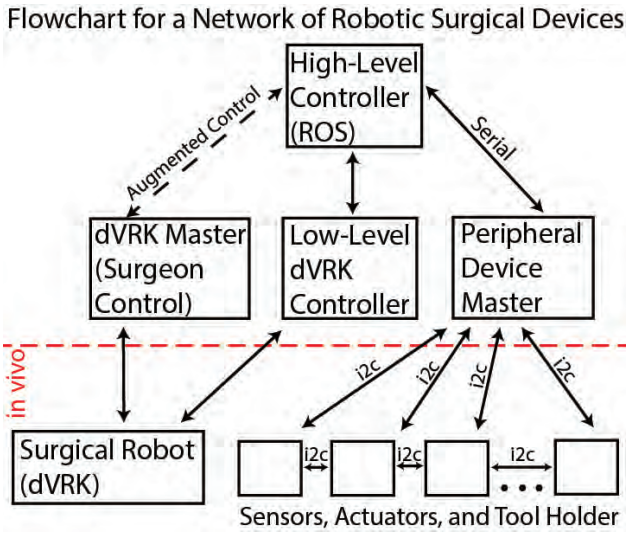

Figure 4.4: The injection device communicates with a suite of instruments that accompany the da Vinci Robotic Surgical Assistant which allows for automation of surgical sub-tasks such as injection.

Interchangeable Instruments for RMIS

5.1 Overview

Tumor resection is a multi-step multilateral surgical procedure to localize, expose, and remove a subcutaneous tumor, then seal the resulting wound. This process requires several tools and is currently practiced in clinic with no automation. This chapter describes an interchangeable instrument mount that uses the jaws and wrist of a standard RMIS tool to securely hold and manipulate a variety of end-effectors and an interchangeable device to assist autonomous tool-changing within confined spaces. Initial experiments suggest that an automated Intuitive Surgical dVRK system using these devices can successfully complete the entire procedure.

5.2 Introduction

Robotic Surgical Assistants (RSAs) are frequently used with high success rates for Robotic Minimally Invasive Surgical (RMIS) procedures such as prostatectomy, ureterectomy, tumorectomy, and nephrectomy within the abdominal and thoracic cavities [26, 111]. Intuitive

Surgical's *da Vinci* Robotic Surgical Assistant (RSA) facilitated over 570,000 procedures in 2014 with 3000 RSA systems worldwide [61]. RSAs are currently controlled by surgeons via pure tele-operation, requiring constant surgeon attention and control. Supervised autonomy of surgical sub-tasks has the potential to reduce surgeon tedium, fatigue, and operation time.

In 2009, Miller et al. [99] labeled video data to measure elapsed time of fourteen different laparoscopic surgical procedures; 24% of the total procedure time involved the task of changing instruments for specialized surgical sub-tasks. Miller et al. concluded surgery time and costs could be decreased by use of a quick-change instrument system: they proposed a concept for devices without wristed articulation to be used in traditional manual laparoscopy; these tools would be unable to function in a tele-operable way because of their limited degrees of freedom.

Interchangeable surgical end-effectors allow for smaller incision wounds [116] and decreased surgical time [99], but currently available modular tools do not have a wristed degree of freedom thus decreasing surgeon efficacy. To address the problem of modularity and interchangeability, we have developed several novel devices, including interchangeable low-cost instrument mounts for retractors with wristed articulation as illustrated in figures 5.1 and 5.2, to be used to explore automated tumor resection.

We consider the multilateral surgical procedure of tumor resection which includes four sub-tasks: (a) *Palpation*, (b) *Incision*, (c) *Debridement*, and (d) *Adhesive Injection*. These sub-tasks represent a selection of those included in the *Fundamental Skills of Robotic Surgery* (FSRS) [139] used for training laparoscopic surgeons [131, 33]. We explore the automation of this procedure using the da Vinci Surgical Research Kit (dVRK), a commercial RMIS system from Intuitive Surgical [72] with silicone-based simulated tissue phantom. Tumor resection requires multiple instruments: a haptic device for palpation, a blade for incision, grippers for debridement, and a syringe pump for injection. Changing instruments during surgery is time consuming and currently requires a pause in the surgical procedure for human intervention. We consider a scenario where the standard surgical grippers can interface with multiple tool-tips to increase the automation during robotic laparoscopy.

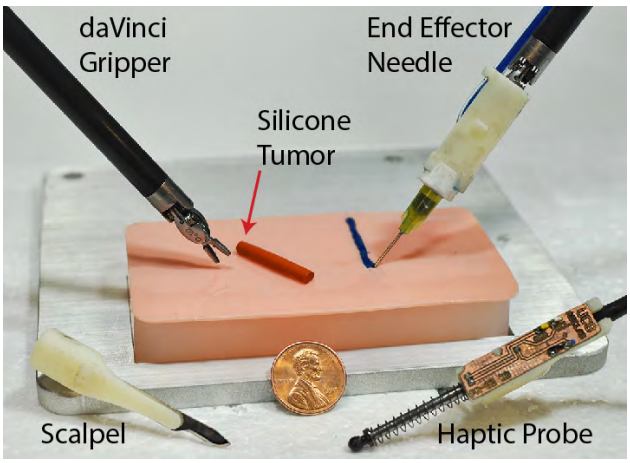

Figure 5.1: The injection tool is used as part of an autonomous surgical pipeline to inject fluid at the site of a simulated tumor resection using the dVRK Robotic Surgical Assistant.

Contributions

1. Designs of novel interchangeable instrument mount compatible with standard RMIS gripper.

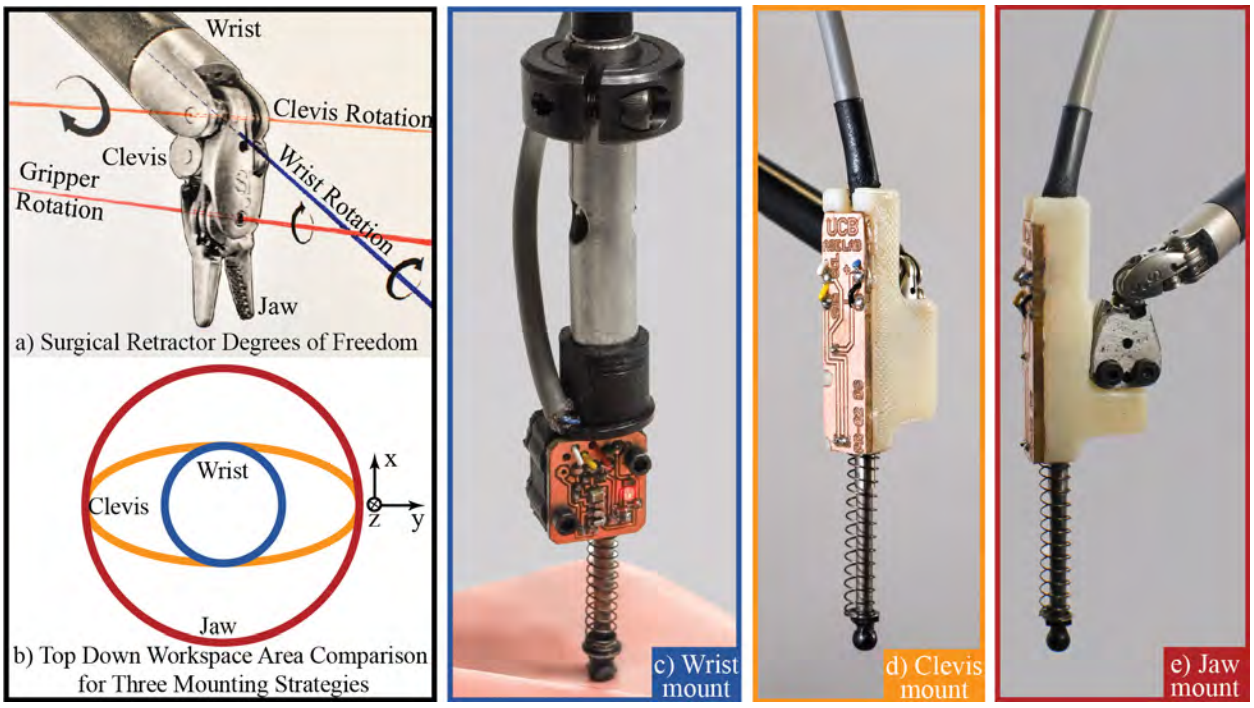

Figure 5.2: Three designs for end-effector instrument mounts differentiated by attachment strategies to the surgical retractor. We found that the usable workspace of the Palpation Probe decreases as degrees of freedom (a) are restricted. The surgical retractor in (c) extends axially within the mount. The retractor in (d) is inserted at level with the clevis pulley seen in (a).

2. Design of a novel tool-guide and sleeve to facilitate automated switching between instruments.

3. Application of the interchangeable instrument system to multi-step supervised autonomous surgical tumor resection involving changes between haptic probe, scalpel, fluid injector, and standard grippers.

5.3 Related Work

Interchangeable MIS Instrument Systems

There have been a number of studies on non-robotic laparoscopic instruments with interchangeable end-effectors [74, 119]. However, the end-effectors of these instruments allow only a single degree-of-freedom (jaw opening/closing) and do not interface with existing surgical retractors. Most existing robotic systems such as the da Vinci and DLR MICA exchange the entire instrument instead of the end effector [160, 1].

Implementation of Interchangeable Systems: Currently, the instrument change procedure for the da Vinci RSA involves the complete removal of the instrument from within

the abdominal cavity through the trocar port (see Figure 2.2). To make interchangeable instrument end-effectors beneficial to RMIS, end-effectors can be introduced through a separate utility trocar port as described in [144]. The utility trocar port can also be the point of entry for electronic cables and catheters as described in [74] allowing for sensorized and fluid delivery end-effectors to be introduced into the RMIS workspace.

Robotic Interchangeable Instrument Systems: In 2007, Friedman et al. proposed the early use of a robotic system to automate instrument change on the da Vinci RSA [39]. However, their method required additional automated infrastructure including an industrial arm used to change the entire da Vinci instrument after removing it from the abdominal cavity.

Commercially Available Devices: In 2015, Teleflex Medical was granted FDA clearance to market interchangeable instrument-tips for *non-robotic* MIS instruments with a single degree of freedom [157].

Existing non-robotic interchangeable instrument end-effectors are not compatible with existing retractor geometry, limiting the combination of possible instrument configurations. Additionally, all of these devices allow only a single controllable degree-of-freedom at the instrument tip with similar limitations as in the initial design for a wrist mount (described in Figure 5.2(b) and shown in Figure 5.2(c)).

	Wrist Mount	Clevis Mount	Jaw Mount
Wrist Rotation	(full) 360°	(full) 360°	(full) 360°
Clevis Rotation	(none) 0°	(full) 180°	(full) 180°
Jaw Rotation	(none) 0°	(none) 0°	(restricted) 60°

Figure 5.3: Comparison of mounting strategies.

Autonomous Multilateral Surgical Tumor Resection

This chapter focuses on the demonstration of *tumor resection* as imagined in a silicone-phantom tumorectomy which includes four sub-tasks [37]: *Palpation*, *Incision*, *Debridement*, and *Injection*, using the finite element approach described in a previous work [102]. Several researchers have explored autonomous performance of RMIS sub-tasks [2, 10, 155, 173]. Moustris et al. [101] and Kranzfelder et al. [76] provide reviews of recent developments in semi-autonomous and autonomous execution of various experimental and clinical surgical procedures.

Palpation is necessary for surgeons to find inclusions within tissues. Konstantinova et al. [75] provide an extensive survey on recent advances for sensor design and deployment to enable successful haptic palpation. Algorithms for active exploration in tumor localization [106] and tumor ablation [58] offer new methods to consider for improved robotic palpation outcomes. Sterilization of instruments remains a challenging limitation for clinical use of tactile force sensing in RMIS [6]. In this work, the palpation probe design presented by the authors in 2015 is automated [97].

Scalpel instruments are available as stand-alone tools for the da Vinci. However, they do not allow for interchangeability of instrument-tips. A scalpel instrument-tip is used (shown in Figure 5.1), compatibly with the proposed instrument mount for use in the auto-

mated tumor resection pipeline as described in Section 5.6. In surgical theaters, electrical cauterization is generally used for resection. However, these instruments will function properly in a silicone-based phantom tissue.

Surgical debridement is a tedious surgical sub-task in which foreign inclusions or damaged tissues are removed from the body [7, 49]. Automated brain tumor ablation and resection with the RAVEN II has been explored in simulation [58]. Kehoe et al. [73] used motion planning to perform multilateral surgical debridement using the Raven II surgical robot. Tissue debridement and multilateral cutting on deformable materials with the dVRK has been explored [102].

Targeted fluid injection allows for controlled and precise delivery of materials such as chemotherapy drugs, surgical glues, and stem cells. However, delivery to organs in inaccessible locations such as in the thorax, abdomen and pelvis is challenging because of the relatively high degree of trauma required [71]. Non-MIS robot injection tools have been developed and evaluated in the past [147]. Robotic catheter injection tools have also been studied [4]. However, there is a need for low-cost RMIS compatible delivery devices which enable access to internal organs and deliver controlled quantities of localized fluids [68].

There are a number of clinically used methods for **wound closure** including suturing, staples [166] and surgical adhesives. Padoy et al. [113] demonstrated execution of a human-robot collaborative suturing task on the daVinci platform with a research interface. Surgical glue has shown promise in closing small scale inter-cavity hernias [82], but little work exists on the use of RSAs for precision application of fluids.

5.4 System Design and Interfacing

The design motivation is to develop modular tooling for the dVRK to allow for the demonstrable automation of a multi-step surgical procedure. The interchangeable mounting system has:

1. Kinematically constrained mounting on a standard surgical retractor end-effector using existing geometric features
2. Self-actuating retractor fixation requiring minimal grip force
3. Preservation of existing retractor articulation
4. Form factor to fit through a 15 mm cannula during minimally invasive procedures
5. Low-cost for single-use disposability.

Clevis Mount Design

A low-cost wrist-mounting design is introduced in recent work for use as a minimally invasive palpation sensor [97] shown in Figure 5.2(c). However, due to the sleeve enclosure, the motion

of the end-effector is restricted to only wrist rotation as shown in Figure 5.3. This limits the range of motion of the surgical retractor as illustrated in Figure 5.2(b).

An interchangeable instrument-tip mount is presented to address these limitations by mounting on the 'clevis' link of the surgical retractors (see Figure 5.2(a)) providing stabilization (as shown in Figure 5.2(d)). The cavity on the clevis mount (illustrated in Figure 5.5) was designed to help funnel the dVRK needle driver into its proper orientation, allowing a higher tolerance for misalignment in settings without visual feedback and easing the demands on software. The furthest proximal extent of the mount extends up to the clevis joint linkage; any further extension along this axis would limit clevis rotation as shown in Figure 5.2(b). The cavity of the mount mates with the side contour of the surgical retractor to limit rotation away from the 'z' axis (defined in Figure 5.5) yet maintains a sliding fit to allow the retractor to detach easily.

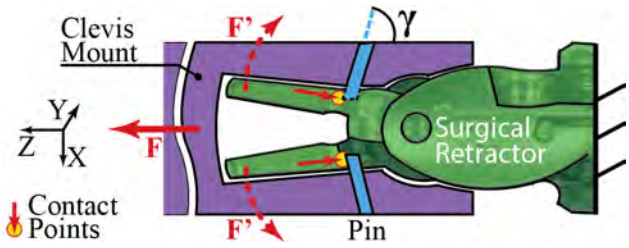

Figure 5.4: A self-actuating mount: Disturbance F in the negative z direction is countered by the contact points between the mount pins and the retractor shoulder. This results in an outwards clamping force F' to the clevis mount. The interchangeable mount can be designed with any external shape.

The internal cavity of the clevis mount is designed with locking pins extending from the walls of the interchangeable mount. The pins securely engage shoulders located on the retractor jaw when open ('Contact Points' marked on Figure 5.5). The angle of these pins (angle 'γ' shown in Figure 5.5) matches the angle of the shoulders on the opened jaws to maximize contact area. A self-actuating lock is achieved as the points of contact on the jaw are angles such that a disturbance forces the jaws further open in contact with the internal cavity of the mount as a force in the positive 'z' direction is applied (shown in Figure 5.5). Movement in the negative 'z' direction is limited by contact between the clevis linkage and the internal cavity of the interchangeable mount.

The clevis mount allows greater range of motion along the 'x-y' plane as shown in Figure 5.2(b). However, because jaw rotational motion was restricted, the workspace is limited to a narrow ellipse along the 'x' axis as shown in Figure 5.2(b). Despite these limitations, utility of a self-engaging interchangeable instrument-tip mount is demonstrated by performing tumor resection surgeries in silicon flesh phantoms as described in Sections 5.7 and 5.6.

Jaw Mount Design

The jaw mount design was created to extend the utility of the clevis mount design by allowing greater range of motion in jaw rotation axes. Mount movement in the negative 'z' direction is constrained by an internal spur that mates with the 'palm' of the surgical retractor clevis between the two retractor jaws. The mating cavity was created by laminating water-jetted 1095 spring steel sheets of 0.025 *in* thickness using two M2 machine screws. Points to engage the retractor shoulders were designed integrally to the laminate layers. This

interchangeable mount is affixed to modular instrument tips and end-effectors as shown in figures 5.2(e) and 5.5.

5.5 Design for Autonomous Tool-Changing

The methods above describe interfacing tools and devices affixed temporarily to the tips of surgical retractors. An extension of this concept would be to develop an interchangeable tool attachment for the 3-D printed jaw-tip mount that enables changing tools autonomously. A novel Tool-Changing Adapter (TCA) is presented that mounts on an 8mm Needle Driver as shown in Figure 5.6. The tool changer can be used with a two- or three-arm surgical robot. Tools can be loaded onto the tool-changer and inserted into the body cavity through the cannula to be affixed to the surgical arm(s) already within he body. The tool changing attachment consists of an indexing channel and a finger-tip mount that interfaces to the 8 mm Needle Driver as discussed in section 5.4.

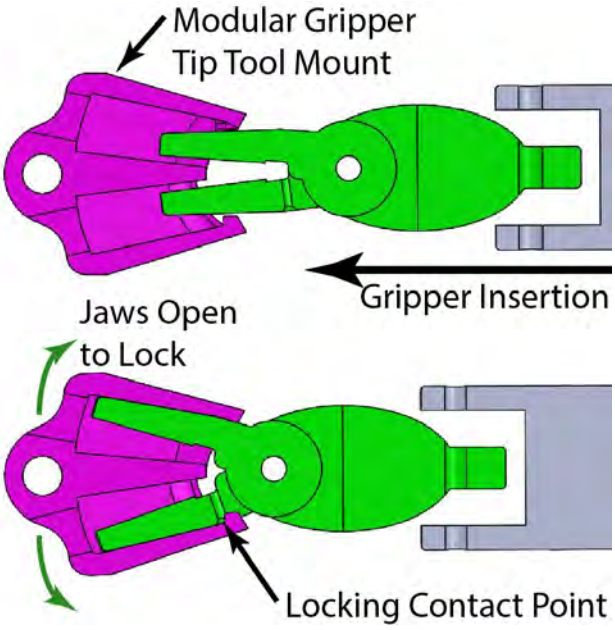

Figure 5.5: The Jaw-Tip mount allows a smaller form factor and can be 3D printed as a single piece shown in purple (requiring no additional manufacturing steps). This component can be added to surgical peripherals to interface the Robotic Surgical Assistant to a wide variety of user-defined devices.

Aspects of the TCA design that were motivated by autonomous robotic interaction are highlighted in Figure 5.6; in this figure, the orange arm is removing the palpation probe for use elsewhere in surgery and is the *retrieving* tool. The modular jaw-tip tool mount described in Section 5.4 can be used for the point of attachment for the TCA, and remains the starting point for additional modular tools. The *Retaining Catch* holds the jaw-tip mount in place during repeated tool exchanges; this is a passive fixation. The *Tool Return Guides* force the returning jaw-tip mount to mate with the base of the catch basin, indexing the jaw-tip mount for the next removal. The *Shaft Catch Basin* provides a large landing area for the retrieving surgical arm to mate with the TCA rather than attempting to visually servo the points of the gripper jaws into the jaw-tip mount. The *Gripper Ramp* passively forces the retrieving arm to rotate its shaft such that the tips of the gripper jaws insert properly within the retrieved tool. The *Indexing Slot* guides larger tools (such as the Palpation Probe shown in Figure 5.6) into place within the catch basin.

Autonomous Tool-Changing Evaluation: A static third arm was added to the DVRK as shown in blue in Figure 5.6 and is know as the *presenting arm*. The position of the

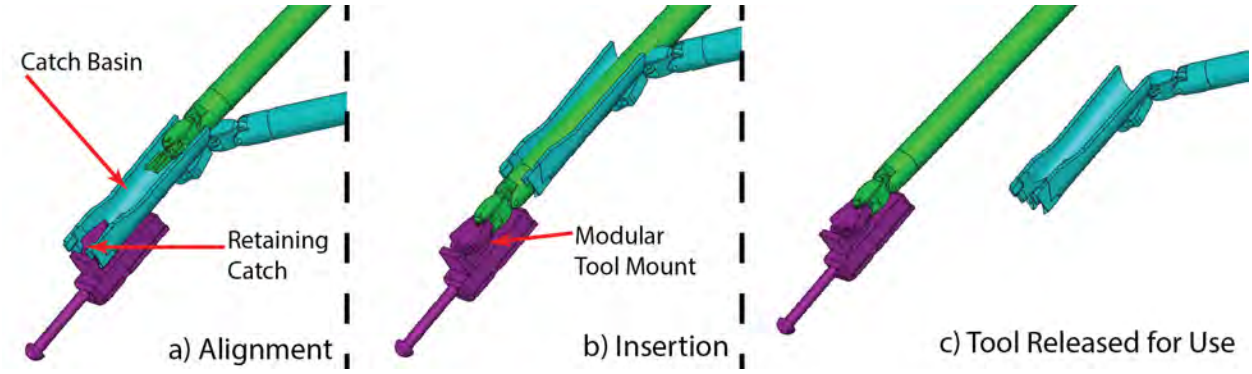

Figure 5.6: Changing tools within the body cavity could reduce surgical time. In this configuration the blue arm carries a new tool into the surgical workspace, the green arm interfaces with the tool and carries it to the point of use.

presenting arm was calibrated to the global coordinate frame of the DVRK by tele-operating the individual arms to the location of the indexing channel on the tool-changing interface. Once the location of the static presenting arm is known the tool change process is repeatable. Experiments demonstrated robust results by exceeding 30 repeated tool change operations with the same hardware being re-used. However, this trial was performed 'open-loop': once the position of the presenting arm deviates from the initial setup, all repeatability is lost. Further development of the TCA will include features that are designed to facilitate visual servoing of the retrieving arm into the Shaft Catch Basin.

5.6 Experiments

Tumor resection includes four sub tasks: *Palpation*, *Incision*, *Debridement*, and *Injection*. Palpation of tissues is a means by which surgeons verify the location of tumors to make precise incisions using their sense of touch. Retraction and debridement require the interaction of the dVRK with flexible tissues. Surgical adhesive applications require the placement of discrete amounts of fluid to precise locations.

Experimental Setup: The palpation probe was affixed to the 8mm Needle Driver (as shown in Figure 5.7) by manually placing the clevis-mounted probe below the surgical retractor, then prompting the jaws to open. The location of the flesh phantom was registered to the dVRK robot by manually tele-operating to the corners of the phantom and recording the global robot pose when palpation probe end effector distance was non-zero. These recorded points were used to fit a plane to the surface of the tissue.

For wound closure, an automated injection instrument with three components is presented: end-effector mounted needle (seen in Figure 5.1), a flexible catheter assembly, and a drive motor assembly mounted to the upper portion of the dVRK arm behind the sterile barrier. The Fluid Injector precision constraint is guided a theoretical dose volume of surgical glue (6 uL dose for each 2 mm of wound closure) based on clinical reports [82]. Injec-

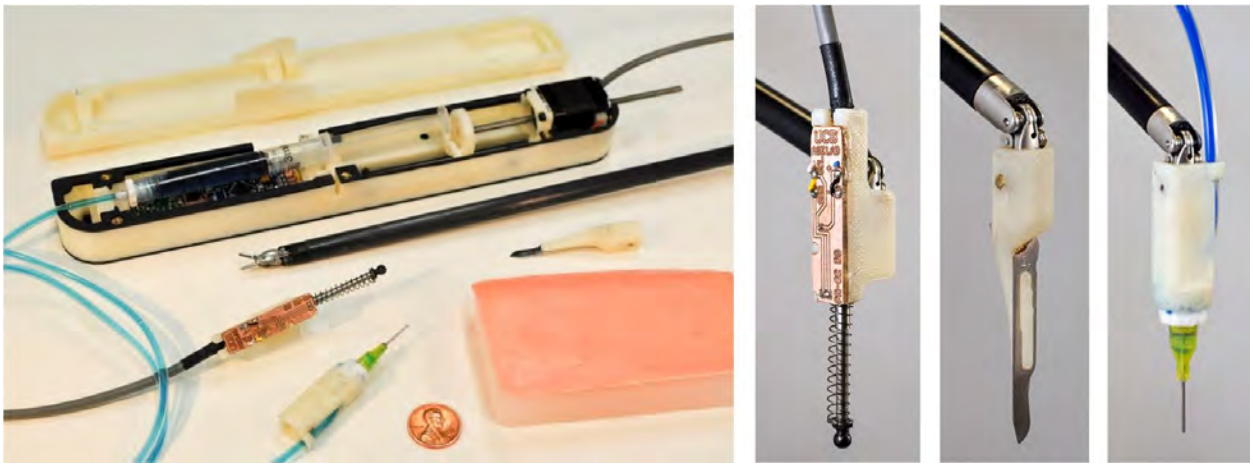

Figure 5.7: The suite of surgical tools created for increased autonomy in Robotic Minimally Invasive Surgery. **At Left:** The surgical adhesive injector and other tools shown with a US penny for scale. **At Right:** Tools mounted on a daVinci surgical retractor (featuring PALP, a scalpel, and FLIP)

tion force is provided by a Haydon-Kerk 21F4AC-2.5 linear actuator, powered by Allegro's A4988 micro-stepping bipolar stepper motor driver, and controlled by an Arduino Pro Mini 328 microcontroller. Syringes up to 10 mL in volume are carried by a 3D-printed enclosure along a linear stage which is mounted to the RSA arm.

Palpation: The dVRK retractor manipulates a palpation probe (as shown in Figure 5.2(d)) affixed to a modular instrument-tip mount to search for inclusions within a tissue phantom. The dVRK slides the lubricated end effector of the probe over the surface of the tissue in eight parallel passes while the end-effector deflection is recorded by the ROS node. Each parallel pass covers the entire 150 mm length of the tissue phantom (details in [97]). In each palpation pass the relatively stiff tumor causes a local maxima in end-effector displacement indicating the position of the tumor. Robot position data associated with the probe deflection data is used to filter out noisy data near the edges of the tissue where the probe loses contact with the surface of the tissue. In Figure 5.8(a), a haptic probe is shown palpating a flesh phantom; the position estimate of the underlying tumor is shown in the inset.

Incision: The surgical retractor is prompted to close and the palpation probe is detached and replaced with a clevis-mounted type-15 scalpel shown in Figure 5.1. A linear incision is made in the cutaneous phantom at a fixed offset from the estimated location of the tumor to create a retractable flap. The incision is performed in 1 cm linear slicing motions rather than incising continuously in one single pass because of friction at the blade-silicone interface. Once all the segments are complete, a finishing pass is made along the full length of the incision to ensure a single continuous incision.

Without jaw articulation, this instrument is used to cut only in lines parallel to the 'y' axis. A third redesign allows for full articulation (similar to the mount shown in Figure 5.2(e)).

Debridement - Retraction and Resection: After removing the clevis-mounted scalpel,

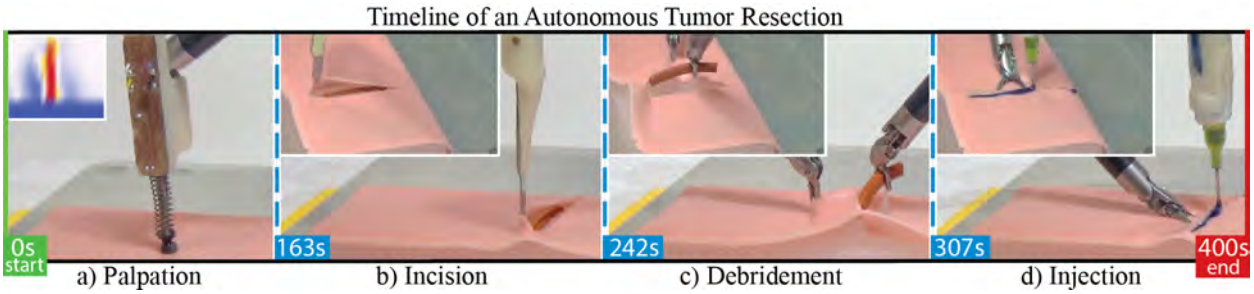

Figure 5.8: An autonomous simulated-tumor resection was performed using a suite of interchangeable instrument-tips and the da Vinci 8 mm Needle Driver; the dVRK performed a) Palpation with a haptic probe, b) Incision using a scalpel, c) Debridement using the Needle Drivers, and d) Injection of a surgical adhesive. Full video of the task is available at: http://bit.ly/29LhVXr

the left retractor grasps the cutaneous flap created during incision by moving to a pose below the surface of the tissue and closing the jaws then retracting the skin to reveal the tumor. The right arm approaches the tumor and uses repeated grasping-and-retracting motions to incrementally resect the tumor from the subcutaneous tissue before removing it from the workspace. Depth of each arm is controlled as offsets from the surface plane created during indexing.

Injection: In the final step, the clevis-mounted injector tip (shown in Figure 5.1) connected to the Fluid Injection Device is affixed to the surgical retractor on the right. The left surgical retractor then restores the skin flap to its original location before opening its jaws and depressing the cutaneous layer to stabilize the wound. The right arm uses the Fluid Injector to seal the incision with surgical adhesive. The needle tip passes over the incision at a constant rate as the externally mounted syringe pump injects the adhesive to facilitate uniform coverage of the incision site.

Design of Tissue Phantoms: Tissue phantoms as shown in Figure 5.8 were created for testing. A cylindrical tumor of Silicone Rubber (thickness 3 mm; Shore hardness 70A) was coated in Vaseline and placed in the bottom of a 100 mm long, 50 mm wide, 20 mm deep *Delrin* mold prior to casting. Silicone Rubber *Ecoflex 00-30* (*Smooth-On*) was cast into the mold to create subcutaneous tissue. After setting, the subcutaneous phantom was demolded and inverted. A cutaneous phantom was created using a stiffer (shore hardness 2A) *DragonSkin 10 Medium* Silicone Rubber (*Smooth-On*). Opaque pigmentation was achieved using a 0.5% by volume addition of Oil Pigment (Winton Oil Colour, Flesh Tint). The dermal layer was cast at a thickness of 1 mm into a *Delrin* mold (width 60 mm and length 100 mm). Upon solidification, the dermal phantom was overlaid on the subcutaneous phantom to create the final tissue phantom setup.

dVRK Hardware and Software: The Intuitive Surgical da Vinci Research Kit (dVRK) is used as described in [102] along with open-source electronics and software developed by WPI and Johns Hopkins University [72]. The software system is integrated with ROS, and controls robot pose in Cartesian space by interpolating between requested points. The manually created finite state machine consists of four segments with a manual tool change

start	Palpation	Tool Change	Incision	Tool Change	Debridement: Skin Retraction	Debridement: Tumor Resection	Tool Change	Injection	end
Trial 1	1:58	0:17	0:43	0:04	failed (0:31) - incorrect palpation estimate				FAILURE
2	1:58	0:18	0:51	0:03	0:49		0:11	1:03	SUCCESS
3	1:58	0:12	0:48	0:03	0:47		0:08	1:02	SUCCESS
4	1:58	0:15	0:47	0:06	failed (0:24) - improper skin retraction				FAILURE
5	1:58	0:19	0:55	0:03	0:49		0:06	1:06	SUCCESS
6	1:58	0:13	failed - incorrect palpation estimate						FAILURE
7	1:58	0:23	0:52	0:06	failed (0:29) - skin not grasped				FAILURE
8	1:58	0:23	0:51	0:03		failed (0:45) - tumor not grasped			FAILURE
9	1:58	0:17	0:56	0:03	0:51		0:08	1:05	SUCCESS
10	1:57	0:11	0:51	0:04	0:49		0:12	1:05	SUCCESS

Table 5.1: Autonomous Tumor Resection Open-Loop Automation Results and Sub-Task Timing (min:sec). The cause of failure for each trial is shaded in dark red. Visual feedback for the *Skin Retraction* subtask was implemented which raised success rates for the skin retraction phase to 100%. Visual feedback for tumor resection was implemented but did not yield greater accuracy.

occurring between each as described in Figure 5.8.

5.7 Experimental Results

Tumor Resection End-to-End Performance: The end-to-end tumor resection was repeated ten times with no prior knowledge of tumor location; results are tabulated in Table 5.1. Each phantom had a skin-phantom layer of thickness (1 mm +/- 0.25 mm), tumor-phantom 25 mm in length and 3 mm in diameter. Success was determined based on a complete tumor removal and wound closure. During trial 1 and trial 6, the position of the tumor was incorrectly estimated by the palpation probe resulting in respective failures in *Debridement* and *Incision*. In trial 4 and 7, the left retractor failed to grasp the dermal phantom fully and the tumor was not uncovered during skin retraction. In trial 8, the tumor was not fully resected from the flesh phantom during *Debridement*. Five of the ten trials were successful.

Visual Feedback: Four of five failures occurred in the debridement sub-task with two of these due to failure of the jaws to properly retract the skin layer before extracting the tumor. The system is sensitive to the insertion depth, which also varies with skin thickness, which varies from $1 - 2$ mm. Insertion too deep can cause pinching of the layer beneath the skin, preventing retraction, and if too shallow the jaws will fail to grasp the skin layer. The open-cv computer vision toolkit is used to create a visual feedback filter to detect if the tumor is properly revealed by thresholding on color in the zone below the gripper. If the tumor is not visible, the system increases the insertion depth by 1 mm and makes another attempt. In ten independent trials the system succeeded the first time only once. Eight trials required two attempts, and one trial required three attempts. All trials were able to successfully complete debridement with visual feedback. In future work more visual feedback conditions will be incorporated.

Palpation Subtask Evaluation: Metrics such as sensitivity to speed, sliding direction, inclusion diameter, and inclusion depth were evaluated in a prior study by the authors using a probe similar to that shown in Figure 5.2.c [97] (see Chapter 3).

Incision Subtask Evaluation: The scalpel attachment for the clevis-mount was successfully used in nine of the ten recorded trials while cutting through 1 mm thick silicone phantom skin. Incision failed (in the sixth trial) when palpation data created an incorrect target estimate.

Debridement Subtask Evaluation: A flesh phantom with tumors of known position and varying diameter (1, 2, 3 and 4) mm was created to test the efficacy of debridement strategies. In all trials, a single retraction (grasp-and-pull) attempt was found to be insufficient to resect the tumor from the flesh phantom. Using two attempts increased efficacy to 75%, and three attempts were successful in all of 20 trials.

Sensitivity to tumor diameter was tested using a 3-grasp-and-retract strategy on tumors of (1, 2, 3, and 4) mm. Retraction was successful in all of ten trials on each of the 1 mm, 2 mm, and 3 mm tumors; none of the 10 attempts for the 4 mm tumor were successful.

Sensitivity to approach accuracy to proper palpation-localization estimate was tested by offsetting the horizontal approach of the retractor by (0, 1, and 2) mm. After establishing a baseline approach that was successful in 10 out of 10 debridement trials at 0 mm horizontal offset, the success rate dropped to 25% at 1 mm offset, and 0% at 2 mm approach offset. This result suggests that the palpation estimate is within 1 mm from the true position. Debridement results may benefit from visual feedback.

Fluid Injection Subtask Evaluation: To test precision of volume injection, an array of small droplets was injected with the Fluid Injector (shown in Figure 5.1) onto an even surface and was visually measured by area from above; 24 drops were deposited at a mean overhead surface area of 37 mm^2 with 1.7 mm^2 standard deviation. A grid array target pattern was created to test the positional accuracy of the injection instrument and to evaluate its use in a tele-operated setting. The dVRK injected a pattern of droplets in a 3-by-3 grid covering an area of $20x16$ mm which was visually graded and compared to an expert demonstration provided by a surgeon who had been asked to place the same pattern of droplets via tele-operation of the dVRK in a $10x10$ mm area by sight. The expert demonstration had an average deviation from desired droplet position of 1.6 mm over 8 droplets; the autonomous injection was had an average deviation of 1.4mm over 8 droplets. These results suggest that the injection tool was useful in both tele-robotic and supervised autonomous control.

5.8 Discussion and Future Work

This chapter describes an interchangeable instrument system that can be contained within the body cavity. It is based on a novel mounting mechanism compatible with a standard RMIS gripper and tool-guide and sleeve to facilitate automated instrument switching. A prototype of the system on the dVRK with da Vinci Classic Large Needle Driver instruments

is evaluated. Experiments suggest that this interchangeable instrument system can perform a multi-step tumor resection procedure that uses a novel haptic probe to localize the tumor, standard scalpel to expose the tumor, standard grippers to extract the subcutaneous tumor, and a novel fluid injection tool to seal the wound. In future work additional experiments will be performed with tumor resection and other surgical procedures. Design files and fabrication instructions are available online at: http://berkeleyautomation.github.io/surgical-tools/.

Co-Design of Retractors and Mounts: In this work, we present interchangeable mounts to be self-actuating by using existing geometric features of the da Vinci Large Needle Driver jaws. If both the retractor (Needle Driver) jaws and the mount were co-designed, a smaller and more robust implementation of the interchangeable mount could be achieved. A consideration for retractor jaw redesign would be the introduction of a shoulder feature with inverted angle, γ, shown in Figure 5.5 allowing the mount to apply self-actuated forces inwards (pinching upon an internal support) rather than externally (wedging against an outer cavity) when the mount is exposed to a force in the positive 'x' direction (as shown in Figure 5.5).

Chapter 6: Alignment

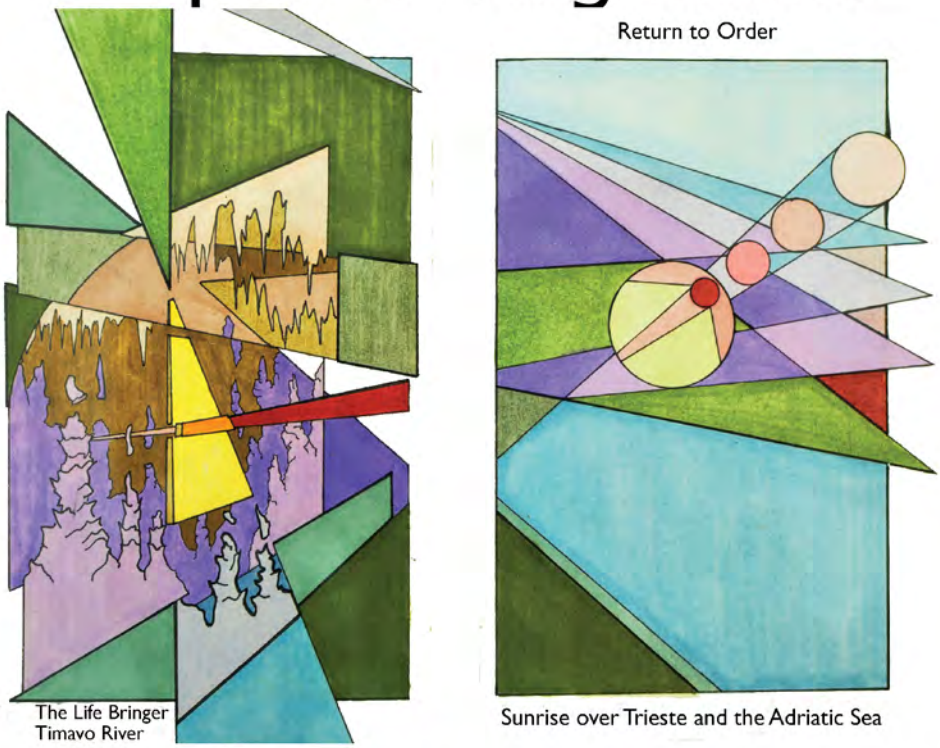

A Surgical Needle Positioner for RMIS

6.1 Overview

The designs presented in this dissertation focus on the demonstration of *tumor resection* as imagined in a silicone-phantom tumorectomy which includes four subtasks [37]: *Palpation*, *Incision*, *Debridement*, and *Closure*. In Chapter 5 a procedure was described which uses surgical adhesive as a closure method after excising a phantom tumor.

Suturing is a more common practice in clinical surgical interventions but is difficult to automate because of the small size of surgical needles. This chapter addresses the design and evaluation of a device for passively orienting a needle within the jaws of a surgical retractor to allow for automation of suturing. Refer to Sen et al. for more information on needle trajectory optimization and path planning using this device [136].

The Surgical Needle Positioner (SNAP) improved grasp repeatability by 10**x** and orientation accuracy by 3**x** as compared with standard 8mm needle driver. Utility of the SNAP was demonstrated on 4-throw suturing – a subtask from the Fundamental Skills of Robotic Surgery [146]. In physical experiments, the robot acheived a success rate of 50% for the 4-throw task and 86% of attempted suture throws were completed. The system is currently 3**x** slower than human surgeons [43].

6.2 Introduction and Related Work

The use of surgical adhesives is one of several clinically used methods for wound closure including staples and suturing [166]. Sutures have been used for autonomous anastamosis by Shademan et al in recent work which automated the placement and application of a standard laparoscopic surgical suturing tool (endoEvolution Endo360) in a living porcine intestine [137]. This work required a human to mark the contour of the flexible intestinal tissue with near infra red dye injections by hand before the algorithm autonomously positioned the device. This study highlights the importance of imaging within a surgical environment for the success of autonomy [179].

Suturing without specialized tools remains a difficult task to automate because of perception difficulties in small scale threads and needles. *Running Sutures* are a commonly used method for closing tissue in open and laparoscopic surgery and must be used in situations where both sides of the tissue are not accessible to a specialized tool (as used in [137]). Running sutures are beneficial for minimizing wound tension; and are frequently used in surgery for external tissues such as facial and abdominal [56], as well as for internal tissues such as intestinal anastomosis [19].

The *Fundamental Skills of Robotic Surgery* (FSRS), is a representative set of frequently occurring procedures in surgery, used for surgical training and evaluation [146]. Running a multi-throw suturing (MTS) is also one of the tasks described as fundamental to laparoscopic surgery.

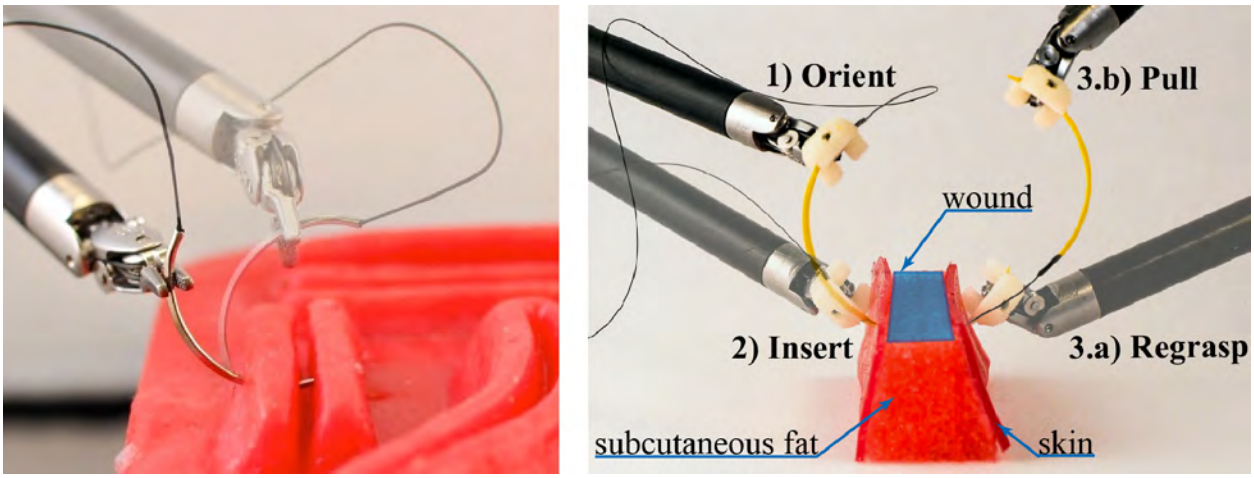

Figure 6.1: **Left:** Proper suturing is critical for scar-free surgery. **Right:** Each suturing throw consists of four steps: (1) Needle Orientation (2) Needle Push, (3.a) Needle Grasp, and (3.b) Suture Pull shown here in time-lapse view with two da Vinci Needle Driver tools. Step (4) Needle hand-off after the suture pull is not shown here. It also shows the experimental suturing setup developed for this dissertation: a tissue phantom which mimics two layers of skin surrounding subcutaneous fat.

A running suture subtask requires four surgemes: 1) Orientation of the needle; 2) Needle insertion; 3.a) Regrasping and 3.b) Pulling the thread through the tissue; and 4) Tying a

knot to secure the suture. The first three steps of this process are illustrated in Figure 6.1 and constitute a single *throw* of suturing. A *multi-throw* suture consists of multiple throws before ending with a knot to secure the wound.

Autonomous suturing algorithms have been proposed for a variety of hardware configurations. Knot tying using the Berkeley Surgical Robot [22] (see Section 2.1) was accomplished at super human speeds by van den Berg et al. using iterative learning control on human demonstrations [164]. Autonomous knot tying has also been accomplished on a modified Kuka industrial arm by Mayer et al. using a recurrent neural net trained on motion primitives from human demonstrations [91]. The needle insertion sugeme has been investigated on the modified Kuka system by Staub et al. [145]. Needle pass-through has been investigated as a human-robot collaboration on the daVinci Research Kit [114]. This demonstration shows partially autonomous suturing with human assistance during hand-off and needle insertion. Other groups have explored individual challenges in (a) interaction with deformable tissue [62, 63], (b) multilateral manipulation of needle and suture [145], and (c) hierarchical models for multi-step task planning [69].

Suturing success is dependent on planning complex needle motions, needle handling dexterity, and maintaining correct needle orientation during the needle insertion in tissue. Incorrect placement of the needle in the gripper may result in a bent needle, difficult skin penetration, or an undesirable tissue entry angle. However, maintaining and estimating needle orientation is a challenge without accurate needle tracking. Authors of [63] also note that a system for MTS would need both planning and visual feedback. There have been studies focusing on needle tracking within surgical settings as shown in [105, 143].

6.3 Motivation for SNAP

The difficulty faced in automating suturing has been the lack of perception at the scale of surgical needles (10mm) in surgical environments (with high specularity and noise). This limitation was illustrated in a 2013 case study by Schulman et al. who investigated algorithms for suturing using a learning by demonstration approach to warp recorded expert demonstrations and perform suturing in simulation. Schulman then implemented the learned trajectories on a large-scale experimental setup using the PR2 robot (see Figure 2.6) and knitting needles [135]. A key insight from this study is that the task of suturing could be learned and executed by an autonomous robot provided with adequate knowledge of needle pose and environmental state.

The motivation for the SNAP is to facilitate the automation of multi-throw running sutures by overcoming the perceptual deficiencies of the robotic surgical assistant.

Medical device manufacturers have explored the use of self-righting needle holders for manually held laparoscopic tools [90, 124]. However, these instruments have not been used for automated control and are not available for robotic MIS systems. There have been some commercial efforts to mitigate back-and forth hand-offs and uncertainty in laparoscopic surgery through passively orienting the needle upon gripper closure using a '*self-righting*'

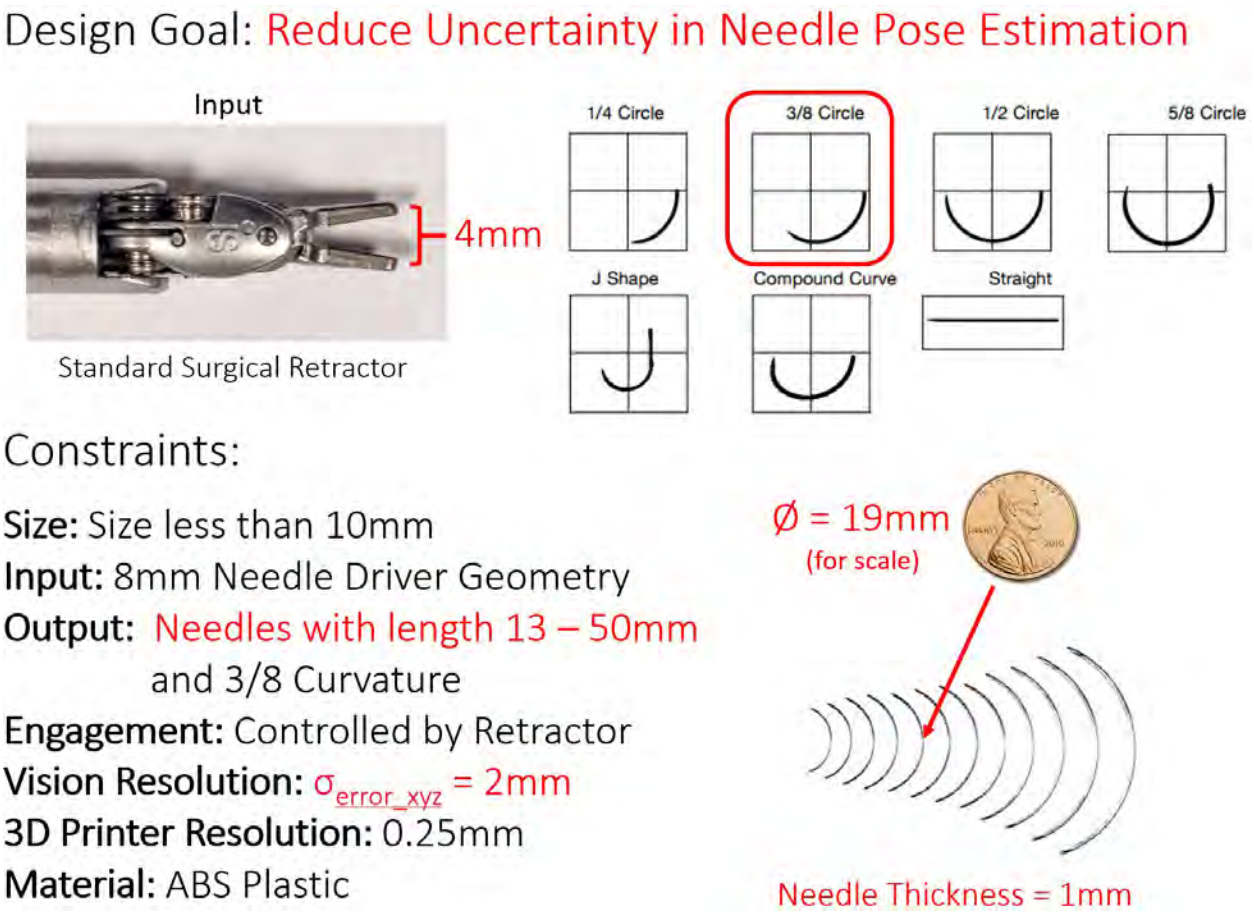

Figure 6.2: Design Goals for the Surgical Needle Alignment Positioner (SNAP)

gripper jaw design [90, 124]. However, these are not designed for automation, and require a complete tool-redesign.

6.4 SNAP Design Constraints

The design constraints of the SNAP are centered on the perception abilities of the vision algorithm (illustrated in Figure 6.3) and the comparative size of the surgical grippers and needles to be used. To determine the perception accuracy of the camera setup shown in Figure 6.3, a 30mm needle was held in the 8mm Needle Driver and moved to 20 poses within the surgical workspace. The standard deviation in needle position estimation (camera estimate with-respect-to surgical workspace) is shown in Table 6.1.

Based on the results from camera position estimation (Table 6.1), the SNAP needed to overcome 2mm of positional error in all axes, and up to 5 degrees of angular error. The input to the SNAP is an 8mm Needle driver (for consistency with the other tools used in the Tumor Resection), and the output devices are surgical needles of length 13 - 50mm with

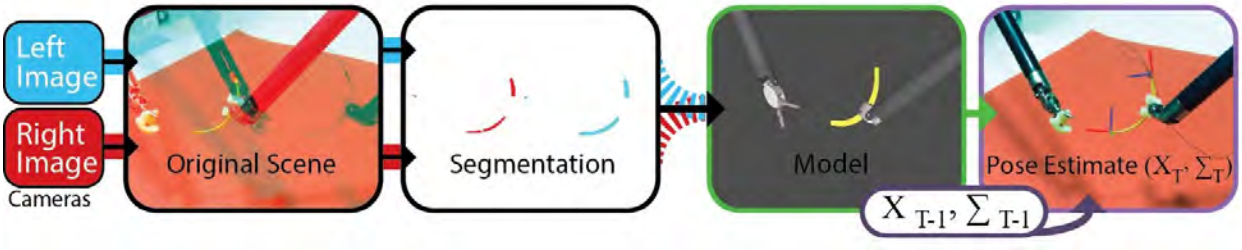

Figure 6.3: An estimate of the needle position within the surgical workspace found from segmented stereo images is combined (using a Kalman filter) with the pose model of the surgical grippers to determine the pose estimate for the needle.

Figure 6.4: Two Allied Vision Technologies Prosilica GC1290C were used to support stereoscopic vision during suturing experiments. These cameras were chosen because they can be set up with a larger baseline (distance between optics) than standard endoscopes.

	Position (mm)			Orientation (degrees)		
	x	y	z	Yaw	Pitch	Roll
Std. Dev.	2.182	1.23	1.54	2.495	4.699	4.329

Table 6.1: Error in Visual Pose Estimation (for 20 Trials)

3/8 curvature. The total size of the SNAP is to stay below 12mm in all dimensions to fit within the cannula for RMIS.

SNAP is mounted axially on one of the needle driver jaws. It is designed to guide the needle toward a groove running perpendicular to the length of the gripper jaws 6.5(b), (c). Upon closing the jaws, the needle rolls to a stable pose passing through contact points C_1 and C_2 as shown in the section view in 6.5(b).

The size of the needle gripper is parameterized by the distance between contact points C_1, C_2 which is dependent on the curvature of the needle – a needle with a larger radius needs a wider contact grasp to enable the needle rolling upon jaw closure. As illustrated in

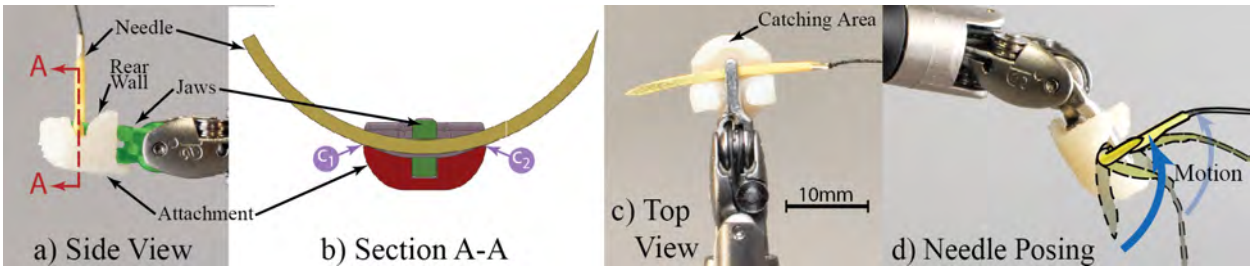

Figure 6.5: This figure illustrates the design and function of the Surgical Needle Angular Positioner (SNAP) made from 3D Printing. Figures (a) and (b) show a convex depression in which the needle rests upon gripper closure. Figure (d) shows a time-lapse figure of the gripper closing action on needle orientation.

Error in Stationary Grasp Orientation (Standard Deviation)

	Succ. Grasps	x (mm)	y (mm)	z (mm)	Yaw (deg)	Pitch (deg)	Roll (deg)
Without Snap	100%	2.511	1.434	4.838	20.547	7.584	6.472
With SNAP	100%	0.199	0.158	0.177	0.926	1.094	0.664

Error in Perturbed Grasp Orientation (Standard Deviation)

	Succ. Grasps	x (mm)	y (mm)	x (mm)	Yaw (deg)	Pitch (deg)	Roll (deg)
Without Snap	100%	2.01	2.59	5.95	15.54	12.74	7.62
With Snap	91.66%	1.58	1.15	1.19	5.55	3.97	6.34

Table 6.2: A comparison of error in stationary and perturbed grasp orientation before and after use of the SNAP.

the 6.5(a), SNAP has a rear-wall which allows the gripper to overshoot during the pre-grasp approach. It also has a needle *catching area* in the front (6.5(c)) which guides the needle in the groove compensating for undershoot during pre-grasp. These features increasing robustness of needle manipulation.

The SNAP is fabricated from ABS plastic using a Stratysys uPrint 3D printer. For an 8mm classic needle driver, using a $\frac{3}{8}$ circumference, 39mm length needle, the SNAP is designed with $C_1 - C_2$ span of 10mm. Through experimental evaluation, the SNAP design was improved to include a larger rear wall. This enables a wider jaw opening during approach allowing for larger tolerance in needle pose uncertainty.

The SNAP guides and passively re-orients a curved needle into a stable pose upon closure of gripper jaws as illustrated in 6.5(d). SNAP reduces needle pose uncertainty in two rotational axes as shown in Table 6.2. This allows for higher tolerances during needle hand-off, to relax accuracy requirements of needle tracking.

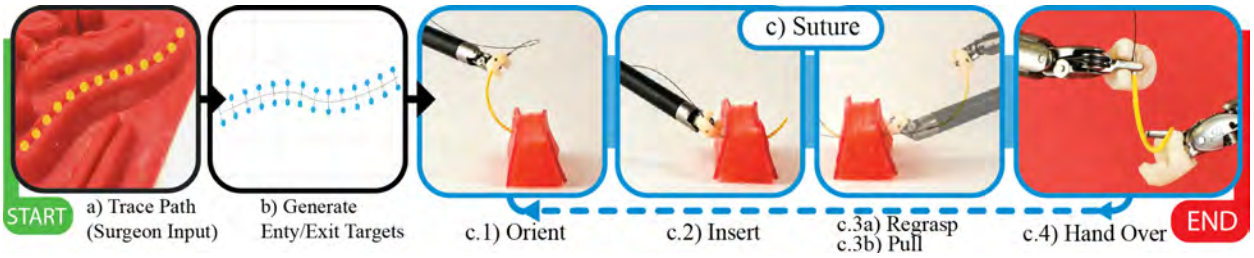

Figure 6.6: The Multi-Throw Suturing Finite State Machine. First, the surgeon specifies a wound shape along with wound width, depth, and suture pitch. Then, the system computes entry and exit points, and generates optimized trajectory and needle size for every suture throw. Then Single-throw Suture steps (c)-(f) are repeated with visual feedback for each suture throw until completion.

Evaluation of Surgical Needle Allignment Positioner (SNAP)

1. Stationary Needle Pick-up: The needle is placed in the same location for each trial. The robot is instructed to grasp the needle using the SNAP. After the needle is picked up, the robot brings the needle to a known location (with known gripper orientation) and the needle's pose is recorded using the needle tracker described in [136]. This process is repeated over ten trials. Due to noise in robot kinematics and needle starting pose, the needle is grasped slightly differently each time, resulting in variances in needle pose.

In the second part of the experiment, the orientation of the robot grasp pose is perturbed from -30 degrees to 30 degrees in yaw, pitch, and roll to evaluate robustness to uncertainty in orientation. The grasp pose is perturbed. Results show that the use of SNAP results in a 3x reduction in needle pose uncertainty over standard Needle Driver as shown in Table 6.2.

Robot Experiments: Four Throw Task

A suturing phantom (shown in Figure 6.1) was constructed using foam to mimic subcutaneous fat tissue and a layer of 1mm thick skin (shore hardness 2A) *DragonSkin 10 Medium* Silicone Rubber (*Smooth-On*).

In this experiment, the system tries to complete a closed loop four throw suturing task illustrated in Figure 6.6. The system is provided entry and exit poses on opposite surfaces of the tissue phantom as well as a desired suture depth. Based on the output needle curvature, a 39mm long, 3/8 reverse cutting needle is used to perform the suturing throws. For each trial time-to-completion is recoreded. The robot moves at a top speed of 3cm/s.

6.5 Conclusions and Future Work

Initial experiments suggest the multi-throw suturing (MTS) can be automated using the proposed framework but performance times are only 30% that of human tele-operation.

These observations suggest the use of SNAP along with Needle Tracking substantially improves needle orientations and enables automation of the MTS task. In future work, SNAP will be modified to enable knot tying.

Part 3: Frugal Design Theory

Chapter 7: Design

Riddarholms kyrkan, Stockholm

Balcony Study

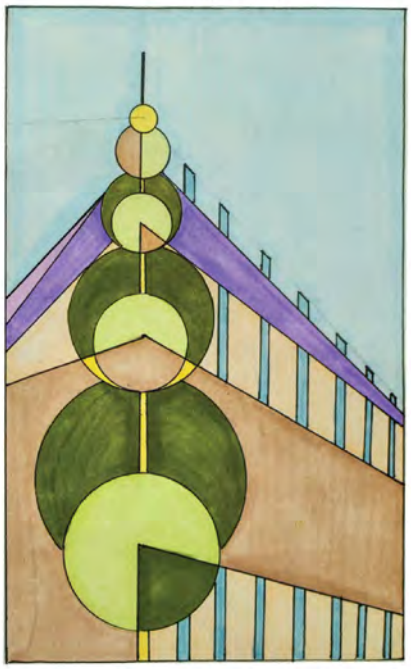

Kungsholmsgatan & Kungsgatan

Bauhaus in the Second Machine Age

7.1 Motivation for Formulation of Design Theory

A designer must understand the relationship between the user's aesthetic response to a creation and the creation's physical characteristics (including color, form, texture, size, context, etc). Design theory can be borne from artistic study in the systematic creation of physical objects with specific intent for evocation of user experience [163, p. 97]. In this chapter, examples of this form of study will be discussed.

Artwork included below represents a collection of the author's experimental work into the individual components of the artistic styles that merged to form the Bauhaus. For each piece, the specific design intent present will be discussed.

7.2 Background in the Bauhaus Design Theory

The Bauhaus existed to bridge art and design that the objects within our lives could be impactful [171]. Walter Gropius, director of the Bauhaus at its conception in 1919, actively worked to blur the boundaries between art, design, and engineering [112, p. 77]. As design

theory is the study surrounding the act of creation itself, it can be applied to analyse how objects can be designed to evoke emotions within their users. Just as a building or painting can inspire awe or reverence, so too can a designed product evoke a feeling of respect and identity (consider the iPod as a contemporary example of this attachment). See Veryzer et al. for an empirical study discussing the importance of aesthetics in form [168].

The style that Bauhaus popularized is 'functionalism,' which is aesthetic minimalism. Many of the designs created by the designers of the Bauhuas are still in use today. To understand this style's lasting efficacy, the author found it useful to prise apart the art theory behind the Bauhaus before applying it to engineering design.

A Brief Art History behind the Bauhaus

Artistically, a transition can be traced across the Machine Age through Impressionism (beginning in the 1860's) to Art Deco (ending in the 1940's) that can be classified as 'Expressionism'. The beginning of this movement can be associated with the posthumous dissemination of Vincent van Gogh's work in Germany and France [12, p. 56].

Figure 7.1: "Night Walk (Impressionism to Cubism)" *S. McKinley 2016* explores the relationship between color and depth in mapping hues of purple and brown to distance. The analogous constructavist rendition of the same scene uses layout and repetition to recreate a similar emotional response.

Although the movements that occurred during this time are primarily associated with decorative arts (such as painting), their influence extends to other forms of design including

prose, poetry, interior design, product design, and architecture.

Impressionism (1890-1910) and Cloisonnism (1900-1910):
Impressionism disregarded realism to explore the sensations evoked by a work of art. Unrealistic application of color and light were used to accentuate a desired aesthetic response (See Figure 7.1 left). Cloisonnism borrowed from Japanese wood block printing (typified in Ukiyo-e, a style that quickly gained popularity following the opening of Japan's border in 1868), merging areas of color into forms with bold outlines (see Figure 7.2). The fusion of Ukiyo-e with impressionism marked a shift in the way Western artists represented reality and began the era of modern art.

Figure 7.2: "Heron with Chrysanthemums" *S.McKinley, 2016* Impressionism was influenced by Japanese art, primarily woodblock printing, which studied the edge textures of forms in their interaction with light.

Cubism (1908-1919):
Cubism continued the work started by the late impressionists (especially Cezanne) and began creating work that served as representations of multiple viewpoints, whole time sequences, and freely associative volumes in space. Cubism, led by Picasso, Juan Gris, and George Braque, forced a viewer to consider multiple abstractions of a single object. This technique has direct application in engineering during the design process, when an initial problem statement is reconsidered (such as in TRIZ [3]). The artwork for the Chapter 4 header on page 35 is representative of cubism in a multi-view approach.

The cubist view was manifested in architecture and design through the Dutch movement of **De Stijl (1917-1931)** which created highly abstracted physical design forms. The cubist vision, while novel, did not necessarily yield forms of economy and so was less influential in conventional design.

Constructivism (Moscow) (1917):
Constructivism focused on designing pure forms so as to impact culture as a whole (without need for previous art theory). This led the constructivists to strive for aesthetic perfection and minimalism. The constructivist movement originated in Moscow during the Bolshevik revolution and was concerned with justifying the existence of an artist for a greater social good. This movement popularized the stark propaganda posters common with the Russian revolution and the USSR and celebrated technology as a liberating force for the worker.

Figure 7.1 (right) is a representation of the forest scene in constructivist style. The Chapter 7 and 6 headers on pages 61 and 52 are representative of constructivist design theory. Page layout and composition was chosen to fall along points of golden ratio intersections so

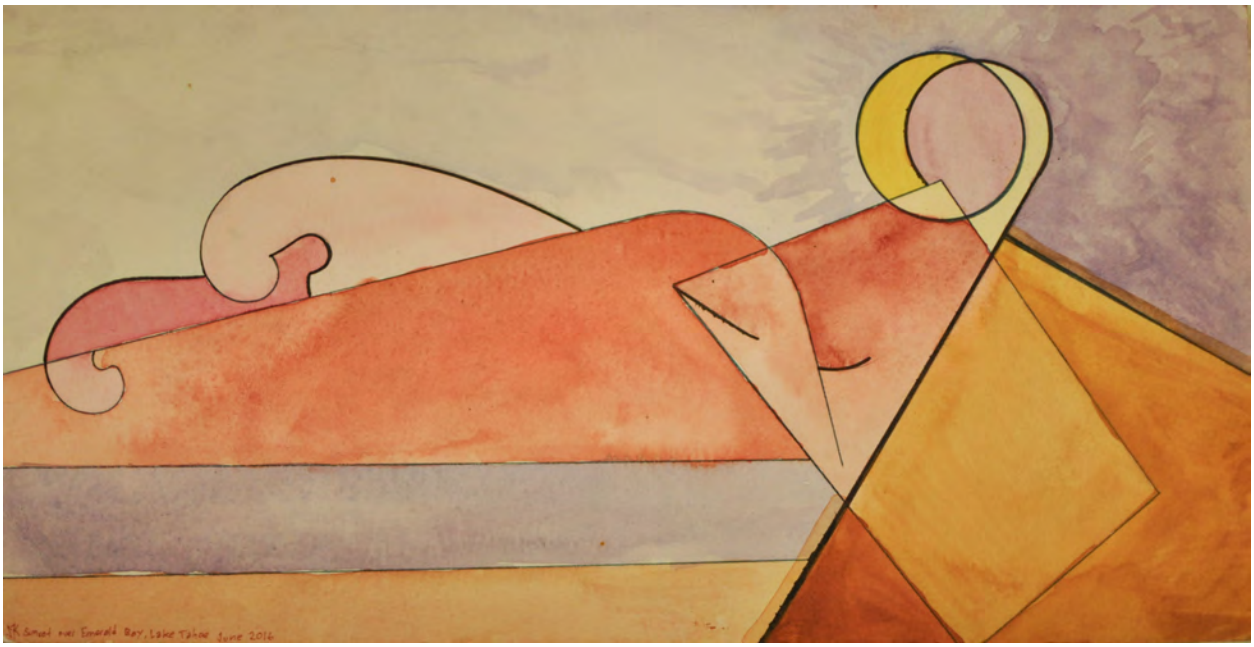

Figure 7.3: "Emerald Bay Moonrise" *S.McKinley 2016* presents a functionalist study of the sky during moonrise in the style of the Bauhaus.

as to be more readily experienced by a user.

Bauhaus (German) (1919-1933):
The Bauhaus brought together an eclectic group of designers from Europe and the United States under the banner of a reunification of art, craft, and design. The new approach in style borrowed from the De Stijl and Cubist movements in its abstraction of form into elemental form while simplifying the design to the fewest possible components necessary [9, p. 43]. An example of this style is shown in Figure 7.3.

The Bauhaus adopted the socialist intentions of the constructivists (born from the Bolshevik party in Moscow) but was quick to distance itself politically. What was left, is the ideology that designs should have impact societally, not simply serving as an outlet of expression for the artist.

On socially conscious art and design at the Bauhaus: ". . . [An] apolitical approach to art is a deception. Politics is not intended here in its sense of political parties but as a path to realizing ideals of the welfare of the general population." [171, p. 148]

The Bauhaus distanced itself from a purely artistic approach by focusing on applied design. Teaching workshops were expected to design objects that could be commercialized for a monetary return to support the institution. Faculty members were also encouraged to take commercial commissions (mostly for architecture) [171, p. 120].

7.3 Bauhaus Design Ideology

The Bauhaus also borrowed the celebration of technology from the constructavist movement (especially after the appointment of Lázló Muholy-Nagy as director of the Bauhaus Introductory Course).

Muholy-Nagy embodied the Bauhaus design ideal (the reunification of art and technology) by implementing production using artistically 'productive' design and thus relieving the act of creation from the constraints of consumerism [171, p. 135]. Specifically, Muholy-Nagy sought to lessen the creative constraints imposed by the ever-increasing mechanization of the machine age through the celebration of mass-production techniques.

Figure 7.4: "Human Augmentation I." *S.McKinley, 2016* The Bauhaus movement celebrated technological progress and the embraced the augmentation of man through machine. Robotic surgery represents a technology that can greatly improve the human experience through augmentation (as discussed in Chapter 2).

The 'Machine Age' lasted from 1880 to 1945 and described the era that gave rise to the telephone; mass marketing; consumerism; rapid travel by railroad, airplane, and automobile; war machines such as tanks, aircraft, and battleships; and mass production assembly lines. Increased automation in society brought about fears that human creativity would be usurped by mechanized production.

The term 'Robot' was fist used in 1921 in the title of the Czech play "Rossums Universal Robots" which depicted the invention of artificial workers who ultimately overthrow the human race. In the dawn of consumerism, mass production had allowed for the creation of great volumes of human artifacts. However, these were not aesthetically pleasing and did not connect with the human beings that used them. The Bauhaus was founded to train a generation of designers who would augment human creativity with the powerful new abilities of the Machine Age rather than allow human creativity be usurped (or comparatively undervalued) by mass production. The Bauhaus affinity for socialized design (as engendered by the constructivist movement) is similar to today's democratic design movement which enables the public to take part in a social design process [30].

7.4 Relating Abstract Art to Design

Designing objects (in engineering or art) relies on the repeated cycling in conceptualization and realization of imagined ideas. At the beginning of the design process, a need (represented by a string of words) is abstracted to be represented by many independent possibilities. These individual concepts can be written (such as finding analogies in poetry) or drawn (as imagined through artistic inference) to initially gauge their merit. Continued practice in abstraction without constraint (as in art) will allow for a designer to more confidently create without feeling the need to imitate existing solutions. Instead, the designer may realize new visions of reality [100].

> The engineer, inspired by the law of economy and governed by mathematical calculation, puts us in accord with universal law.
>
> *Le Corbusier*

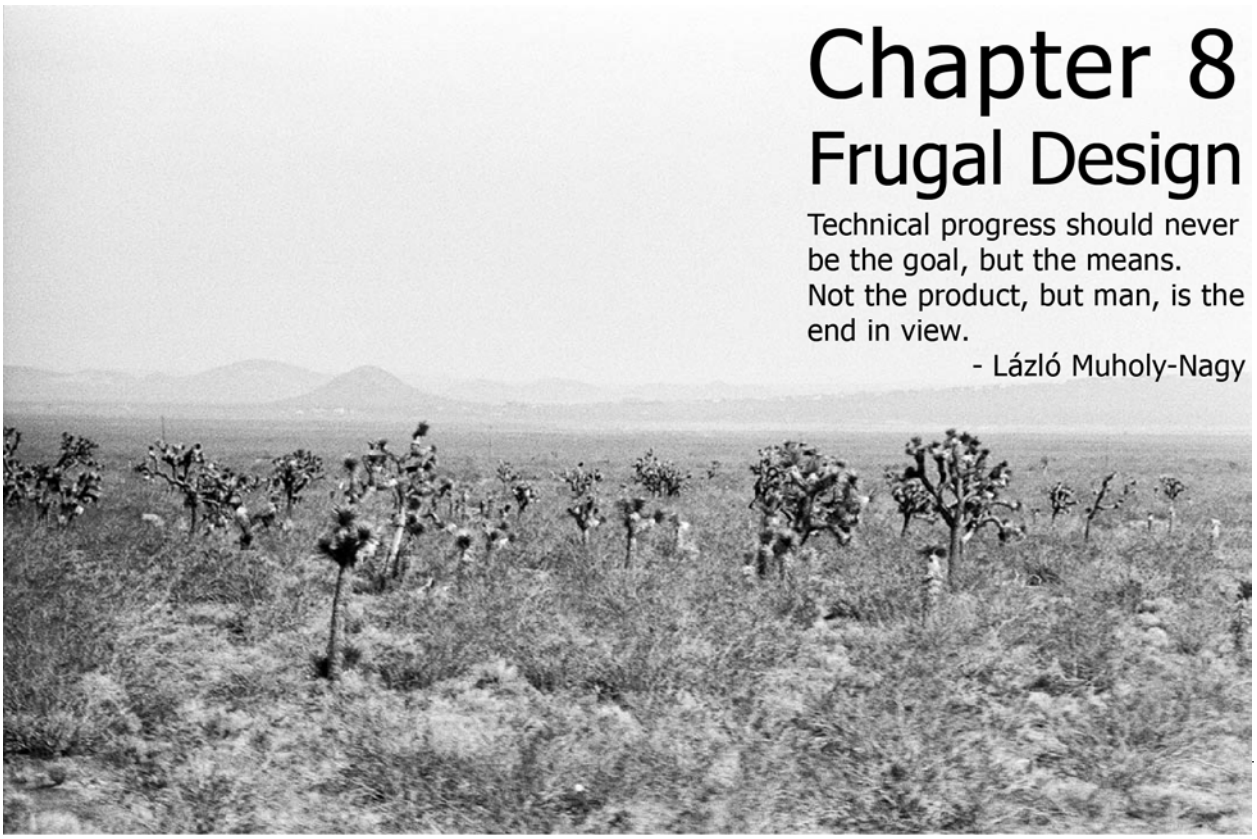

Relating the Bauhaus to Engineering

8.1 An Overview of Frugal Innovation in Existing Literature

'Frugal design' is functionalism (a Bauhaus design theory) with the direct goal of improving global accessibility to technology. This ideal can employ any other engineering design methodology for its purpose. In this design ideology a parallel can be made to the Bauhaus movement, who (as discussed in Chapter 7) had similar civic intentions to combat growing consumerism with functional inexpensive designs that appealed to the mass market [140].

Frugal innovation has been placed alongside the practices of 'inclusive', 'catalytic', 'trickle-up', and bottom of pyramid innovation in existing literature since the 1990's [15]. Frugal innovation can be thought of as a reaction against capitalist production (for explicit profit) in existing markets [178] and can be observed in the past as a cyclic response to economies of scarcity such as post-WWI Germany (creating the Bauhaus) or post-WWII Britain (Art-Deco) [16]. Recently, current developing economies in India, China and Africa exhibit similar 'Less-is-More' approaches to innovation [126].

The first instance of the term 'Frugal Innovation' was used by Wooldridge in 2010 for an article in *The Economist* to address several groups (including Tata and General Electric) who

were working to address significant health crises in India (heart disease and contaminated water) through frugal innovation by design teams stationed within the markets they hoped to serve [174]. The first use of the term 'Frugal Engineering' was made by Renault-Nissan CEO Carlos Ghosen (in 2009) to describe how the manufacturing processes of Indian auto manufacturers differed from their Chinese counterparts (which were modeled after Japanese and Western practices) [20].

8.2 Related Research in Frugal Innovation

Of specific interest to this dissertation, Zeschky et al. performed a case study of **frugal medical innovations** in emerging rural Chinese markets [178]. This study examined GE's portable ultrasound machine, Philip's bedside patient monitoring system, and Siemen's computed tomography scanner (among other non-medical products). With respect to medical equipment, Zeschky et al. cite difficulties faced by large traditional corporations in engaging the growing set of middle class users in developing areas. Firstly, corporations traditionally develop high-margin products for a few affluent users (in the case of medical devices, these are hospitals and clinics) rather than creating functionalist versions accessible to rural populations. The second, and more important challenge, is that most large corporations have central research and development divisions located near their headquarters geographically distanced from the needs of marginalized populations. Pearce addresses this concern with an extensive investigation of the (strongly positive) effects of decentralized Research and Development departments upon large Multi-National Enterprises [117].

Ray and Ray conducted a longitudinal study of corporate managers involved in technological development for developing rural Indian communications markets [128]. This work was focused on examining product design strategies for Indian telecommunications manufacturers to uncover how developers in resource-constrained environments continue to innovate. Ray identified three factors as critical: "entrepreneurial leadership and vision; modular designs to meet user demands of affordability, functionality and operability through architectural innovation; and the exploitation of the local knowledge base and the creation of local innovation clusters" [128].

Navi Radjou presented his qualitative experience on 'jugaad' innovation in a 2010 *Harvard Business Review* blog post [127] and a 2014 *TED Talk* [125]. 'Jugaad' is a Hindi-Urdu word that can mean an innovative fix or a simple work-around, used for solutions that bend rules to find solutions, a term similar to the definition of Frugal explored by this dissertation. Radjou et al. went on to connect 'jugaad' to 'Frugal Innovation' in a book on frugal innovation that extracted principles from a selection of case studies in product design for rural markets in India and Europe [126]. Among these principles are guidelines the author of this dissertation find useful for resource-limited innovation. These include: engaging and iterating upon design through user studies, using local assets and talent, focused development for future architecture, overcoming 'cheap' connotations of low-cost solutions for user adoption, and design team diversity [126].

The rules defined as 'jugaad' by Radjou are as follows [126]:

Thrift not waste. This first rule which promotes frugality helps tackle scarcity of all forms of resources.

Inclusion, not exclusion. This second rule helps entrepreneurial organizations put inclusiveness into practice by tightly connecting with, and harnessing, the growing diversity that permeates their communities of customers, employees, and partners.

Bottom-up participation, not top-down command and control. This third rule drives collaboration. CEOs who tend to act as conductors must learn to facilitate collaborative improvisation just as players in jazz bands do.

Flexible thinking and action, not linear planning. This fourth rule facilitates flexibility in thinking and action. Jugaad-practicing firms are highly adaptable as they are not joined to any single business model and pursue multiple options at any time.

Since 2002, Prahaled has promoted a Bottom of Pyramid approach to invigorating developing economies [121]. Alternate views to the success (and utility) of bottom of the pyramid approaches are provided by Jaiswal and Karnani [65, 70]. A positive case study of Chinese frugal innovation was undertaken by Hang et al. who posit that 'reverse innovation' will create simpler solutions to established economies [54], and can be thought of as a type of 'trickle up' innovation.

An Alternate (Negative View) of Frugal Innovation

Zeschky et al. (and much of the other related work cited above) view emerging markets as 'fertile ground' for frugal entrepreneurship [178]. Viewing an emerging market as 'fertile ground' suggests a capacity for exploitation of cultures eager to keep up with Western materialistic tastes. Indeed, Ray et al. focus their research on 'technocrats' with highly capitalist intentions in Indian Telecom markets [128]. Wooldrige (whose article coined the term 'frugal innovation') focused on the Shanzai entrepreneurs who bring technology to the rural masses through mass-production [174]. Wooldridge explores the term 'Shanzai' as the negative instantiation of entrepreneurship in a fringe market. Shanzai is a Chinese term that refers to the rapid (illegal) copying of consumer products developed by large corporations for resale into lower income markets. This practice is explored alongside 'jugaad' and 'frugal' innovation by Wooldridge [174], who emphasizes rule-breaking as a top priority of frugal development (the word 'Shanzai' literally refers to a mountain stronghold used by bandits). This practice is a good example of strongly capitalist predation on emerging markets by entrepreneurs.

8.3 Tenants of Frugal Design

0) Envision Accessibility

Frugal Design represents accessibility. A critical component of Frugal Design borrowed from the Bauhaus ideology discussed in the previous chapter is **social progressivism:** objects should not be created simply to be consumed by individuals with lower income, but are intended to help better their condition. Examples are discussed above in Related Work [174, 178].

1) Engage and Iterate

Design starts by interviewing potential users; observe natural behavior if possible. Consider how to create designs that are as relevant to the user as possible (instead of creating novel, but orthogonal solutions).

2) Use & Re-use local Assets

Re-use materials whenever possible. Develop a culture of rapid response to problems and embrace creative use of found objects. Whenever possible, use off-the-shelf solutions to minimize time (and money) wasted through resolving an existing solution. Use components from well-established high-volume industries (such as MEMS sensors from the automotive industry). Rapidly iterate on inexpensive prototypes using 3D printing, Circuit Board Printing, and cardboard/plywood prototyping.

3) Develop for future success

During the build process, create infrastructure to further continued growth. Modular solutions that adapt to subsequent improvements in technology are ideal in a resource-constrained environment [128].

4) Consider Presentation [163, p. 102]

Frugal does not mean 'cheap.' Strive to create objects that are visually appealing and aesthetically fluent (embrace Bauhaus functionalism). Allow your proof-of-concepts and novel devices to communicate their value to the users. There is never a need to apologize for an inexpensive prototype: instead, communicate what specific goals were being pursued by the project.

5) Collaborate Diversely

Build a design team that is vibrant, energetic, positive, and from a diverse set of backgrounds. There will always be more than one solution to a design problem; engaging a diverse team in solving a challenge will yield a more robust result.

8.4 Relating Frugal Design to Maker Culture

The Maker movement is a modern-day extension of the Do-It-Yourself (DIY) movement and the 'hacking' culture that surrounded early electronics community [152]. The success of the Maker movement has shown that individuals desire control over their environment and the devices they use [130]. This movement towards democratized design represents a reaction to current electronic device manufacturing practices of monolithic design (such as in the iPhone, which is very difficult to modify).

Additive manufacturing (3D Printing), digital design tools, internet community, and open-source hardware have opened a path for individuals to contribute to design. 'Democratic design, influenced by the entirety of a user-base creates a sense of communal connection to design. However, the Maker movement is primarily focused on empowering hobbyists [31], and democratic design can be detrimental to product design cycles [108]. Design convergence, in the democratic design setting, is dependent upon a small group of designers guiding the design process towards consensus. There are great benefits to the Maker movement: exposure to design knowledge among the general population will create a sustainable future [30] through the increased awareness that we may realize our individual desires or needs through design rather than continued consumption.

Frugal Design shares similar roots as the Maker movement. However, Frugal Design outlines explicit design considerations that exist beyond hobbyists and DIY access to fabrication.

[1] "Intuitive Surgical, EndoWrist®/Single-Site® Instrument & Accessory Catalog."

[2] R. Alterovitz and K. Goldberg, *Motion Planning in Medicine: Optimization and Simulation Algorithms for Image-guided Procedures.* Springer, 2008.

[3] G. Altshuller, L. Shulyak, and S. Rodman, *40 Principles: TRIZ keys to innovation.* Technical Innovation Center, Inc., 2002, vol. 1.

[4] J. Alvarez, G. Stahler, F. Barbagli, and C. Carlson, "Endoscopic robotic catheter system," Jan. 20 2011, US Patent App. 12/504,559.

[5] F. Anooshahpour, I. G. Polushin, and R. V. Patel, "Tissue compliance determination using a da vinci instrument," in *Robotics and Automation, 2015. ICRA 2015. IEEE International Conference on*, May 2015, pp. 5344–5349.

[6] *ST79-Comprehensive guide to steam sterilization and sterility assurance in health care facilities,*, ANSI/AAMI Std. ST79:2010/A4:2013.

[7] C. E. Attinger, E. Bulan, and P. A. Blume, "Surgical Debridement: The Key to Successful Wound Healing and Reconstruction," *Clinics in podiatric medicine and surgery*, vol. 17, no. 4, p. 599, 2000.

[8] G. H. Ballantyne, "The pitfalls of laparoscopic surgery: challenges for robotics and telerobotic surgery," *Surgical Laparoscopy Endoscopy & Percutaneous Techniques*, vol. 12, no. 1, pp. 1–5, 2002.

[9] M. Bax and J. J. van der Linden, *Bauhaus lecture notes, 1930-1933: ideal and practice of architectural training at the Bauhaus, based on the lecture notes made by the Dutch ex-Bauhaus student and architect JJ van der Linden of the Mies van der Rohe curriculum.* Architectura & Natura Press, 1991.

[10] R. A. Beasley, "Medical Robots: Current Systems and Research Directions," *Journal of Robotics*, vol. 2012, 2012.

[11] M. Beccani, C. Di Natali, L. J. Sliker, J. A. Schoen, M. E. Rentschler, and P. Valdastri, "Wireless tissue palpation for intraoperative detection of lumps in the soft tissue," *Biomedical Engineering, IEEE Transactions on*, vol. 61, no. 2, pp. 353–361, 2014.

[12] T. O. Benson, *Expressionism in Germany and France: From van Gogh to Kandinsky*. Los Angeles County Museum of Art, 2014.

[13] D. Berenson, P. Abbeel, and K. Goldberg, "A robot path planning framework that learns from experience," in *Robotics and Automation (ICRA), 2012 IEEE International Conference on*. IEEE, 2012, pp. 3671–3678.

[14] R. Berguer, D. Forkey, and W. Smith, "Ergonomic problems associated with laparoscopic surgery," *Surgical Endoscopy*, vol. 13, no. 5, pp. 466–468, 1999.

[15] Y. A. Bhatti, "What is frugal, what is innovation? towards a theory of frugal innovation," 2012.

[16] Y. A. Bhatti and M. Ventresca, "How can frugal innovationbe conceptualized?" *Available at SSRN 2203552*, 2013.

[17] A. Bolopion and S. Regnier, "A review of haptic feedback teleoperation systems for micromanipulation and microassembly," *Automation Science and Engineering, IEEE Transactions on*, vol. 10, no. 3, pp. 496–502, 2013.

[18] I. Brouwer, J. Ustin, L. Bentiey, A. Dhruv, and F. Tendick, "Measuring in vivo animal soft tissue properties for haptic modeling in surgical," in *Medicine meets virtual reality*, vol. 81, 2001, p. 69.

[19] J. M. Burch, R. J. Franciose, E. E. Moore, W. L. Biffl, and P. J. Offner, "Single-layer continuous versus two-layer interrupted intestinal anastomosis: a prospective randomized trial," *Annals of surgery*, 2000.

[20] G. "Carlos. (2009) Now is the time for the electric car. [Online]. Available: http://whr.tn/1GT17VM

[21] M. C. Çavusoglu, "Control of a telesurgical workstation," 1997.

[22] M. C. Cavusoglu, F. Tendick, M. Cohn, and S. S. Sastry, "A laparoscopic telesurgical workstation," *IEEE Transactions on Robotics and automation*, vol. 15, no. 4, pp. 728–739, 1999.

[23] M. C. Cavusoglu, J. Yan, and S. S. Sastry, "A hybrid system approach to contact stability and force control in robotic manipulators," in *Intelligent Control, 1997. Proceedings of the 1997 IEEE International Symposium on*. IEEE, 1997, pp. 143–148.

[24] T. G. Cooper, "Multi-component telepresence system and method," Oct. 17 2000, uS Patent 6,132,368.

[25] M. R. Cutkosky, R. D. Howe, and W. R. Provancher, "Force and tactile sensors," in *Springer Handbook of Robotics*. Springer, 2008, pp. 455–476.

[26] A. Darzi and Y. Munz, "The impact of minimally invasive surgical techniques," *Annu. Rev. Med.*, 2004.

[27] S. A. Darzi and Y. Munz, "The impact of minimally invasive surgical techniques," in *Annu Rev Med.*, vol. 55, 2004, pp. 223–237.

[28] B. Demi, T. Ortmaier, and U. Seibold, "The touch and feel in minimally invasive surgery," in *Haptic Audio Visual Environments and their Applications, 2005. IEEE International Workshop on.* IEEE, 2005, pp. 6–pp.

[29] S. M. Devine, A. M. Bartholomew, N. Mahmud, M. Nelson, S. Patil, W. Hardy, C. Sturgeon, T. Hewett, T. Chung, W. Stock *et al.*, "Mesenchymal stem cells are capable of homing to the bone marrow of non-human primates following systemic infusion," *Experimental Hematology*, vol. 29, no. 2, pp. 244–255, 2001.

[30] I. Digranes and L. B. Fauske, "The reflective citizen–general design education for a sustainable future," in *DS 62: Proceedings of E&PDE 2010, the 12th International Conference on Engineering and Product Design Education-When Design Education and Design Research meet..., Trondheim, Norway, 02.-03.09. 2010*, 2010.

[31] D. Dougherty, "The maker movement," *innovations*, vol. 7, no. 3, pp. 11–14, 2012.

[32] S. d.School". "design for extreme affordability". [Online]. Available: "http: //extreme.stanford.edu/course-information"

[33] G. Dulan, R. V. Rege, D. C. Hogg, K. M. Gilberg-Fisher, N. A. Arain, S. T. Tesfay, and D. J. Scott, "Developing a Comprehensive, Proficiency-based Training Program for Robotic Surgery," *Surgery*, vol. 152, no. 3, pp. 477–488, 2012.

[34] A. Escoto, S. Bhattad, A. Shamsil, A. Sanches, A. L. Trejos, M. D. Naish, R. A. Malthaner, and R. V. Patel, "A multi-sensory mechatronic device for localizing tumors in minimally invasive interventions," in *Robotics and Automation, 2015. ICRA 2015. IEEE International Conference on*, May 2015, pp. 4742–4747.

[35] R. S. Fearing, "Tactile sensing mechanisms," *The International Journal of Robotics Research*, vol. 9, no. 3, pp. 3–23, 1990.

[36] R. S. Fearing and J. M. Hollerbach, "Basic solid mechanics for tactile sensing," *The International journal of robotics research*, vol. 4, no. 3, pp. 40–54, 1985.

[37] Y. Fong, W. Jarnagin, K. Conlon, R. DeMatteo, E. Dougherty, and L. Blumgart, "Hand-assisted laparoscopic liver resection: Lessons from an initial experience," *Archives of Surgery*, 2000.

[38] A. J. Friedenstein, K. V. Petrakova, A. I. Kurolesova, and G. P. Frolova, "Heterotopic transplants of bone marrow." *Transplantation*, vol. 6, no. 2, pp. 230–247, 1968.

[39] D. C. Friedman, J. Dosher, T. Kowalewski, J. Rosen, and B. Hannaford, "Automated tool handling for the trauma pod surgical robot," in *ICRA*, 2007.

[40] L. M. Funk, T. G. Weiser, W. R. Berry, S. R. Lipsitz, A. F. Merry, A. C. Enright, I. H. Wilson, G. Dziekan, and A. A. Gawande, "Global operating theatre distribution and pulse oximetry supply: an estimation from reported data," *The Lancet*, vol. 376, no. 9746, pp. 1055–1061, 2010.

[41] N. Futai, K. Matsumoto, and I. Shimoyama, "A flexible micromachined planar spiral inductor for use as an artificial tactile mechanoreceptor," *Sensors and Actuators A: Physical*, vol. 111, no. 2, pp. 293–303, 2004.

[42] J. B. Gafford, S. B. Kesner, A. Degirmenci, R. J. Wood, R. D. Howe, and C. J. Walsh, "A monolithic approach to fabricating low-cost, millimeter-scale multi-axis force sensors for minimally-invasive surgery," in *Robotics and Automation (ICRA), 2014 IEEE International Conference on*. IEEE, 2014, pp. 1419–1425.

[43] Y. Gao, S. S. Vedula, C. E. Reiley, N. Ahmidi, B. Varadarajan, H. C. Lin, L. Tao, L. Zappella, B. Béjar, D. D. Yuh *et al.*, "Jhu-isi gesture and skill assessment working set (jigsaws): A surgical activity dataset for human motion modeling," *Modeling and Monitoring of Computer Assisted Interventions*, pp. 1–10, 2014.

[44] A. Garg, S. Sen, R. Kapadia, Y. Jen, S. McKinley, L. Miller, and K. Goldberg, "Tumor localization using automated palpation with gaussian process adaptive sampling," *International Conference on Automation Science and Engineering (CASE)*, 2016.

[45] D. V. Gealy, S. A. McKinley, M. Guo, L. Miller, S. Vougioukas, J. Viers, S. Carpin, and K. Goldberg, "Co-robotic device for automated tuning of emitters to enable precision irrigation." *IEEE International Conference on Automation Science and Engineering (CASE)*, 2016.

[46] P. S. Girão, P. M. P. Ramos, O. Postolache, and J. M. D. Pereira, "Tactile sensors for robotic applications," *Measurement*, vol. 46, no. 3, pp. 1257–1271, 2013.

[47] P. H. Gleick, "Water use," *Annual Review of Environment and Resources*, vol. 28, no. 1, pp. 275–314, 2003.

[48] R. E. Goldman, A. Bajo, and N. Simaan, "Algorithms for autonomous exploration and estimation in compliant environments," *Robotica*, vol. 31, no. 01, pp. 71–87, 2013.

[49] M. Granick, J. Boykin, R. Gamelli, G. Schultz, and M. Tenenhaus, "Toward a Common Language: Surgical Wound Bed Preparation and Debridement," *Wound repair and regeneration*, 2006.

[50] E. Graves, "Vital and health statistics," *Data from the National Health Survey*, no. 122, 1993.

[51] B. L. Gray and R. S. Fearing, "A surface micromachined microtactile sensor array," in *Robotics and Automation, 1996. Proceedings., 1996 IEEE International Conference on*, vol. 1. IEEE, 1996, pp. 1–6.

[52] P. Green, "Advanced teleoperator technology for enhanced minimally invasive surgery," in *Proc. Medicine Meets Virtual Reality Conference*, 1992, pp. 4–7.

[53] J. C. Gwilliam, Z. Pezzementi, E. Jantho, A. M. Okamura, and S. Hsiao, "Human vs. robotic tactile sensing: Detecting lumps in soft tissue," in *Haptics Symposium, 2010 IEEE*. IEEE, 2010, pp. 21–28.

[54] C.-C. Hang, J. Chen, and A. M. Subramian, "Developing disruptive products for emerging economies: Lessons from asian cases," *Research-Technology Management*, vol. 53, no. 4, pp. 21–26, 2010.

[55] W. Hayes, L. Keer, G. Herrmann, and L. Mockros, "A mathematical analysis for indentation tests of articular cartilage," *Journal of biomechanics*, vol. 5, no. 5, pp. 541–551, 1972.

[56] J. Hochberg, K. M. Meyer, and M. D. Marion, "Suture choice and other methods of skin closure," *Surgical Clinics of North America*, vol. 89, no. 3, pp. 627–641, 2009.

[57] R. Howitt, J. Medellin-Azuara, D. MacEwan, J. Lund, and D. Sumner, "Economic analysis of the 2014 drought for california agriculture," *Center for Watershed Sciences, University of California, Davis*, 2014.

[58] D. Hu, Y. Gong, B. Hannaford, and E. J. Seibel, "Semi-autonomous simulated brain tumor ablation with ravenii surgical robot using behavior tree," in *IEEE Int. Conf. Robotics and Automation*, 2015.

[59] Y. Hu, R. Katragadda, H. Tu, Q. Zheng, Y. Li, and Y. Xu, "Bioinspired 3-d tactile sensor for minimally invasive surgery," *Microelectromechanical Systems, Journal of*, vol. 19, no. 6, pp. 1400–1408, Dec 2010.

[60] R. Ibrayev and Y.-B. Jia, "Recognition of curved surfaces from one-dimensional tactile data," *Automation Science and Engineering, IEEE Transactions on*, vol. 9, no. 3, pp. 613–621, 2012.

[61] Intuitive Surgical, "Annual report 2014," 2014. [Online]. Available: http://investor.intuitivesurgical.com/phoenix.zhtml?c$=122359$|&p=irol-IRHome

[62] M. C. Jackson, Russell C.and Cavusoglu, "Modeling of needle-tissue interaction forces during surgical suturing," in *2012 IEEE International Conference on Robotics and Automation (ICRA)*, 2012.

[63] R. C. Jackson and M. C. Cavusoglu, "Needle path planning for autonomous robotic surgical suturing," in *ICRA*. IEEE, 2013, pp. 1669–1675.

[64] B. Jaffray, "Minimally invasive surgery," *Archives of disease in childhood*, vol. 90, no. 5, pp. 537–542, 2005.

[65] A. K. Jaiswal, "Fortune at the bottom of the pyramid: An alternate perspective," *Indian Institute of Management*, 2007.

[66] R. Jansen, K. Hauser, N. Chentanez, F. van der Stappen, and K. Goldberg, "Surgical retraction of non-uniform deformable layers of tissue: 2d robot grasping and path planning," in *2009 IEEE/RSJ International Conference on Intelligent Robots and Systems*. IEEE, 2009, pp. 4092–4097.

[67] P. Joice, G. Hanna, and A. Cuschieri, "Errors enacted during endoscopic surgerya human reliability analysis," *Applied ergonomics*, vol. 29, no. 6, pp. 409–414, 1998.

[68] Y. Jung, G. Bauer, and J. A. Nolta, "Concise review: Induced pluripotent stem cell-derived mesenchymal stem cells: progress toward safe clinical products," *Stem cells*, vol. 30, no. 1, pp. 42–47, 2012.

[69] H. Kang and J. T. Wen, "Autonomous suturing using minimally invasive surgical robots," in *Control Applications, 2000. Proceedings of the 2000 IEEE International Conference on*. IEEE, 2000, pp. 742–747.

[70] A. Karnani, "The mirage of marketing to the bottom of the pyramid: How the private sector can help alleviate poverty," *California management review*, vol. 49, no. 4, pp. 90–111, 2007.

[71] J. M. Karp and G. S. L. Teo, "Mesenchymal stem cell homing: the devil is in the details," *Cell stem cell*, vol. 4, no. 3, pp. 206–216, 2009.

[72] P. Kazanzides, Z. Chen, A. Deguet, G. S. Fischer, R. H. Taylor, and S. P. DiMaio, "An open-source research kit for the da vinci® surgical system," in *IEEE Int. Conf. Robotics and Automation (ICRA)*, 2014.

[73] B. Kehoe, G. Kahn, J. Mahler, J. Kim, A. Lee, A. Lee, K. Nakagawa, S. Patil, W. D. Boyd, P. Abbeel *et al.*, "Autonomous multilateral debridement with the raven surgical robot," in *2014 IEEE International Conference on Robotics and Automation (ICRA)*. IEEE, 2014, pp. 1432–1439.

[74] T. Kheir, "Multi-purpose minimally invasive instrument that uses a micro entry port," Feb. 23 2010, uS Patent 7,666,181.

[75] J. Konstantinova, A. Jiang, K. Althoefer, P. Dasgupta, and T. Nanayakkara, "Implementation of tactile sensing for palpation in robot-assisted minimally invasive surgery: A review," *Sensors Journal, IEEE*, vol. 14, no. 8, pp. 2490–2501, Aug 2014.

[76] M. Kranzfelder, C. Staub, A. Fiolka, A. Schneider, S. Gillen, D. Wilhelm, H. Friess, A. Knoll, and H. Feussner, "Toward increased autonomy in the surgical or: needs, requests, and expectations," *Surgical endoscopy*, 2013.

[77] E. Kroll, S. S. Condoor, and D. G. Jansson, *Innovative conceptual design: theory and application of parameter analysis.* Cambridge University Press, 2001.

[78] M. Laskey, J. Lee, C. Chuck, W. Hseih, F. T. Pokorny, A. D. Dragan, and K. Goldberg, "Robot grasping in clutter: Using a hierarchy of supervisors for learning from demonstrations." *IEEE International Conference on Automation Science and Engineering (CASE)*, 2016.

[79] M. Laskey, S. Staszak, W. Hseih, J. Mahler, F. T. Pokorny, A. D. Dragan, and K. Goldberg, "Shiv: Reducing supervisor burden in dagger using support vectors for efficient learning from demonstrations in high dimensional state spaces." *IEEE International Conference on Robotics and Automation (ICRA)*, 2016.

[80] H. Liu, J. Li, X. Song, L. D. Seneviratne, and K. Althoefer, "Rolling indentation probe for tissue abnormality identification during minimally invasive surgery," *Robotics, IEEE Transactions on*, vol. 27, no. 3, pp. 450–460, 2011.

[81] H. Liu, D. P. Noonan, B. J. Challacombe, P. Dasgupta, L. D. Seneviratne, and K. Althoefer, "Rolling mechanical imaging for tissue abnormality localization during minimally invasive surgery," *Biomedical Engineering, IEEE Transactions on*, vol. 57, no. 2, pp. 404–414, 2010.

[82] P. Losi, S. Burchielli, D. Spiller, V. Finotti, S. Kull, E. Briganti, and G. Soldani, "Cyanoacrylate surgical glue as an alternative to suture threads for mesh fixation in hernia repair," *Journal of Surgical Research*, 2010.

[83] E. Lupton and J. A. Miller, *ABC's of the Bauhaus: The Bauhaus and Design Theory.* Princeton Architectural Press, 1991.

[84] A. J. Madhani and J. K. Salisbury, "Articulated surgical instrument for performing minimally invasive surgery with enhanced dexterity and sensitivity," Aug. 11 1998, uS Patent 5,792,135.

[85] ——, "Force-reflecting surgical instrument and positioning mechanism for performing minimally invasive surgery with enhanced dexterity and sensitivity," Sep. 15 1998, uS Patent 5,807,377.

[86] ——, "Wrist mechanism for surgical instrument for performing minimally invasive surgery with enhanced dexterity and sensitivity," Aug. 25 1998, uS Patent 5,797,900.

[87] J. Mahler, S. Krishnan, M. Laskey, S. Sen, A. Murali, B. Kehoe, S. Patil, J. Wang, M. Franklin, P. Abbeel *et al.*, "Learning accurate kinematic control of cable-driven surgical robots using data cleaning and gaussian process regression," in *2014 IEEE International Conference on Automation Science and Engineering (CASE)*. IEEE, 2014, pp. 532–539.

[88] J. Mahler, F. T. Pokorny, B. Hou, M. Roderick, M. Laskey, M. Aubry, K. Kohlhoff, T. Kröger, J. Kuffner, and K. Goldberg, "Dex-net 1.0: A cloud-based network of 3d objects for robust grasp planning using a multi-armed bandit model with correlated rewards," *ICRA*.

[89] J. Mahler, F. T. Pokorny, S. Niyaz, and K. Goldberg, "Synthesis of energy-bounded planar caging grasps using persistent homology." *Workshop on the Algorithmic Foundations of Robotics (WAFR)*, 2016.

[90] D. T. Martin, J. A. Woodard, C. J. Shurtleff, and A. C. Yoo, "Articulating needle driver," Tech. Rep., 2012.

[91] H. Mayer, F. Gomez, D. Wierstra, I. Nagy, A. Knoll, and J. Schmidhuber, "A system for robotic heart surgery that learns to tie knots using recurrent neural networks," *Advanced Robotics*, vol. 22, no. 13-14, pp. 1521–1537, 2008.

[92] G. L. McCreery, A. L. Trejos, M. D. Naish, R. V. Patel, and R. A. Malthaner, "Feasibility of locating tumours in lung via kinaesthetic feedback," *The International Journal of Medical Robotics and Computer Assisted Surgery*, vol. 4, no. 1, pp. 58–68, 2008.

[93] D. McKay and G. Blake, "Optimum incision length for port insertion in laparoscopic surgery," *Annals of the Royal College of Surgeons of England*, vol. 88, no. 1, p. 78, 2006.

[94] S. McKinley, A. Garg, S. Lim, S. Patil, and K. Goldberg, "Automated delivery instrument for stem cell treatment using the da vinci robotic surgical system," http://bit.ly/29Kzog2, 2015, poster presented at International Society for Stem Cell Research Conference 2015, Stockholm, Sweeden.

[95] S. McKinley, A. Garg, J. McKinley, Y. Jen, D. Gealy, D. J. Boyd, P. Abbeel, and K. Goldberg, "Robot-assisted surgery: Autonomous tumor localization and extraction," http://bit.ly/29LhVXr, 2016, best Video Winner at Hamlyn Surgical Challenge 2015.

[96] S. McKinley, A. Garg, S. Sen, D. V. Gealy, J. P. McKinley, Y. Jen, M. Guo, D. Boyd, and K. Goldberg, "An interchangeable surgical instrument system with application to supervised automation of multilateral tumor resection," *International Conference on Automation Science and Engineering (CASE)*, 2016.

[97] S. McKinley, A. Garg, S. Sen, R. Kapadia, A. Murali, K. Nichols, S. Lim, S. Patil, P. Abbeel, A. M. Okamura, and K. Goldeberg, "A disposable haptic palpation probe for locating subcutaneous blood vessels in robot-assisted minimally invasive surgery," in *CASE*, 2015.

[98] S. McKinley, S. Sen, A. Garg, Y. Jen, D. Gealy, P. Abbeel, and K. Goldberg, "Autonomous Tumor Localization and Extraction: Palpation, Incision, Debridement and Adhesive Closure with the da Vinci Research Kit," June 2015, Hamlyn Surgical Robotics Conference, London. [Online]. Available: j.mp/palpation-vid

[99] D. J. Miller, C. A. Nelson, and D. Oleynikov, "Shortened OR time and decreased patient risk through use of a modular surgical instrument with artificial intelligence," *Surgical endoscopy*, vol. 23, 2009.

[100] L. Moholy-Nagy, "In defense of" abstract" art," *The Journal of Aesthetics and Art Criticism*, vol. 4, no. 2, pp. 74–76, 1945.

[101] G. Moustris, S. Hiridis, K. Deliparaschos, and K. Konstantinidis, "Evolution of autonomous and semi-autonomous robotic surgical systems: a review of the literature," *The International Journal of Medical Robotics and Computer Assisted Surgery*, 2011.

[102] A. Murali, S. Sen, B. Kehoe, A. Garg, S. McFarland, S. Patil, W. D. Boyd, S. Lim, P. Abbeel, and K. Goldberg, "Learning by observation for surgical subtasks: Multilateral cutting of 3d viscoelastic and 2d orthotropic tissue phantoms," in *2015 IEEE International Conference on Robotics and Automation (ICRA)*. IEEE, 2015, pp. 1202–1209.

[103] Y. Murayama, M. Haruta, Y. Hatakeyama, T. Shiina, H. Sakuma, S. Takenoshita, S. Omata, and C. E. Constantinou, "Development of a new instrument for examination of stiffness in the breast using haptic sensor technology," *Sensors and Actuators A: Physical*, vol. 143, no. 2, pp. 430–438, 2008.

[104] G. F. Muschler, C. Nakamoto, and L. G. Griffith, "Engineering principles of clinical cell-based tissue engineering," *The Journal of Bone & Joint Surgery*, vol. 86, no. 7, pp. 1541–1558, 2004.

[105] F. Nageotte, C. Doignon, M. de Mathelin, P. Zanne, and L. Soler, "Circular needle and needle-holder localization for computer-aided suturing in laparoscopic surgery," pp. 87–98.

[106] K. Nichols, A. M. Okamura *et al.*, "Methods to segment hard inclusions in soft tissue during autonomous robotic palpation," *Robotics, IEEE Transactions on*, 2015.

[107] K. A. Nichols and A. M. Okamura, "Methods to segment hard inclusions in soft tissues," *IEEE Transactions on Robotics*, accepted.

[108] L. Nielsen and I. Digranes, "User participation-real influence or hostage-taking?" in *DS 43: Proceedings of E&PDE 2007, the 9th International Conference on Engineering and Product Design Education, University of Northumbria, Newcastle, UK, 13.-14.09. 2007*, 2007.

[109] M. Ohka, N. Morisawa, H. Suzuki, J. Takata, H. Koboyashi, and H. Yussof, "A robotic finger equipped with an optical three-axis tactile sensor," in *Robotics and Automation, 2008. ICRA 2008. IEEE International Conference on*, May 2008, pp. 3425–3430.

[110] K. Ohuchida and M. Hashizume, "Robotic surgery for cancer," *The Cancer Journal*, vol. 19, no. 2, pp. 130–132, 2013.

[111] C. C. L. or Open Resection Study Group *et al.*, "Laparoscopic surgery versus open surgery for colon cancer: short-term outcomes of a randomised trial," *The lancet oncology*, 2005.

[112] P. Oswalt, *Bauhaus conflicts, 1919-2009: controversies and counterparts*. Hatje Cantz Pub, 2009.

[113] N. Padoy and G. Hager, "Human-Machine Collaborative Surgery using Learned Models," in *ICRA*, 2011, pp. 5285–5292.

[114] N. Padoy and G. D. Hager, "Human-machine collaborative surgery using learned models," in *Robotics and Automation (ICRA), 2011 IEEE International Conference on*. IEEE, 2011, pp. 5285–5292.

[115] J. H. Palep *et al.*, "Robotic assisted minimally invasive surgery," *Journal of Minimal Access Surgery*, vol. 5, no. 1, p. 1, 2009.

[116] S. Parihar, "Percutaneous instrument and method," Sep. 18 2014, US Patent App. 13/832,496.

[117] R. D. Pearce, "Decentralised r&d and strategic competitiveness: globalised approaches to generation and use of technology in multinational enterprises (mnes)," *Research Policy*, vol. 28, no. 2, pp. 157–178, 1999.

[118] P. Peng and R. Rajamani, "Handheld microtactile sensor for elasticity measurement," *Sensors Journal, IEEE*, vol. 11, no. 9, pp. 1935–1942, 2011.

[119] C. Penna, "Laparoscopic instruments, attachable end effectors and methods relating to same," Aug. 7 2014, US Patent App. 13/756,777.

[120] D. G. Phinney and D. J. Prockop, "Concise review: mesenchymal stem/multipotent stromal cells: the state of transdifferentiation and modes of tissue repaircurrent views," *Stem cells*, vol. 25, no. 11, pp. 2896–2902, 2007.

[121] C. K. Prahalad, "Bottom of the pyramid as a source of breakthrough innovations," *Journal of Product Innovation Management*, vol. 29, no. 1, pp. 6–12, 2012.

[122] P. Puangmali, K. Althoefer, L. D. Seneviratne, D. Murphy, and P. Dasgupta, "State-of-the-art in force and tactile sensing for minimally invasive surgery," *Sensors Journal, IEEE*, vol. 8, no. 4, pp. 371–381, 2008.

[123] M. Qasaimeh, S. Sokhanvar, J. Dargahi, and M. Kahrizi, "Pvdf-based microfabricated tactile sensor for minimally invasive surgery," *Microelectromechanical Systems, Journal of*, vol. 18, no. 1, pp. 195–207, Feb 2009.

[124] S. U. Qureshi, K. M. Rupp, and B. Thompson, "Needle holder with suture filament grasping abilities," Sep. 14 1999, uS Patent 5,951,587.

[125] N. Radjou", "Creative problem-solving in the face of extreme limits," http://bit.ly/29RZDFe, 2014.

[126] N. Radjou, J. Prabhu *et al.*, *Frugal Innovation: How to do more with less*. PublicAffairs, 2015.

[127] N. Rajdou, J. Prabhu, and S. Ahuja. (2010) Jugaad: a new growth formula for corporate america. [Online]. Available: http://bit.ly/29SWGG6

[128] P. K. Ray and S. Ray, "Resource-constrained innovation for emerging economies: The case of the indian telecommunications industry," *IEEE Transactions on Engineering Management*, vol. 57, no. 1, pp. 144–156, 2010.

[129] C. E. Reiley and G. D. Hager, "Task versus subtask surgical skill evaluation of robotic minimally invasive surgery," in *International Conference on Medical Image Computing and Computer-Assisted Intervention*. Springer, 2009, pp. 435–442.

[130] M. Richardson, S. Elliott, and B. Haylock, "This home is a factory: Implications of the maker movement on urban environments," *Craft+ design enquiry*, vol. 5, pp. 1–3, 2013.

[131] E. Ritter and D. Scott, "Design of a Proficiency-based Skills Training Curriculum for the Fundamentals of Laparoscopic Surgery," *Surgical Innovation*, vol. 14, no. 2, pp. 107–112, 2007.

[132] A. Sarvazyan, "Computerized palpation is more sensitive than human finger," in *Proceedings of the 12th International Symposium on Biomedical Measurements and Instrumentation*, 1998, pp. 523–24.

[133] S. Sastry, M. Cohn, and F. Tendick, "Milli-robotics for remote, minimally invasive surgery," *Robotics and Autonomous Systems*, vol. 21, no. 3, pp. 305–316, 1997.

[134] J. Schulman, A. Gupta, S. Venkatesan, M. Tayson-Frederick, and P. Abbeel, "A Case Study of Trajectory Transfer through Non-Rigid Registration for a Simplified Suturing Scenario," in *IROS*, 2013, pp. 4111–4117.

[135] ——, "A case study of trajectory transfer through non-rigid registration for a simplified suturing scenario," in *2013 IEEE/RSJ International Conference on Intelligent Robots and Systems*. IEEE, 2013, pp. 4111–4117.

[136] S. Sen, A. Garg, D. V. Gealy, S. McKinley, Y. Jen, and K. Goldberg, "Automating multiple-throw multilateral surgical suturing with a mechanical needle guide and sequential convex optimization," *IEEE International Conference on Robotics and Automation (ICRA)*, 2016.

[137] A. Shademan, R. S. Decker, J. D. Opfermann, S. Leonard, A. Krieger, and P. C. Kim, "Supervised autonomous robotic soft tissue surgery," *Science translational medicine*, vol. 8, no. 337, pp. 337ra64–337ra64, 2016.

[138] A. Shashank, M. Tiwana, S. Redmond, and N. Lovell, "Design, simulation and fabrication of a low cost capacitive tactile shear sensor for a robotic hand," in *Engineering in Medicine and Biology Society, 2009. EMBC 2009. Annual International Conference of the IEEE*, Sept 2009, pp. 4132–4135.

[139] R. Smith, V. Patel, and R. Satava, "Fundamentals of robotic surgery: a course of basic robotic surgery skills based upon a 14-society consensus template of outcomes measures and curriculum development," *The International Journal of Medical Robotics and Computer Assisted Surgery*, vol. 10, no. 3, pp. 379–384, 2014.

[140] W. Smock, *The Bauhaus Ideal Then and Now: An Illustrated Guide to Modern Design*. Chicago Review Press, 2009.

[141] *Dragon Skin Series: Addition Cure Silicone Rubber Compounds*, Smooth-On, 6 2015.

[142] *Ecoflex Series: Super-Soft, Addition Cure Silicone Rubbers*, Smooth-On, 6 2015.

[143] S. Speidel, A. Kroehnert, S. Bodenstedt, H. Kenngott, B. Mueller-Stich, and R. Dillmann, "Image-based tracking of the suturing needle during laparoscopic interventions," in *SPIE Medical Imaging*, 2015.

[144] J. Spivey, K. Huey, R. Nobis, and S. Conlon, "Method for exchanging end effectors in vivo," Apr. 14 2011, US Patent App. 12/576,578.

[145] C. Staub, T. Osa, A. Knoll, and R. Bauernschmitt, "Automation of tissue piercing using circular needles and vision guidance for computer aided laparoscopic surgery," in *Robotics and Automation (ICRA), 2010 IEEE International Conference on*. IEEE, 2010, pp. 4585–4590.

[146] A. P. Stegemann, K. Ahmed, J. R. Syed, S. Rehman, K. Ghani, R. Autorino, M. Sharif, A. Rao, Y. Shi, G. E. Wilding *et al.*, "Fundamental skills of robotic surgery: a multi-institutional randomized controlled trial for validation of a simulation-based curriculum," *Urology*, vol. 81, no. 4, pp. 767–774, 2013.

[147] D. Stoianovici, J. A. Cadeddu, R. D. Demaree, S. A. Basile, R. H. Taylor, L. L. Whitcomb *et al.*, "An efficient needle injection technique and radiological guidance method for percutaneous procedures," in *CVRMed-MRCAS'97*. Springer, 1997.

[148] N. P. Suh, "Axiomatic design: Advances and applications (the oxford series on advanced manufacturing)," 2001.

[149] H. Takao, K. Sawada, and M. Ishida, "Monolithic silicon smart tactile image sensor with integrated strain sensor array on pneumatically swollen single-diaphragm structure," *Electron Devices, IEEE Transactions on*, vol. 53, no. 5, pp. 1250–1259, 2006.

[150] S. Takenawa, "A soft three-axis tactile sensor based on electromagnetic induction," in *Mechatronics, 2009. ICM 2009. IEEE International Conference on*, April 2009, pp. 1–6.

[151] A. Talasaz and R. Patel, "Integration of force reflection with tactile sensing for minimally invasive robotics-assisted tumor localization," *Haptics, IEEE Transactions on*, vol. 6, no. 2, pp. 217–228, April 2013.

[152] J. G. Tanenbaum, A. M. Williams, A. Desjardins, and K. Tanenbaum, "Democratizing technology: pleasure, utility and expressiveness in diy and maker practice," in *Proceedings of the SIGCHI Conference on Human Factors in Computing Systems*. ACM, 2013, pp. 2603–2612.

[153] E. Tateishi-Yuyama, H. Matsubara, T. Murohara, U. Ikeda, S. Shintani, H. Masaki, K. Amano, Y. Kishimoto, K. Yoshimoto, H. Akashi *et al.*, "Therapeutic angiogenesis for patients with limb ischaemia by autologous transplantation of bone-marrow cells: a pilot study and a randomised controlled trial," *The Lancet*, vol. 360, no. 9331, pp. 427–435, 2002.

[154] R. Taylor, J. Funda, D. Grossman, J. Karidis, and D. Larose, "Improved remote center-of-motion robot for surgery," *European Patent No. EP0595291*, 1994.

[155] R. Taylor, A. Menciassi, G. Fichtinger, and P. Dario, "Medical Robotics and Computer-Integrated Surgery," *Springer Handbook of Robotics*, pp. 1199–1222, 2008.

[156] R. H. Taylor, J. Funda, B. Eldridge, S. Gomory, K. Gruben, D. LaRose, M. Talamini, L. Kavoussi, and J. Anderson, "A telerobotic assistant for laparoscopic surgery," *IEEE Engineering in Medicine and Biology Magazine*, vol. 14, no. 3, pp. 279–288, 1995.

[157] Teleflex, "Teleflex press release," 2015. [Online]. Available: http://bit.ly/29F0Lry

[158] F. Tendick and M. C. Cavusoglu, "Human-machine interfaces for minimally invasive surgery," in *Engineering in Medicine and Biology Society, 1997. Proceedings of the 19th Annual International Conference of the IEEE*, vol. 6. IEEE, 1997, pp. 2771–2776.

[159] F. Tendick, R. W. Jennings, G. Tharp, and L. Stark, "Sensing and manipulation problems in endoscopic surgery: experiment, analysis, and observation," *Presence: teleoperators & virtual environments*, vol. 2, no. 1, pp. 66–81, 1993.

[160] S. Thielmann, U. Seibold, R. Haslinger, G. Passig, T. Bahls, S. Jörg, M. Nickl, A. Nothhelfer, U. Hagn, and G. Hirzinger, "Mica-a new generation of versatile instruments in robotic surgery," in *Intelligent Robots and Systems (IROS), 2010 IEEE/RSJ International Conference on*. IEEE, 2010, pp. 871–878.

[161] M. I. Tiwana, S. J. Redmond, and N. H. Lovell, "A review of tactile sensing technologies with applications in biomedical engineering," *Sensors and Actuators A: Physical*, vol. 179, pp. 17–31, 2012.

[162] A. L. Trejos, J. Jayender, M. Perri, M. D. Naish, R. V. Patel, and R. Malthaner, "Robot-assisted tactile sensing for minimally invasive tumor localization," *The International Journal of Robotics Research*, 2009.

[163] K. T. Ulrich, *Design: Creation of Artifacts in Society*. University of Pennsylvania, 2011.

[164] J. Van Den Berg, S. Miller, D. Duckworth, H. Hu, A. Wan, X.-Y. Fu, K. Goldberg, and P. Abbeel, "Superhuman performance of surgical tasks by robots using iterative learning from human-guided demonstrations," in *Robotics and Automation (ICRA), 2010 IEEE International Conference on*. IEEE, 2010, pp. 2074–2081.

[165] R. Veldkamp, E. Kuhry, W. Hop, J. Jeekel, G. Kazemier, H. J. Bonjer, E. Haglind, L. Pahlman, M. A. Cuesta, S. Msika *et al.*, "Laparoscopic surgery versus open surgery for colon cancer: short-term outcomes of a randomised trial," *Lancet Oncol*, vol. 6, no. 7, pp. 477–484, 2005.

[166] M. Velez, J. Velez, and A. Velez, "Surgical staple and endoscopic stapler," Feb. 28 1995, US Patent 5,392,978.

[167] S. K. Venkatesh, M. Yin, J. F. Glockner, N. Takahashi, P. A. Araoz, J. A. Talwalkar, and R. L. Ehman, "Magnetic resonance elastography of liver tumors-preliminary results," *AJR. American Journal of Roentgenology*, vol. 190, no. 6, p. 1534, 2008.

[168] R. W. Veryzer and J. W. Hutchinson, "The influence of unity and prototypicality on aesthetic responses to new product designs," *Journal of consumer research*, vol. 24, no. 4, pp. 374–394, 1998.

[169] C. J. Vörösmarty, P. Green, J. Salisbury, and R. B. Lammers, "Global water resources: vulnerability from climate change and population growth," *science*, vol. 289, no. 5477, pp. 284–288, 2000.

[170] S. Wang, X. Qu, and R. C. Zhao, "Clinical applications of mesenchymal stem cells," *J Hematol Oncol*, vol. 5, no. 1, p. 19, 2012.

[171] R. K. Wick", *Teaching at the Bauhaus*. Hatje Cantz Publishers, 2000.

[172] S. B. Williams, M.-H. Chen, A. V. D'Amico, A. C. Weinberg, R. Kacker, M. S. Hirsch, J. P. Richie, and J. C. Hu, "Radical retropubic prostatectomy and robotic-assisted laparoscopic prostatectomy: likelihood of positive surgical margin (s)," *Urology*, vol. 76, no. 5, pp. 1097–1101, 2010.

[173] A. Wolf and M. Shoham, "Medical Automation and Robotics," in *Springer Handbook of Automation*, 2009, pp. 1397–1407.

[174] A. Wooldridge, "First break all the rules: The charms of frugal innovation," *The Economist*, 2010.

[175] J. Yan, P. K. Scott, and R. S. Fearing, "Inclusion probing: signal detection and haptic playback of 2d fem and experimental data," in *1999 ASME International Mechanical Engineering Congress and Exposition*, 1999, pp. 14–19.

[176] K. Yang and H. Zhang, "A comparison of triz and axiomatic design," *TRIZ Journal*, vol. 8, 2000.

[177] W. Yu, Y. Li, Y. Zheng, N. Lim, M. Lu, and J. Fan, "Softness measurements for open-cell foam materials and human soft tissue," *Measurement Science and Technology*, vol. 17, no. 7, p. 1785, 2006.

[178] M. Zeschky, B. Widenmayer, and O. Gassmann, "Frugal innovation in emerging markets," *Research-Technology Management*, vol. 54, no. 4, pp. 38–45, 2011.

[179] S. Zhang. (2016) Why an autonomous robot won't replace your surgeon anytime soon. [Online]. Available: http://www.wired.com/2016/05/robot-surgeon/

[180] A. M. Zysk, F. T. Nguyen, A. L. Oldenburg, D. L. Marks, and S. A. Boppart, "Optical coherence tomography: a review of clinical development from bench to bedside," *Journal of Biomedical Optics*, vol. 12, no. 5, pp. 051 403–051 403, 2007.

9.1 Notes on Artwork Featured in this Dissertation

Decorative piece for Abstract on page 2
Magnolia Tree as seen from the patio of Caffe Strada looking north:a companion to many late-night brainstorming sessions with the collaborators listed in the Acknowledgements section. Watercolors on paper, 3.125in x 3.125in.

Dedication sigil on page i
Oy Logo. A symbol representing the author's endeavors during his time working at the AUTOLAB. The 'Oy' symbol was designed to connote a sense of eagerness and enthusiasm without containing any specific information. The 'Oy' was added to objects as a symbolic punctuation mark to the experiences that ensued within its presence.
Designed in Adobe Illustrator; implemented as stickers, fabric patches, and large-scale magnetic decals.

Preface logo on page v
AUTOLAB Logo with Tagline The Automation Sciences Laboratory was rebranded as the 'AUTOLAB' in May 2016. This logo is designed in homage to Herbert Mayer typography of the Bauhaus school [83, page 45]. The outer line is shaped to connote the visualization of a speech bubble suggesting open communication.
Designed in Adobe Illustrator; implemented as stickers and posters.

Preface header on page iv
Macro Seed Pods. Berkeley, CA. May 2016.
Nikon F; 35mm 400ISO, TriX Film.

Table of Contents header on page iii
Staircase Theme 1 from within the Museo Civico, Trieste, Italy. May 2016.
Nikon F; 35mm 400ISO, FujiFilm Pro.

Part I cover image on page 2
The Future of Intelligence. Lee-Huang Chen's desk following a presentation to the UC Regents: Albany, CA. March 2016.
Holga 120N; 120mm 400ISO, Film, Double Exposure.

Chapter 1 header on page 2
Desert Wind Double exposure of wind turbines and an oil rig near the Mojave Desert, April 2015.
Holga 120N; 120mm 400ISO, Film double exposure.

Part II cover image on page 12
Human Augmentation 3. David Gealy makes an adjustment to an autonomus cutting experiment in the AUTOLAB: Berkeley, CA. June 2016.
Nikon F; 35mm 400ISO, TriX Film.

Chapter 2 header on page 12
Macro Flowers. Berkeley, CA. May 2016.
Nikon F; 35mm 400ISO, TriX Film.

Chapter 3 header on page 20
Beach Roses (collaboration with Zoe McCarthy). Pt. Reyes National Seashore with David Gealy. April 2016. Nikon F; 35mm 400ISO, FujiFilm Pro. Enhanced using Neural Networks to 'hallucinate' a juxtaposed texture of roses onto the beach scene.

Chapter 4 header on page 35
Twisted Canals, No Sky. May 2016. Prismacolor pen and watercolor marker in Moleskine notebook. 7in x 5.5in.
In Venice I was quickly overwhelmed by the density of tourists and architecture around me. The city was beautiful but slowly falling apart. On the left here is my representation of the twisted and crooked island of Lido. Television aerials and church crosses were reflected and multiplied by the sludgy canal waters. On the right is my view across the Guidecca canal from the door of our hostel (staying with Jonathan McKinley). The main features here are the bubbly San Marco basilica and the full moon reflecting off of the canal.

Chapter 5 header on page 39
Box Cars. seen traveling through Utah in the VW van with Nick Um. April 2015.
Nikon F; 35mm 400ISO, TriX Film.

Chapter 6 header on page 52
Return to Order. May 2016. Prismacolor pen and watercolor marker in Moleskine notebook. 7in x 5.5in.
In Trieste Jonathan McKinley and I visited the Grotta Gigante, a 150 meter tall cavern underneath the Karst plateau (reference). In the early 1800's, prospectors were searching

for underground caverns to find the underground Timavo river in hopes to support the growing merchant city of Trieste with water (which rose after Venice collapsed in the late 1700s). The Triestians merchants were responsible for opening the Suez canal and bringing Egyptomania to the rest of the world. In my picture, the pyramid in the cave references Ra (the Egyptian sun god) in place of Mithras (the sun god of antiquity that was worshiped from within the caves of the region). The red beam emanating from the cave represents wine flowing forth to the region. On the right, the repeated circles are meant to evoke the image of a coin flipping: as the city of Trieste has historically been tossed from empire to empire in a near-continuous border struggle. One of the circles represents the sun rising over the Aegean sea.

Part III cover image on page 61
Super Bloom 1 (collaboration with Zoe McCarthy). Traveling to Death Valley, CA with Nick Um to observe an abundance of wildflowers. April 2016.
Nikon F; 35mm 400ISO, TriX Film. Enhanced using Neural Networks to 'hallucinate' a juxtaposed texture of primates onto the flower scene.

Chapter 7 header on page 61
Balcony Study. May 2016. Prismacolor pen and watercolor marker in Moleskine notebook. 7in x 5.5in.
In Stockholm, there is a church steeple that is made of thin metal webbing that has captured my attention each time I visit. The Ryddarholms Kyrkan, where the Swedish monarchy are interred, is decomposed in this drawing into two planes representing the components of its texture. (See for reference: `http://bit.ly/2aa2bPZ` On its right, the lines of the church blend into a representation of the building on the street corner near the 'Lodge 32' hostel on the corner of Kungholmsgatan & Kungsgatan as seen here: `http://bit.ly/2a5mif4`. In this panel I am juxtaposing my experiences at the robotics conference (artificial, metallic, and cold), to the experiences I shared with Jonathan McKinley and Rebecka Öberg while running on the (green, verdant, and warm) island of Lidingö.

Figure 7.1 on page 62
Night Walk. November 2015. Prismacolor pen, pencil, and watercolor marker in Moleskine notebook. 7in x 5.5in.
There is a waterfall near Codornices Park in Berkeley which has become a place of refuge from the excitement of the University. On the background of these pages are notes from a lecture given by Antonio Bicchi (University of Pisa) on robotic grasping and manipulation. Inspiration for this piece was taken from an exhibit at the Asian Art Museum in San Francisco: 'Looking East: How Japan Inspired Monet, van Gogh, and other Western Artists.'

Figure 7.2 on page 63
Night Walk. November 2015. Prismacolor pen, pencil, gesso, tung oil, and watercolor marker in Moleskine notebook. 3.5in x 5.5in.

Inspiration for this piece was taken from an exhibit at the Asian Art Museum in San Francisco: 'Looking East: How Japan Inspired Monet, van Gogh, and other Western Artists.'

Figure 7.3 on page 64
Emerald Bay Moonrise. June 2016, Lake Tahoe, CA. Ink and Watercolor. 6in x 12in.
An aesthetically minimal (Functionalism) interpretation of the sky during moonrise over Emerald Bay in Lake Tahoe.

Figure 7.4 on page 65
Human Augmentation I. June 2016, AUTOLAB: Berkeley, CA.
Professor Ken Goldberg of the AUTOLAB reaches toward the end-effector of a daVinci Surgical Robot. Currently there are 3000 of such machines in use worldwide; for comparison, there are 400,000 operating rooms in the world. The world has only begun to benefit from robotic surgery.
Nikon F; 35mm 400ISO, TriX Film.

Chapter 8 header on page 67
Driving across the Mojave Desert in the VW van with Jeff Mahler and Nick Um.
Nikon F; 35mm 400ISO, TriX Film.

Bibliography header on page 86
Self Portrait in the Train traveling from Venice to Trieste following the ICRA2016 conference.
Nikon F; 35mm 400ISO, TriX Film.

Appendix header on page 87
Setting up the Drone: Crewing an ultramarathon for Jonathan McKinley. Pictured are Jeff Mahler, David Gealy, and Michael McKinley. June 2016
Nikon F2; 35mm 400ISO, Kodachrome Film.

9.2 A Note Regarding Other Figures in this Dissertation

Except for those in Chapter 2, all figures were created with a Nikon D90 DSLR camera using post processing in Adobe Lightroom, and Adobe Illustrator.

9.3 Conceptual Designs for the DATE Device

As referenced in Chapter 1 on Page 9, these are conceptual drawing used to communicate a provision patent on a precision irrigation system and inform the prototype device design.

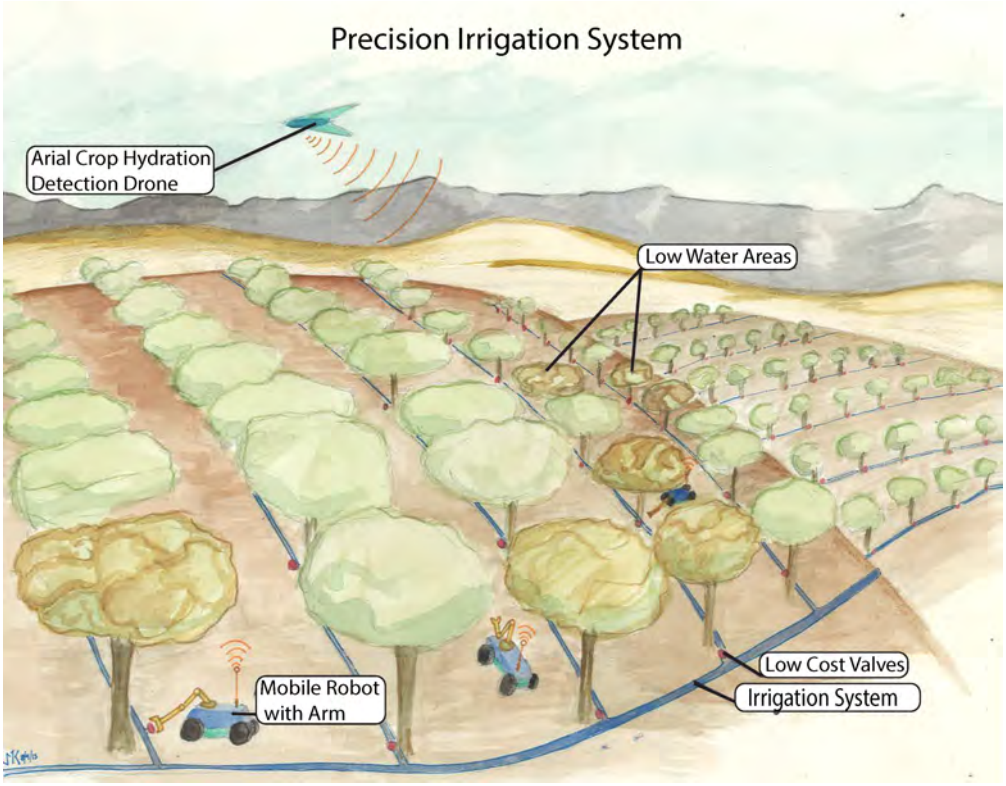

Figure 9.1: "Precision Irrigation System Conceptual Model" *S. McKinley 2016* Watercolors on Paper, 11in x 17in, digital collage

A precision irrigation system is envisioned as Figure 9.1 which includes crop hydration level sensing (as embodied here by an aerial drone), mobile robots equipped with a novel gripper (further visualized in Figures 9.2, 9.3, 9.4, and 9.5). Existing irrigation systems are shown in blue with added valves (emitters) shown in red.

Figure 9.2 is a visualization needed to illustrate the following functional design criteria: A flexible shaft coupling a tool to the plant-located emitter, the presence of a vision system to identify valves, the presence of a knob on the emitter, the presence of some sort of indexing feature on the knob, the transferal of torque between the tool and the emitter so as to change the output water flow delivered to the plant, and additional sensors. Each of these functional constraints were addressed as specific claims within the text of the patent.

The functional requirements of the valve shown in Figure 9.3 included: a component that can control flow of a liquid, fittings to attach the valve to existing piping, a knob to set the flow of the valve, and an indexing feature to verify position with respect to the robot gripper. These functional requirements were written as claims within the patent application.

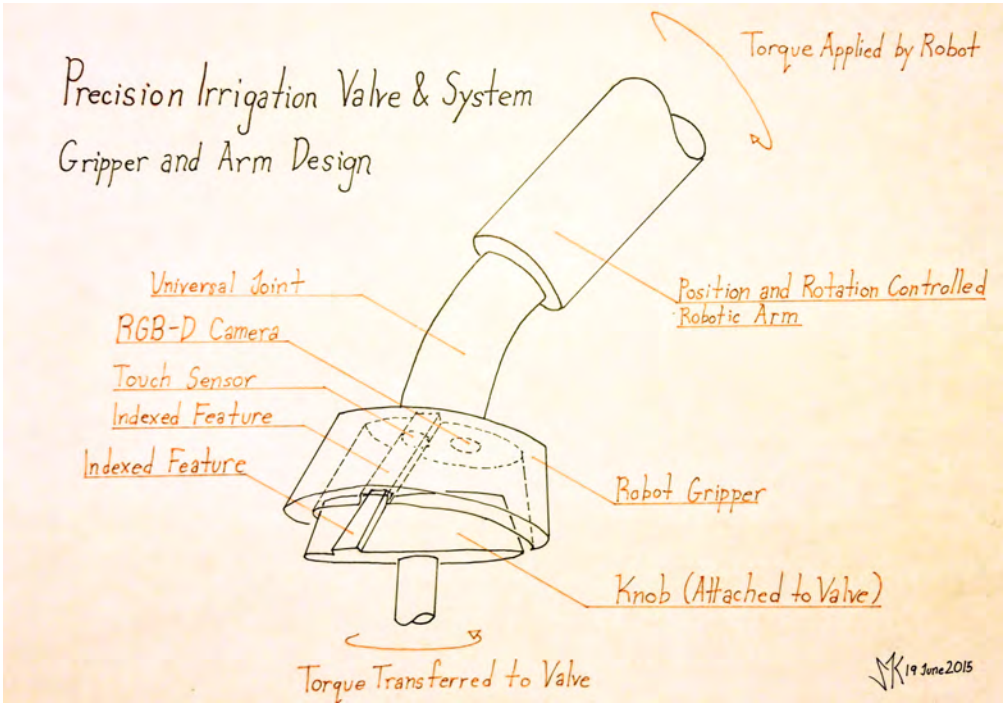

Figure 9.2: "Gripper and Arm Concept" *S. McKinley 2016* Ink on Paper, 8.5in x 11in.

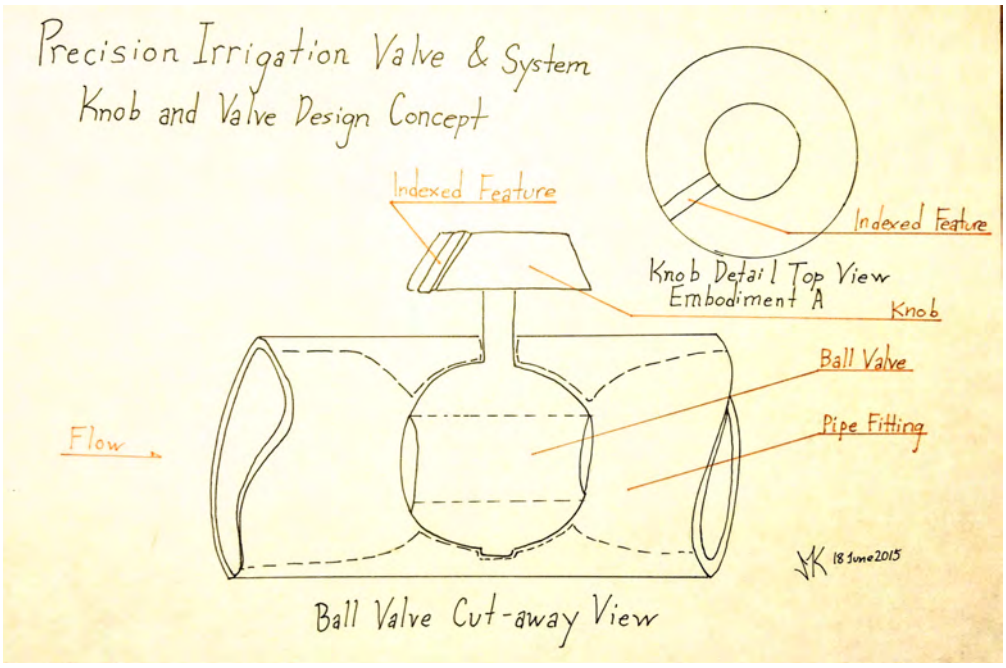

Figure 9.3: "Knob and Valve Design Concept" *S. McKinley 2016* Ink on Paper, 8.5in x 11in.

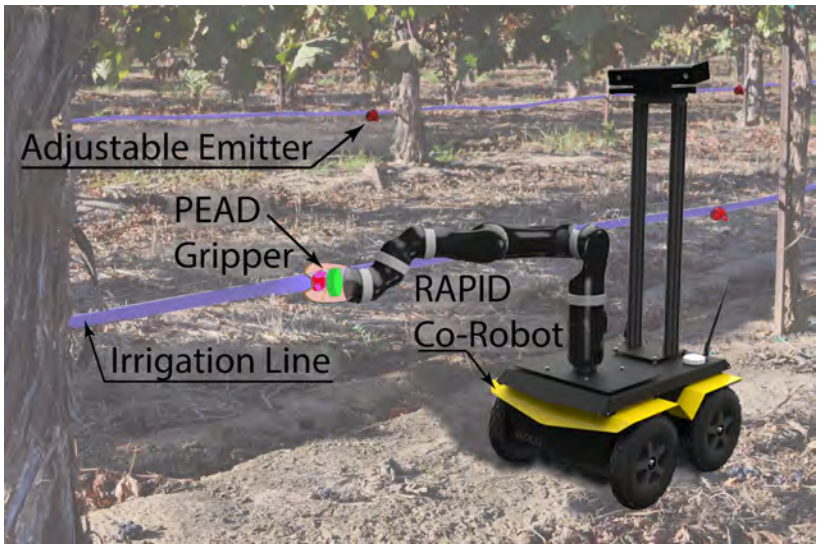

Figure 9.4: "Mobile Robotic Autonomous Interface Concept" *S. McKinley 2016, Digital Collage.* This conceptualization shows an alternate embodiment of the system using a robotic agent in the field in the place of a human worker.

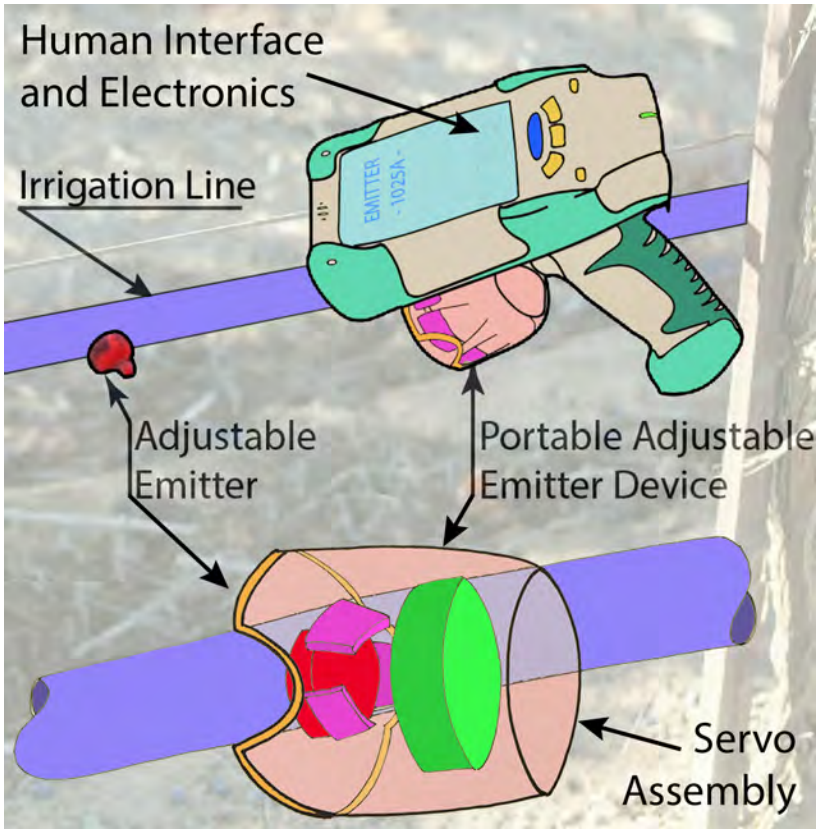

Figure 9.5: "Gripper and Arm Concept" *S. McKinley 2016 Digital Collage.* This figure illustrates functional requirements of the hand-held DATE device (referenced in Chapter 1 on page 9